NTNU

Norwegian University of
Science and Technology

Effects of three metal coupling on galvanic crevice corrosion

Harald Solli

Chemical Engineering and Biotechnology
Submission date: June 2017
Supervisor: Kemal Nisancioglu, IMA
Co-supervisor: Otto Lunder, IMA

Norwegian University of Science and Technology
Department of Materials Science and Engineering

Preface

This thesis was written during spring 2017 at Department of Materials Science and Engineering, at Norwegian University of Science and Technology(NTNU), in Trondheim,Norway. It is a continuation of a ongoing project started by a master thesis written by Sondre Røstbø in the spring of 2016 for the same department.

I would like to thank my supervisors for the thesis, Professor Kemal Nisancioglu, and co-supervisor Dr. Otto Lunder for their guidance and discussions.

Staff Engineer Anita Storsve deserve a big thanks for preparing salt bridges, and responding to my technical problems swiftly.

NTNU's mechanical workshop at Faculty of Natural Science and Technology deserves gratitude for preparing samples and creating devices for the experimental setup.

Lastly, a big thanks goes to Sondre Røstbø for teaching me the experimental method and always being helpful when something about the laboratory work were unclear.

Harald Solli

Summary

The subsea industry is moving its operations down onto the seabed. With this new direction in production solutions a larger emphasis is placed on reducing the weight of the components in the production unit. Finding alternative material solutions to carbon steel in the structures is of high interest, where aluminium might be a fitting solution. A problem with this is that aluminium will experience galvanic corrosion when coupled to steel. Since not all of the steel components can be replaced, the metals will have to be isolated. A different solution could be to apply cathodic protection on both metals by use of a common sacrificial anode.

The purpose of this thesis was to investigate the effects of a three metal coupling on crevice corrosion. Especially aluminium has been found to have poor corrosion properties in galvanic coupling with a crevice present. Experiments were performed with X65 carbon steel and 6005 aluminium. The sacrificial anode for the steel-aluminium coupling were an AlZnIn sacrificial anode. The experiments were performed in synthetic seawater at both 25°C and 10°C. Some parallels was performed without the anode. The tests was a simulation of crevice corrosion with a crevice of 100 μm and tests duration varied between 72,96 and 120 hours. After electrochemical measurements the metal surfaces were inspected and weight loss measurements were performed.

It was found that cathodic protection of steel-aluminium galvanic couples seems possible in galvanic crevice corrosion. Both metals experienced a reduction in current demand as a function of time during the experiments. Reduction rate on steel was found to be 1-2 orders of magnitude higher on steel than on aluminium. Aluminium experienced an anodic current initially which indicates corrosion. It was presumed to be due to development of an alkaline environment inside the crevice. The anodic current decayed with time and passed into the cathodic region for some of the parallels. The electrochemical behaviour were found to be promising for both metals.

Photographs together with SEM micrographs showed that the corrosive attack on aluminium occurred at the crevice mouth during the 25 °C tests. When the temperature was lowered to 10 °C the attack was found over the entire exposed surface. For steel, no corrosive attack was found at 25°C. This was changed when the temperature was lowered and a small corrosive attack was found. Calcareous deposits were also investigated and found to form faster with the AlZnIn anode. Inspection and images indicated that these calcareous deposits could possibly block the crevice when the anode was connected to the system.

The weight loss measurements revealed complete protection of the steel at 25°C and minor corrosion was found at 10°C. It was concluded that the steel is well protected in the three metal coupling. Mass loss rate on aluminium was found to slow down as the duration of the experiments increased. It was concluded that protection of aluminium is possible, but that further testing is necessary.

Sammendrag

Subsea industrien beveger produksjonen sin ned på havbunnen. Med denne nye retningen i produksjonsmetode er det et større fokus på å få redusert vekten til produskjonskomponentene. Å finne alternative materialløsninger til karbonstål i strukturene er av høy interresse og aluminium er en mulig løsning. Et problem med dette er at aluminuium vil oppleve galvanisk korrosjon i kobling med stål. Siden ikke alle stålkomponenter kan bli byttet ut må metallene isoleres fra hverandre. En annerledes løsning ville vært å bruke katodisk beskyttelse på begge metallene, ved bruk av en felles offeranode.

Formålet med denne avhandlingen var å etterforske oppførselen til en tremetallskobling i en spalt. Spesielt aluminium er kjent for å ha dårlig motstand mot spaltkorrosjon. Eksperimentene ble utført med X65 karbonstål og 6005 aluminium. For å beskytte begge metallene ble en AlZnIn offeranode brukt. Eksperimentene ble utført i syntetisk sjøvann ved både 25°C og 10°C. Det ble også kjørt paralleller uten offeranoden. Testene simulerte en 100 μm stor spaltåpning og tidene ble variert mellom 72,96 og 120 timer . Etter de elktrokjemiske målingene ble metalloverflatene inspisert og vekttapsmålinger ble utført.

Det ble funnet at katodisk beskyttelse av stål-aluminium galvanisk kobling virker mulig for spaltkorrosjon. Begge metallene opplevde en nedgang i strømbehov som en funksjon av tid under eksperimentene. Reduskjonsraten på stål ble funnet til å være 1-2 tierpotenser høyere enn for aluminium. Aliminium opplevde en anodestrøm i begynnelsen av forsøkene noe som indikerer korrosjon. Det ble antatt å være grunnet utviklingen av et basisk miljø inni spalten. Den anodiske strømmen ble redusert med tiden og passerte inn i det katodiske området for noen av parallellene. De elektrokjemiske resultatene viste lovende oppførsel for begge metallene.

Bilder sammen med SEM mikrografer avslørte at korrosjonangrepet på alumnium skjedde ved kanten av spalten under 25°C. Med senkning av temperaturen til 10°C dekket angrepet hele overflaten. På stål var det ingen synlig korrosjon ved 25 °C. Når temperaturen ble senket ble det funnet et lite korrosjonsangrep. Kalkbelegg ble også undersøkt og funnet til å vokse fortere når AlZnIn anoden var tilkoblet. Inspeksjon og bilder indikerte at disse beleggene kunne tette igjen spalten når anoden var tilkoblet.

Vektapsmålinger viste komplett beskyttelse av stål ved 25°C og lav korrosjon ved 10°C. Det ble konkludert med at stålet er bra beskyttet i tremetallskobling. Massetapsraten på alumnium sakket ned ved lengre forsøk. Det ble konkludert med at beskyttelse av aluminium er lovende, men vil kreve mer testing.

Table of Contents

Chapter 1

Introduction

1.1 Background

Use of aluminium in the subsea industry today is limited. The metal is often used as construction material for remote operated vehicles (ROVs), and not in larger installations. For structural applications it's often used as sacrificial anodes and is associated with poor corrosion resistance to some structural designers[1]. The engineering experience with aluminium alloys in seawater is limited in comparison to steel.

With a larger emphasis on moving offshore production onto the seabed, a reduction in weight is is desired. Here aluminium can prove to be a competent solution with its excellent weight to strength ratio and immunity to hydrogen induced stress cracking (HISC)[2]. To perform maintenance on a subsea installation they have to be lifted up from the bottom. Replacing components of steel, with aluminium can therefore resolve problems experienced with transport and maintenance.

When steel and aluminium are coupled together in seawater the aluminium will suffer from galvanic corrosion.This is often avoided by insulating the two metals from each other. Complete insulation between the metals is impossible in practise and a proposed solution is to protect both the steel and the aluminium by a common sacrificial anode system. The system needs to provide good protection of both metals, and has to be resistant towards other common problems that occur when dissimilar metals are joined. A good example would be resistance against crevice corrosion.

1.2 Aim for the project

The aim for this project is to investigate a protection system for both steel and aluminium in metallic coupling with an emphasis on crevice corrosion. Especially if it's possible to protect aluminium in a crevice. The thesis is a continuation of a master thesis conducted by Sondre Røstbø. Electrochemical behaviour for galvanic crevice corrosion will be

measured, with subsequent surface characterization and weight loss measurements. The alloys will be X65 carbon steel coupled with 6005 aluminium alloy with an AlZnIn sacrificial anode.

Chapter 2

Theory

2.1 Galvanic Corrosion

Galvanic corrosion will occur if two or more different metals are coupled together in a common corrosive medium. Under these circumstances an increase in corrosion can be found on the active metal N, while the noble metal M will experience a decrease or complete stop in corrosion [3], and hence be ”protected”. With no ohmic resistance in the electrolyte or in the metallic circuit, the system will reach a common potential expressed as E_C or coupling potential. This potential will be sustained by a flow of electrons from the active metal(N) to the noble metal(M) as illustrated in figure 2.1

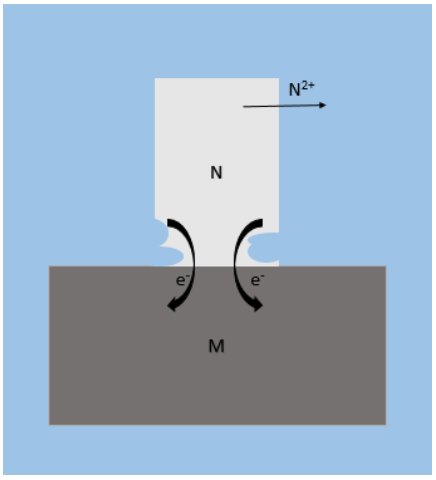

Figure 2.1: Galvanic corrosion. Electrons flow from active metal N to noble metal M, causing dissolution of metal N

The mixed potential theory states that a corrosive attack can be divided into oxidation and reduction reactions[3]. The theory suggests that the rates of oxidation and reduction is the same during corrosion. The oxidation reactions are metal dissolution which are shown in equation (2.1). Reduction reactions are divided into oxygen reduction which are shown in equations (2.2) and (2.3). The other form is hydrogen evolution which are shown in equations (2.4) and (2.5).

$$M \rightarrow M^{n+} + ne^- \tag{2.1}$$

Oxygen reduction reactions in acidic and alkaline environment[3]:

$$O_2(dissolved) + 2H_2O + 4e^- \rightarrow 4OH^- \tag{2.2}$$

$$O_2(dissolved) + 4H^+ + 4e^- \rightarrow 2H_2O \tag{2.3}$$

Reactions for hydrogen evolution at acidic and alkaline conditions respectively:

$$2H^+ + 2e^- \rightarrow H_2 \tag{2.4}$$

$$2H_2O + 2e^- \rightarrow H_2 + 2OH^- \tag{2.5}$$

This principle is important if the rate of galvanic corrosion is to be measured. A zero resistance ammeter can be used to measure the current precisely . The current will then be the difference in oxidation and and reduction reactions on both metals, since the circuit is resistance free. When the system is at the coupling potential, the measured current can be expressed as:

$$I_{net} = \Sigma I_{ox,N} - \Sigma |I_{red}|_{,N} = \Sigma |I_{red}|_{,M} - \Sigma I_{ox,M} \tag{2.6}$$

With the assumption that the only oxidation reactions that occur are metal dissolution, equation (2.6)can be expressed in the form of:

$$I_{net} = \Sigma I_{corr(M-\underline{\mathbf{N}})} - \Sigma |I_{red}|_{,N} = \Sigma |I_{red}|_{,M} - \Sigma I_{corr(\underline{\mathbf{M}}-N)} \tag{2.7}$$

2.2 Cathodic Protection

Cathodic protection utilizes galvanic corrosion to protect a structure or component in an corrosive environment. By connecting the desired structure or component to a more active metal, the corrosion rate will decrease and operational lifetime can be prolonged. The metal dissolution from equation (2.1) will then occur on the active metal as shown in figure 2.1 while the reduction reactions still take place on the now cathodic surface of the noble metal.

Illustrated in figure 2.2 the corrosion potential E_{Corr} is lowered to a protection potential E_P by the active metal, this will in turn decrease the corrosion current i_{Corr} to the protection current i_P. For complete protection of the structure the protection potential would have to be lowered below the reversible potential E_{rev}.

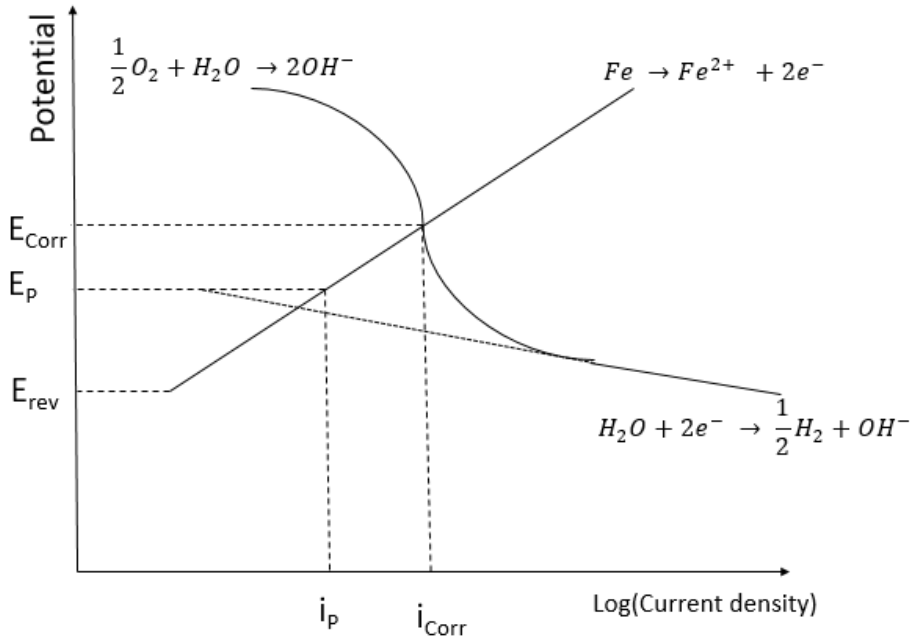

Figure 2.2: Schematic evans diagram adapted from Andresen et al [4] showing relationship between potential lowering and the logarithm of current density on a steel surface in seawater

There are 2 different methods of cathodic protection in use today, these are sacrificial anode or inert anode. Sacrificial anodes will behave like the active metals described, then the oxidation reactions will occur on the anode and it will experience metal dissolution.

With an inert anode system a current has to be provided continuously to keep the structure protected. The difference from the sacrificial anode method is the fact that the inert anode is not consumed during operation.

When applying cathodic protection it's often recommended to keep the potential within a given range. This range depends on the material that is to be protected. If the potential is too high the system will not be able to provide enough current and thus the metal will be "under protected". Then the noble metal will experience corrosion. With a potential to low there will be to much current provided by the anode. This is better known as "over protection" and can cause problems due to a high rate of reduction reactions on the noble metal.

2.2.1 Cathodic protection of steel

Carbon steel is known for its poor resistance to corrosion in most environments. It's very unstable in seawater and thus in need of protection. For a low alloy steel a potential below -0.84V$_{SCE}$ is recommended as a protection potential on steel[2],[5]. This puts

steel in the immune area of the pourbaix diagram shown in figure 2.3. In this area the steel is theoretically completely protected, it's however recommended to consider cathodic protection of steel as a way to decrease and control corrosion, instead of completely stopping it[2],[5].

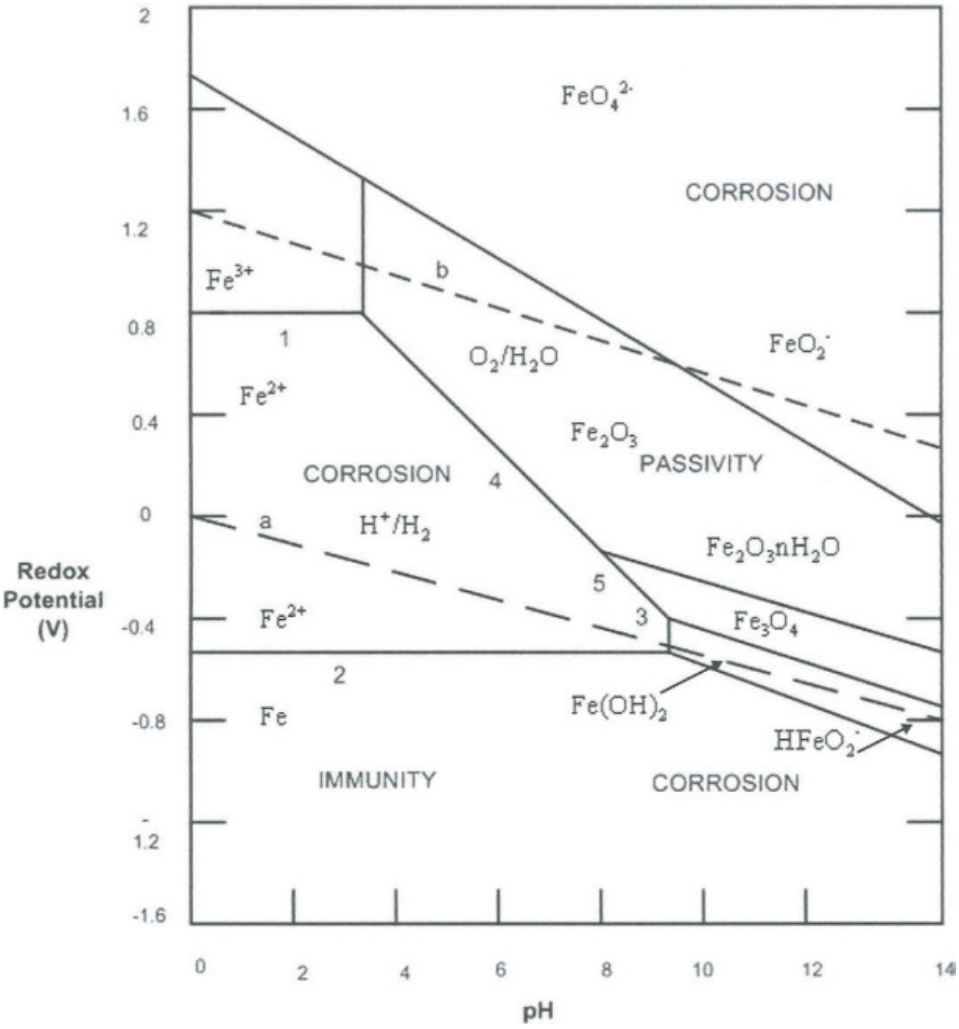

Figure 2.3: Pourbaix diagram of iron in water at showing the immune, passive and corrosion zones. Figure is adapted from Ahmad[6]

Cathodic protection of steel is known to be quite effective. Studies performed in the tidal zone by Refait et al showed that cathodic protection of steel decreased the corrosion rate by orders of magnitudes[7]. Experiments were also conducted on already corroded surfaces and showed that cathodic protection still is effective. Steel is most often susceptible to

uniform corrosion. This means that the entire exposed surface will be in need of protection and thus a high current is demanded of the anode. This demand of the anode will eventually decay in seawater due to formation of calcareous deposits.

2.2.2 Calcareous Deposits

When cathodic protection is applied to a metal submerged in seawater a layer of calcareous deposits will form on the surface. These deposits mainly consist of the two compounds $Mg(OH)_2$ and $CaCO_3$. The deposits have been shown to slow down the reduction rate on the noble metal and thus cause a decrease in the current which the anode has to provide. The layer will act as a physical barrier for the diffusion of oxygen thus slowing down reactions (2.2) and (2.3) which are mass transport controlled. Anode consumption is then decreased and the effectiveness the CP system is increased.

During polarization the reduction reactions given in equations (2.2) and (2.5) cause an alkalization of the metal surface due to the development of hydroksyl ions. These ions can react directly with magnesium ions and thus cause formation of $Mg(OH)_2$:

$$Mg^{2+} + 2OH^- \rightarrow Mg(OH)_2 \tag{2.8}$$

One would expect that $Ca(OH)_2$ also would form during alkalization, but due to a high solubility of the compound, the hydroxides found during calcareous formation mainly consists of $Mg(OH)_2$ [8]. The OH^- ions will however shift the equilibriums given in reactions (2.9),(2.10) and (2.11) to the right, this will facilitate the formation of calcium carbonate as given in equation (2.12)

$$CO_2 + H_2O \rightarrow H_2CO_3 \tag{2.9}$$

$$H_2CO_3 \rightarrow H^+ + HCO_3^- \tag{2.10}$$

$$HCO_3^- \rightarrow H^+ + CO_3^{2-} \tag{2.11}$$

$$Ca^{2+} + CO_2^{2-} \rightarrow CaCO_3 \tag{2.12}$$

The composition becomes important when looking at the protective properties of the layer. It's commonly known that that the calcium carbonate layer is preferred due to its excellent insulating properties. So the protective properties is often expressed through a Ca/Mg factor were a high number is desired. Elbeik et al[8] investigated the protective properties of the calcium carbonate. Here it was found that $CaCO_3$ could inhibit the diffusion of oxygen to the metal surface and thus decrease the oxygen reduction current by a factor of 5[8]. The studies also found that the hydrogen evolution current were halved due to formation of $CaCO_3$. This was interpreted as sign of porosity in the film which could not keep out seawater, but limit the transport of oxygen ions

The magnesium phase is however not known to have the same protective properties as the $CaCO_3$. Studies performed by Okstad et al[9] investigated the influence calcareous deposits has on the hydrogen evolution reaction in natural seawater. It was again found that the calcareous layer slowed down the oxygen current by inhibiting diffusion to the surface. The hydrogen evolution was however not affected which showed that the layer is not able to stop water from reaching the surface. Magnesium hydroxide's effect on hydrogen evolution were studied by Saleh[10]. In these studies it was found that Magnesium hydroxide did not inhibit hydrogen evolution on an iron surface. Further it was found that the layer catalyzed hydrogen evolution, and was 2 to 3 times faster on a $Mg(OH)_2$ coated magnesium surface, rather than on pure Magnesium.

Growth factors

The growth and propagation of the calcareous deposits depend on a number of different factors which are listed beneath:

- current and potential
- temperature
- chemical conditions
- hydrodynamics and flow
- surface morphology and geometry

The Effects of these parameters in combination are often complex and can cause different results on the main compounds $Mg(OH)_2$ and $CaCO_3$. Due to this the results in literature can be contradicting[11]. Flow and surface morphology are factors that are not present in the report and will thus not be discussed.

Chemical conditions and morphology

Considering the solubility factors of the two compounds the critical pH of precipitation has been calculated. Calculations performed by Okstad[12] found the critical pH to be 6.0 for $CaCO_3$ and 9.1 for $Mg(OH)_2$. Yang et al performed similar calculations and found the critical values to be 7.58 and 10 for calcium carbonate and magnesium hydroxide respectively[13]. The kinetics of $Mg(OH)_2$ formation are found to be much faster than those for $CaCO_3$ and hence a larger composition of magnesium phase is expected in conditions where formation of both compounds is possible. Studies also suggest that the Magnesium phase inhibits the formation of the calcium phase and thus further promote a magnesium rich layer[12].

Magnesium hydroxide precipitates as a porous thin film over the entire surface. Calcium carbonate will precipitate either as calcite or argonite. Calcite precipitates with a cubic shape while argonite precipitates in clusters of needles. Calcite is known to be more stable, but is more susceptible to inhibition from the magnesium layer. Thus argonite is often found in seawater when both calcium and magnesium is present. Neville et al

[11] characterized calcareous deposits from cathodic protection under various times and electrolyte composition. Here it was found that calcite will form in an magnesium free electrolyte. This were however changed when the same potential were applied to an artificial seawater solution were argonite seemed to precipitate after an initial layer of containing magnesium were formed.

Potential and current

Since the formation of both $Mg(OH)_2$ and $CaCO_3$ is a result from the reduction reactions described earlier, the potential and provided current will play a major role in the formation of the calcareous layer. Studies performed by Okstad[12] which studied the effect of both potential and flow suggests that the calcium carbonate growth is favoured in an intermediate potential range between too cathodic and too anodic as shown in figure 2.4

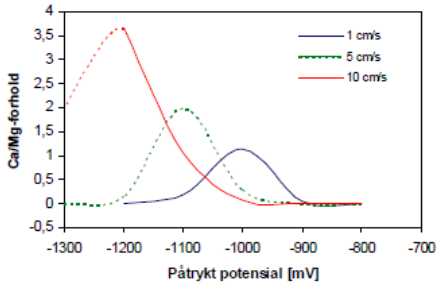

Figure 2.4: Ca/Mg ratio as a function of flow velocity and applied potential the potential is given vs the SCE electrode. Dashed lines represent assumed behaviour [12]

At higher cathodic potentials the reduction reactions on the surface will occur so rapidly that the alkaline environment will favour formation of $Mg(OH)_2$, this is supported by other studies[11]. It can be seen from the figure the Magnesium phase will also be favoured at more anodic potentials. At these conditions the pH at the surface will be considerably lower due a slower rate of reduction reactions. The reason behind the faster formation of $Mg(OH)_2$ is due to its fast kinetics which trumps at pH levels where both compounds can form.

Temperature

With an increasing temperature it's found that the calcareous layer grows faster. This is due to faster kinetics for both calcareous compounds at elevated temperatures. The change in solubility is however opposite for the individual compounds when the temperature is altered. The magnesium phase will see an increase in solubility with temperature, while the solubility of the calcium phase will decrease as a function of temperature[12]. It is thus found that the layer is more protective at higher temperatures due to a larger composition of unsolved $CaCO_3$.

Experiments performed by Barchiche et al[11] showed that the decrease in current requirement were faster at higher temperatures during a polarization potential of -1 V/SCE. This effect were however not present at a potential of -1.2V/SCE. This can be explained by the fact that at such low potential the pH of the surface will cause the layer to consist mostly of $Mg(OH)_2$ and the pH being a more important factor than temperature.

2.2.3 Cathodic protection of aluminium

Oxide layer

Aluminium have great corrosion properties in seawater. This is due the formation of a oxide layer which passivates the surface. This layer is mainly Al_2O_3 and has the following proposed formation mechanism[3] :

$$Al \rightarrow Al^{3+} + 3e^- \tag{2.13}$$

$$2Al^{3+} + 3H_2O \rightarrow Al_2O_3 + 6H^+ \tag{2.14}$$

The formation of this layer is rapid and the layer will renew itself immediately if the surface is scratched[3]. The electrons which are released from equation (2.13) can further react into hydroxide or hydrogen gas:

$$O_2 + 2H_2O + 4e^- \rightarrow 4OH^- \tag{2.15}$$

Or:

$$2H^+ + 2e^- \rightarrow H_2 \tag{2.16}$$

In contrast to the oxide layer found on more noble metals like steel which is dependant on the amount of solved oxygen in the solution, aluminium oxide can form by splitting up water molecules. In these conditions with a depleted oxygen, level the hydrogen evolution from equation (2.16) will be favoured. The layer is amphotericly unstable, which means it's stable at neutral and slightly acidic and alkaline environments. This can be seen from the theoretical pourbaix diagram shown in figure 2.5. Thus aluminium will be susceptible to corrosion in both very acidic and in very alkaline environments.

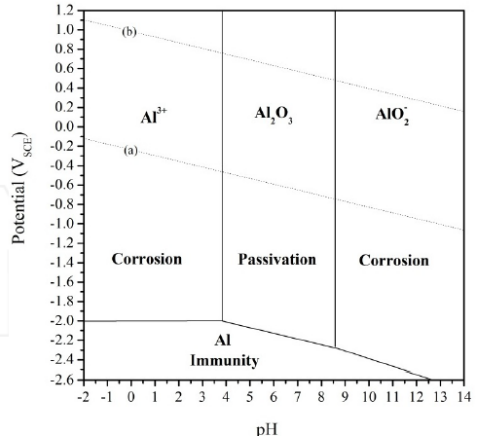

Figure 2.5: Theoretical Pourbaix diagram of pure aluminium in aqueous solution at 25^{o}C. Line (a) corresponds to the hydrogen evolution reaction and line (b) is the oxygen reduction reaction. Figure is taken from [14]

In a study by Perault it was found that there was no immune region for aluminium due to the presence of hydrides on the aluminium surface[15]. It was also found that these hydrides would destabilize the oxide layer and thus cause the aluminium to be more susceptible to corrosion. An experimental construction of a pourbaix diagram of an aluminium alloy in NaCl were created by Gimenez[16].This diagram can be seen in figure 2.6. It was found that aluminium is susceptible to pitting or general attack at lowered potential levels and no immune zone was detected.

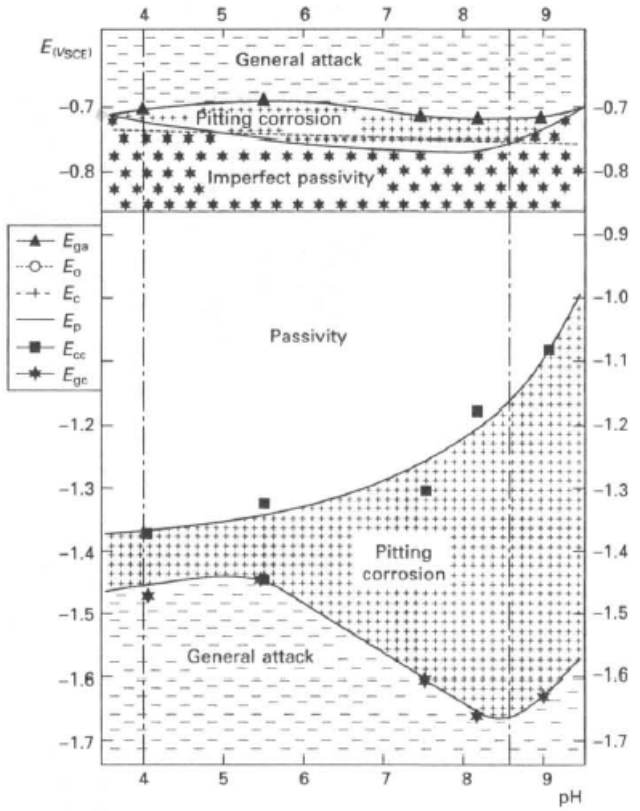

Figure 2.6: Experimental potential-pH diagram for the 5086 alloy in 3% NaCl solution at 20°C. Figure is taken from [16]

Pitting mechanism and current requirement

Under stagnant conditions, corrosion on aluminum is often found in the form a localized pitting attack[17],[18]. These pits stem from iron rich intermetallic particles located in the aluminium matrix that act as weak points on the passivated surface. The particles are nobler than the matrix and will become cathodic in a micro galvanic coupling created on the aluminium surface. Due to the insulating properties of the oxide, the reduction

processes during corrosion can only occur at these particles. As mentioned earlier will reduction reactions cause formation of OH^- ions which will destabilize the oxide layer surrounding the particles. This is illustrated in figure 2.7:

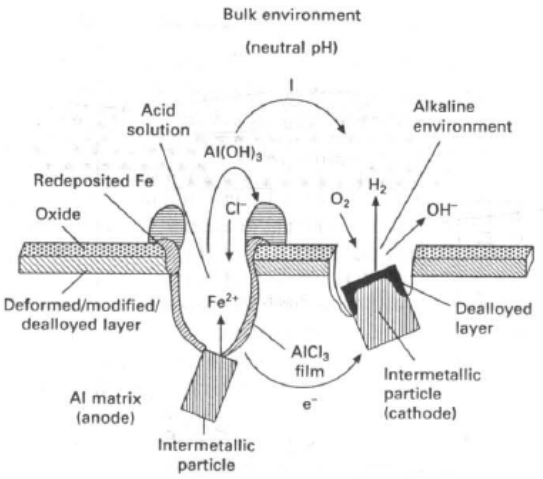

Figure 2.7: Illustration of pitting mechanism for aluminium corrosion at stagnant conditions. Figure taken from[17]

This alkaline etching of the surface will propagate and can eventually result in detachment of the intermetallic particle and a subsequent reapassivation of the surface inside the pit. However in chloride containing mediums, some of the pits can become acidic as seen on the figure. This acidification is due to the hydrolysis during repassivation which is given in equation(2.14). These pits are however only initiated at potential above the critical pitting potential of aluminium which is at -0.75V$_{SCE}$. When initiated the pits can however propagate at potentials lower than E$_P$. In the experimental pourbaix diagram from figure2.6, this is the pitting mechanism placed above the passive zone.

Cathodic protection of aluminum will thus require a potential of at least -0.85V$_{SCE}$[17] to keep the metal in the passive region of the pourbaix diagram. This is called anodic protection and is often done by a potentiostat. Protection of aluminium is found to be very effective against pitting, but do not have any noticeable effect on uniform corrosion[18]. Due to the localized form of corrosion with reduction only occurring at the intermetallic sites .Aluminium will in general demand less current than steel. Studies performed by Gundersen and Nisancioglu [19] showed that the requirement for protection current will decay exponentially as shown in figure 2.8.

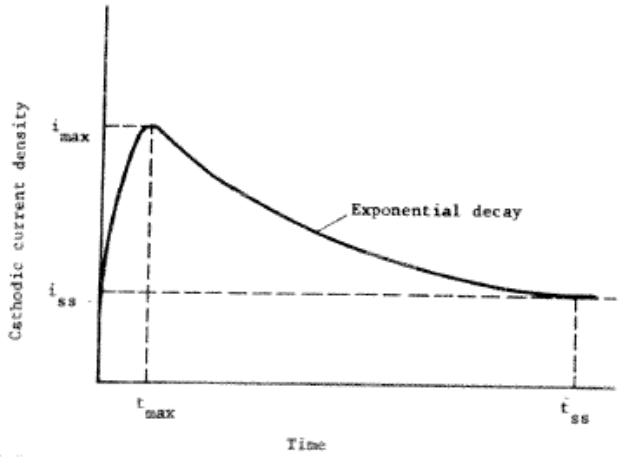

Figure 2.8: Illustrative figure for current demand of an aluminium alloy under cathodic protection with constant potential[19]

This is due to the repassivation of the pits after particle detachment which in conjunction with calcareous formation will decrease the current during polarization. Since the oxide is not stable in alkaline environments there is a danger of "over protection" of the surface. If the surface is polarized to far in the cathodic direction the alkaline etching caused by OH^- ions will continuously expose new intermetallic particles and the oxide layer will not be able to stabilize again[17]. This mechanism is often referred to as cathodic corrosion[3]. This is the pitting zone in figure 2.6 which is located below and to the right of the passive zone.

2.3 Crevice Corrosion

Crevice corrosion occurs at small cavities between dissimilar metals or a metal and an insulator. These small gaps of space usually comes from joining metals with bolts or screws instead of welding. Since the surface inside the crevice is also exposed to the electrolyte, the corrosive reactions will occur both on the inside and the outside. These are the same oxidation and reduction reactions as discussed earlier. For all metals, but especially those with active-passive kinetics a metal oxide can form from the dissolved metal from the oxidation reaction given in (2.1). Formation of this metal is shown in general form [3]:

$$M^+ + H_2O \rightarrow MOH_{(s)} + H^+ \tag{2.17}$$

This reaction will act as a counterbalance to the OH^- production from the reduction reactions in equations (2.2) and (2.5). The amount of dissolved oxygen inside the crevice will be depleted due to a limited transport or diffusion inside the crevice. On the outside there will still be sufficient oxygen supply. This causes the inside of the crevice to become anodic compared to the outside and thus metal dissolution accompanied by hydrolysis will dominate inside the crevice. On the outside which is now cathodic, oxygen evolution will start to dominate. These processes will thus cause a change in the chemistry inside of the crevice since the H^+ ions can not be sufficiently neutralized. The pH inside the crevice will then decrease and an excess of positively charged ions is found. To keep electroneutrality, negatively charged ions will migrate into the crevice. If the electrolyte contains chlorides formation of HCl will develop and which is extremely corrosive and thus further promote corrosion. A schematic representation of initiation and propagation of Crevice corrosion can be found in the figure below:

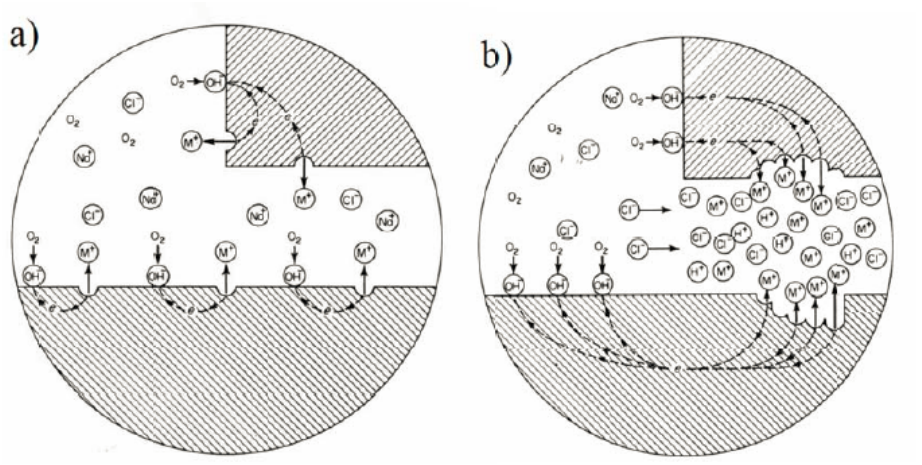

Figure 2.9: a) initiation of crevice corrosion b)Propagation of crevice corrosion. Figure is taken from [20]

An ohmic potential drop inside the crevice will develop in the crevice due to the formation of corrosion products and evolution of hydrogen gas bubbles. Both hydrogen gas and the various corrosion products will not appear uniformly along the crevice and thus the potential distribution will also be non uniform. This nonuniform distribution of potential will also yield a nonuniform current distribution inside the crevice. The distribution inside the crevice will resemble the polarization curve of the metal and its influence on corrosion is illustrated in the figure below.

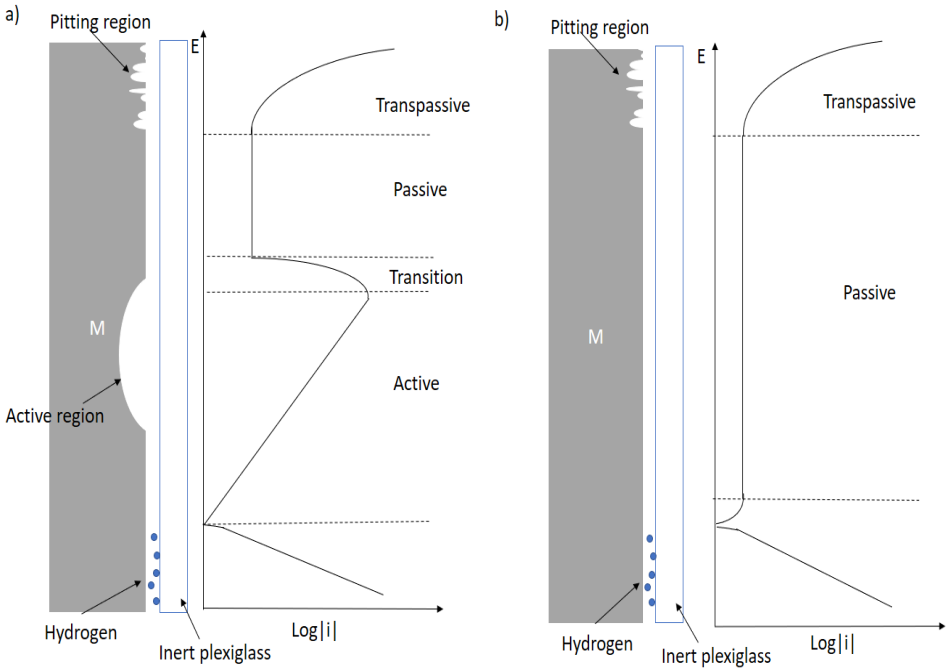

(a) Schematic representation of the relationship between corrosion morphology and polarization curve of an active metal.

(b) Schematic representation of the relationship between corrosion morphology and polarization curve of an active metal.

Figure 2.10: Adapted from Betts [21]

As shown in the figure 2.10 the metals which have active passive kinetics, corrosion can be found deep inside the crevice in the area which is corresponding to the active region on the polarization curve. Hydrogen evolution can also be found deep inside the crevice if the ohmic potential drop is large enough[3]. At the mouth of the crevice it can be found pitting of the metal possess transpassive kinetics.

Metals that have passive kinetics will in general be resistant to crevice corrosion due the oxide layer. It will however experience pitting corrosion near the mouth of the crevice as can be seen in the figure.

2.3.1 Effect of cathodic protection on crevice corrosion

Introducing cathodic protection to a crevice will change the chemistry inside the cavity. The inside will now experience a high rate of reduction reactions due to the polarization from the anode. This will in turn cause the environment inside the crevice to become alkaline due to the formation of OH^- from the increased reduction rates.

The effect of cathodic protection on crevice corrosion were investigated by Li et Al [22]. A mild steel with a simulated disbonded coating were put under cathodic protection in

a dilute NaCl solution. It was reported that the pH inside the crevice increased and the environment turned alkaline. This was as expected due to formation of hydroxyl ions. There were also reported an increase in the conductivity inside the crevice as a consequence of cathodic protection. This was found to be due to migration of Na^+ inside the crevice. The current distribution during cathodic protection were also measured as a function depth in the crevice which can be seen in figure 2.11.

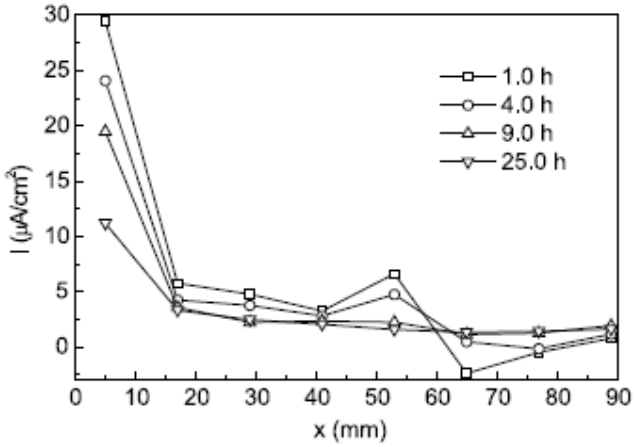

Figure 2.11: Current distribution in crevice at different depths. Thickness of crevice is 1.0 mm, potential at crevice mouth is -1,15 V_{vSCE} and electrolyte is 0.006 M NaCl. Figure is taken from[22]

The anodic current measured at 65 mm into the crevice after 1 hour were interpreted as a sign of corrosion occurring inside the crevice. The current however turned cathodic which is an implication that cathodic protection has the ability to prevent local corrosion inside a crevice.

2.4 Three metal coupling

A three metal coupling will utilize the principle of galvanic corrosion and cathodic protection to protect two different alloys by use of the same sacrificial anode. For a steel and aluminium couple a common AlZnIn anode will provide a potential sufficient to protect both metals. This can be seen in figure 2.12 where the anode has a potential below the recommended protection potential of both aluminium and steel.

Galvanic Series of Metals in Seawater

Metals and Alloys	Corrosion Potential (volts DC ref. Ag/AgCl)
Magnesium and Magnesium Alloys	-1.60 to -1.63
Aluminum - Anode	-1.10
Zinc	-0.98 to -1.03
Aluminum Alloys	-0.76 to -1.00
Mild Steel (clean & shiny)	-0.60 to -0.71
Mild Steel (rusted)	-0.20 to -0.50
Cast Iron (not graphitized)	-0.60 to -0.71

Figure 2.12: Extract of the galvanic series of metals in seawater [23]

The AlZnIn anode is one of the most commonly used anodes in the industry and will keep a stable potential at low current densities[3]. This is due to the fact that the AlZnIn alloy is an active-passive metal which will experience pitting corrosion during operation. This is illustrated in the figure 2.13 where an Evans diagram of cathodic protection in practise is shown. The corrosion of the anode will occur along the pitting line and thus a stable potential is expected in the system

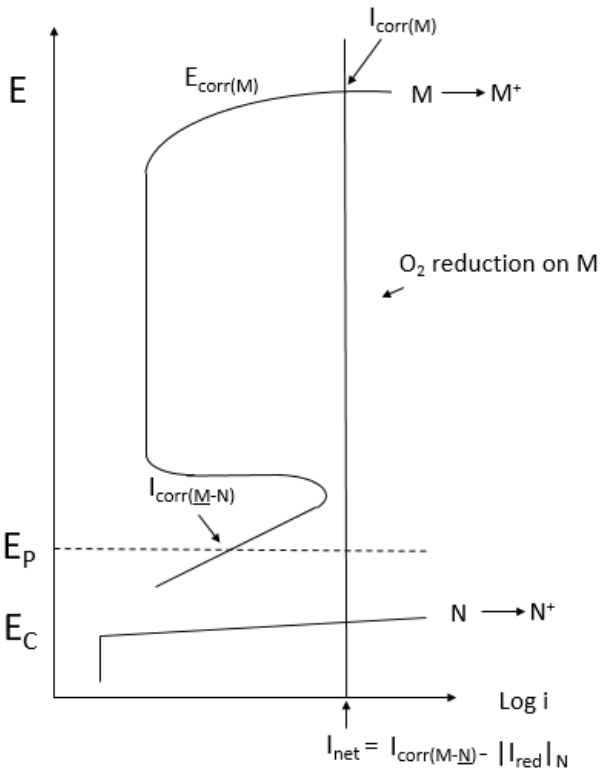

Figure 2.13: Schematic illustration of an evans diagram of cathodic protection with a passive-pitting anode. Illustration is adapted from Nisancioglu [3]

Three metal coupling has been tested by Røstbø[24] and the author[25] as an ongoing project. The work performed by Røstbø were focused on testing of the three metal coupling in both 3.5% NaCl and synthetic seawater. The alloys used were X65 carbon steel, 6005 aluminium and AlZnIn which were the sacrificial anode. The test combined the three metals in different couplings at 25°C in both galvanic corrosion and in crevice corrosion. It was found that both aluminium and steel behaved similar in three metal coupling and two metal coupling with the AlZnIn anode and thus a common anode protection system should be possible[24] without a crevice. The galvanic tests were run for 24 hours and the crevice tests were run for 72 hours. The weight loss measurements showed that steel is completely protected in the three metal coupling and had a big decrease in weight loss compared to open circuit as shown in figure 2.14:

Type	Coupling	NaCl	Seawater
Open circuit	X65	0.92	0.79
Galvanic	X65 CS / 6005 A1	0.18	0.25
	X65 CS / AlZnIn	0.28	0.27
	X65 CS / 6005 A1 / AlZnIn	0	0
	X65 CS / 6005 A1 / AlZnIn (96 h)	-	0.03
Galvanic crevice	X65 CS / 6005 A1	0.02	0.05
	X65 CS / 6005 A1 and AlZnIn	0	0

Figure 2.14: Weight loss measurements for carbon steel in both 3.5% NaCl and synthetic seawater in different metallic couples. Weight loss unit is $\frac{mg}{cm^2 * 24h}$. Figure is taken from[24]

Aluminium also experienced a decrease in weight loss during three metal coupling, there were however not found a decrease for crevice corrosion. This was believed to be because of the alkaline environment inside the crevice which caused a high corrosion rate on aluminium. The weight loss of aluminium can be found in figure 2.15 below:

Type	Coupling	NaCl	Seawater
Open Circuit	6005 Al	0.13	0.16
Galvanic	X65 CS / 6005 Al	0.50	0.18
	6005 Al / AlZnIn	0.11	0.08
	X65 CS / 6005 Al / AlZnIn	0.24	0.11
	X65 CS / 6005 Al / AlZnIn (96 h)	-	0.07
Galvanic crevice	X65 CS / 6005 Al	0.38	0.25
	X65 CS / 6005 Al and AlZnIn	0.39	0.15

Figure 2.15: Weight loss measurements for aluminium in both 3.5% NaCl and synthetic seawater in different metallic couples. Weight loss unit is $\frac{mg}{cm^2 * 24h}$. Figure is taken from[24]

The currents on both the steel and the aluminium were also measured during the experiments. For the galvanic corrosion the current of the steel decayed with time. Both for aluminium and steel a cathodic current were measured. The current measured was in order 1 to 2 magnitudes larger on steel as can be seen in the figure 2.16

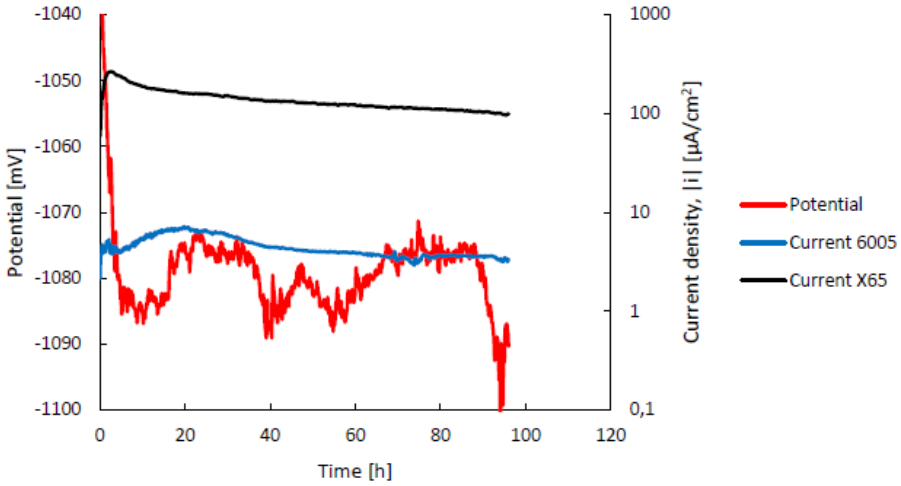

Figure 2.16: Galvanic corrosion test with joint anode system between X65, 6005 and AlZnIn in synthetic seawater. The potential is given against the Ag/AgCl electrode and run for 96 hours. Figure is taken from[24]

During crevice corrosion testing the aluminium experienced an anodic current which indicated high oxidation rates on the surface despite being polarized. As mentioned this caused a higher weight loss and was attributed to an alkaline environment inside the crevice which destabilized the oxide. This was further investigated by use of an electron microscope and clear signs of cathodic corrosion were found with alkaline etching exposing particles as shown in the figure 2.17.

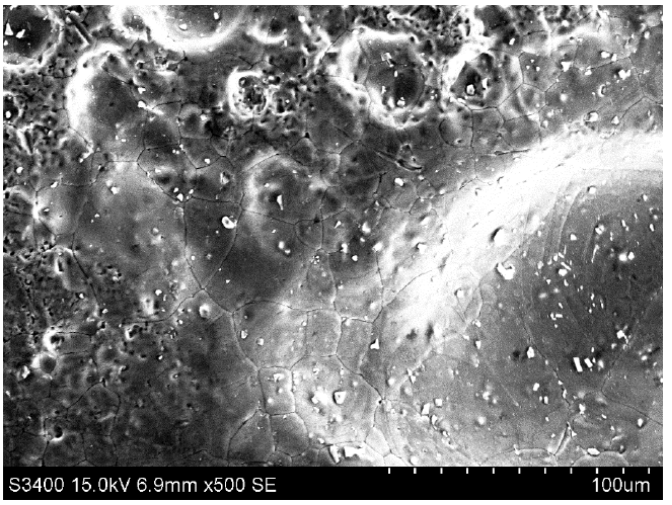

Figure 2.17: SEM image of 6005 aluminium from galvanic crevice corrosion testing with cathodic protection. Image is taken near crevice mouth and post chemical cleaning. Figure is taken from [24]

In the authors specialization project the work were continued, but the focus were shifted to only testing with synthetic seawater and a large focus were put on parallel testing. The galvanic corrosion tests showed moderate weight loss for both steel and aluminium as shown in figure 2.18.

Parallel	X65	6005	AlZnIn
1(24h)	0.24	0.18	2.39
2(24h)	0.21	0	2.68
3(24h)	0.16	0.05	2.13
4(24h)	0.16	0.29	3.53
Average	0.20 ± 0.04	0.15 ± 0.15	2.8 ± 0.7

Figure 2.18: Weight loss measurements for galvanic corrosion testing on seawater. Temperature is 25°C and the weight loss unit is $\frac{mg}{cm^2 * 24h}$. Figure is taken from[25]

The crevice corrosion test were performed for both 72 and 96 hours and also found complete protection of the steel.The weight loss on aluminium were found the be decreasing with increasing test duration. This could indicate a stabilization of the crevice. The weight loss for crevice corrosion can be found in figure 2.19.

Parallel	X65	6005	AlZnIn
1(72h)	0.01	0.12	0.90
2(72h)	0	0.11	0.40
3(96h)	0	0.08	0.27

Figure 2.19: Weight loss measurements for galvanic crevice corrosion testing in seawater. Temperature is 25°C and the weight loss unit is $\frac{mg}{cm^2 * 24h}$. Figure is taken from[25]

The electrochemical behaviour for the galvanic corrosion test showed the same behaviour as is shown in figure 2.16 with a decaying current on both metals. For the crevice corrosion testing it was also found that the aluminium experienced an anodic current and suffered from corrosion. It was however found in the 96 hour parallel that this current turned cathodic as shown in figure 2.20. This was an indication that the CP system could protect both metals at the same time. During such a long polarization time there was also found indication of calcareous deposits blocking the crevice.

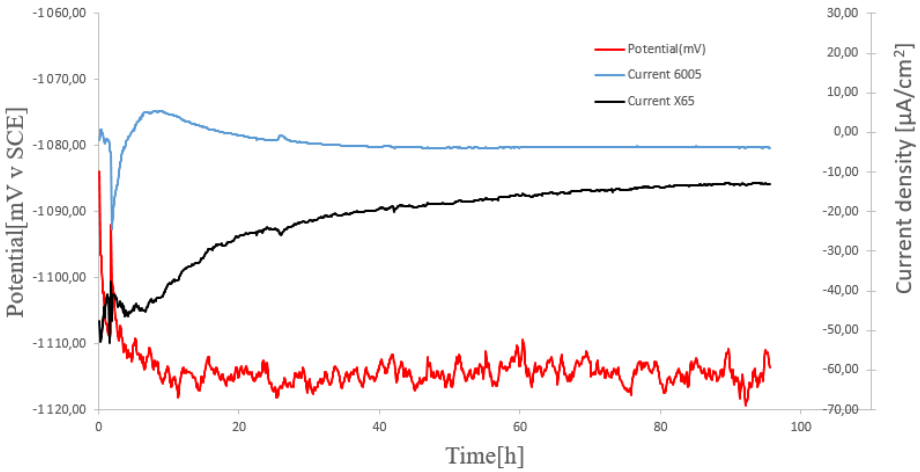

Figure 2.20: Crevice corrosion test between 6005 aluminium and X65 steel with cathodic protection. Crevice size is 100μm and run time is 96 hours at 25 °C. Potential is measured with a saturated calomel electrode. The pH measured after conducted experiment was 9. Figure is taken from [25]

Chapter 3

Experimental

The experimental work in this project follows the methods described in Røstbø's master thesis[24], which were also performed in the authors specialization project[25]. The same lab equipment was used with the same material and electrolyte specifications. The cleaning methods and how the samples was prepared in this report was inspired by the project work of Bergin[26], which worked this out of the ASTM G1 standard[27]. The specifications for the electrolyte was found in the ASTM D1141 standard[28]

3.1 Test Samples

Materials

The materials used was as earlier shown 3 different alloys. The steel came from an oil pipe made of X65 carbon steel which was cut into sample specimens. The aluminium came from a large extruder plate which was an 6005 alloy. Sacrificial anode of AlZnIn was cut from cylindrical anodes. All of the materials were available at NTNU and came from earlier projects. The chemical compositions of the alloys are given in the tables below:

Table 3.1: Composition of X65 Carbon steel [26]

Element[Weight%]								
C	Si	Mn	P	S	V	Nb	Ti	Fe
0.16	0.45	1.65	0.02	0.01	0.09	0.05	0.06	Matrix

Sample preparation

The mechanical preparation of the samples were performed by NTNU's technical laboratory of materials. The steel specimens were milled before the edges were grinded. Both

Table 3.2: Composition of 6005 aluminium [24]

Element[Weight%]						
Mg	Si	Fe	Mn	Cr	Cu	Al
0.51	0.59	0.41	0.14	0.02	0.18	Matrix

Table 3.3: Composition of AlZnIn sacrificial Anode [29]

Element[Weight%]							
Zn	In	Cd	Si	Fe	Cu	Pb	Al
2.65	0.026	0.00021	0.049	0.076	0.00044	0.00007	Matrix

the 6005 and the AlZnIn were first grinded and then polished. The samples had to be cleaned,dried and weighed before they could be connected to the circuitry. The cleaning cycle before weighing were distilled water, acetone and then finalized with ethanol(96%).This was done in quick succession to avoid evaporation of the acetone which can leave impurities on the surface[30]. The samples were dried using an electrical heat gun. To measure the sample weight a standard analytical weight with an error margin of $\pm$ 0.1 mg was used. A test sample with known weight was used for calibration and the samples were corrected accordingly to the found deviation.

3.1.1 Anode connection and coating

A screw hole with a diameter of 3mm were made at the top of the sample to give a connection point for the circuitry. Connection were made by cutting of the top of a banana plug and exposing the copper wire. Half of the wire were removed and then connected to the sample with a screw and washer. Electrical tape were used on the stray wire to keep it in place and ready for coating. This procedure is shown in the figure 3.1 below:

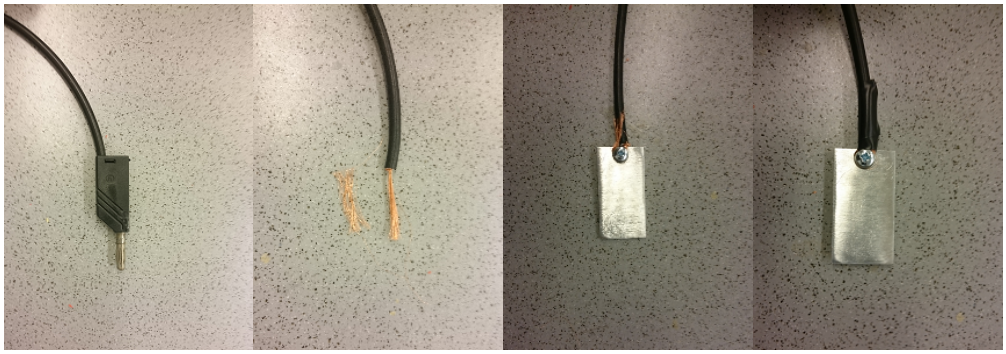

(a) Banana plug **(b)** Cut Banana plug **(c)** Connection with screw and washer **(d)** Electrical tape applied

Figure 3.1

To control the area that were to be exposed the samples were coated with beewax. Masking tape were put on one of the sides of the sample, leaving the exposed area to be 20*19mm(width of sample x width of masking tape). The anode was dipped twice into the beewax and then left to dry. Removing of the tape was done by cutting slightly outside the tape before carefully removing the wax. Appliance of beewax is shown figure3.2 below:

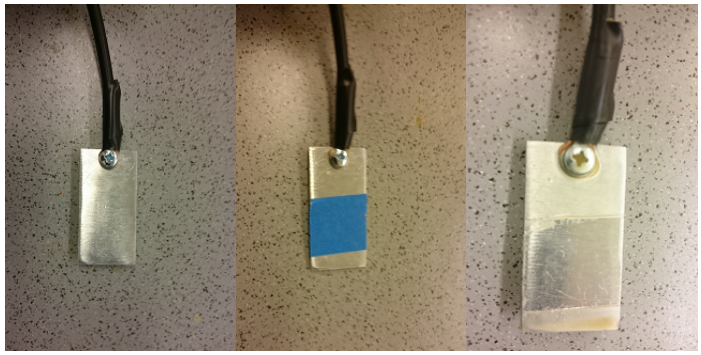

(a) Connected AlZnIn Sample

(b) Maskin tape covering 20 x 19 mm prior to coating

(c) Sample with beewax cut off

Figure 3.2

3.1.2 Galvanic crevice corrosion

Galvanic corrosion testing were performed with the device illustrated in figure3.3.

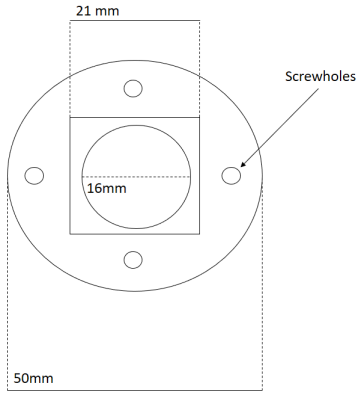

Figure 3.3: Schematic illustration of the crevice device used to simulate galvanic crevice corrosion

The X65 and 6005 samples were cut into dimensions of 20*20*2mm to fit into the device.

To simulate a crevice of 100μm two teflon strips with dimensions 3*20*0.1mm were placed on the edge of the samples. In the back of the samples, screw holes with a depth of 1.8mm were made to create a connection point. Custom screws from the NTNU's technical laboratory of materials was then connected with a cable shoe which had been attached to the wire. After connection the inside of the device were coated with blank nail polish for the 6005 and Miccro Super XP 2000 Stop-Off Lacquer for the steel. The samples were pushed down into the coatings. On the outside both surfaces were coated with 1 layer of nail polish and 2 layers of lacquer, since the circuitry had to be submerged to get the whole device into the electrolyte. Full assembly of the device is shown in the figure3.4:

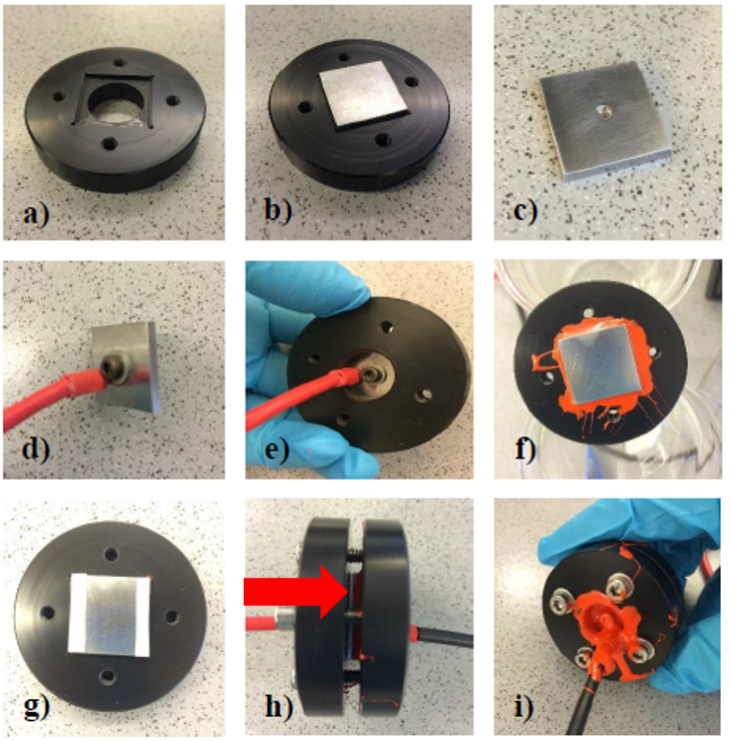

Figure 3.4: Crevice corrosion device with coupling. Figure is taken from[24] a)Sample holder b)Placement of sample c)Backside of sample with screwhole d)Sample connected to wires with cable shoe e)Backside of device with sample connected f)Steel sample in holder with coating g)Teflon strips placement h)Complete device with coupling. The red arrow indicates where the 100μm is i) Coating of the electrical connections

3.2 Electrolyte

The electrolyte used for the testing were artificial seawater. The artificial seawater were made in accordance to the ASTM standard [28] with the exception of KBr which was left out due to HSE reasons. The standard recommends that different stock solutions should be made before being mixed together, but based on earlier experience [24], [26], the decision was made to mix all components together in one big stock. Before use, the pH was adjusted to 8.2$\pm$ 0.1 with 0.1M NaOH as the standard suggests. Full composition is given in table 3.4. The solution were made in stocks of 5L.

Table 3.4: Concentration of different compounds in artificial seawater[28]

Compound	Amount[g/L]
$MgCl_2 \cdot 6\,H_2O$	11.112
$CaCl_2$(anhydrous)	1.158
$SrCl_2 \cdot 6\,H_2O$	0.042
KCl	0.695
$NaHCO_3$	0.201
H_3BO_3	0.027
NaF	0.003
NaCl	24.534
Na_2SO_4	4.094

3.3 Lab equipment

A glass beaker filled with 900 mL of electrolyte was used as the electrochemical cell. All experiments ran over several days and thus distilled water was added to compensate for water evaporation. For reference electrode a saturated calomel electrode(SCE) was used which has a potential of + 0.24V v SHE. A salt bridge made with agar and saturated KCl was used to make ionic contact and close the circuit. Test were performed with both two-metal and three-metal coupling and an illustration of the coupling is shown in figure 3.5:

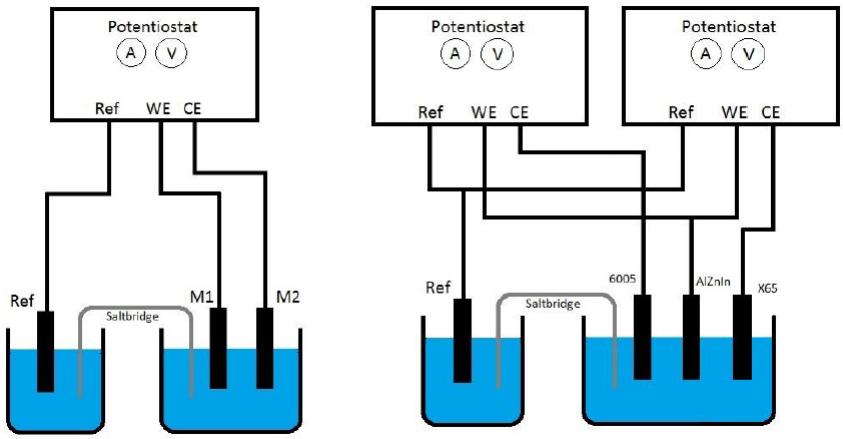

Figure 3.5: Schematic illustration of the experimental setup used in galvanic crevice corrosion testing. The two-metal circuit is shown to the left, and three-metal coupling to the right. The illustration is taken from [24]

In both coupling configurations a gamry potentiostat was used with a zero resistance ammeter configuration. As can be seen in the figure the three metal coupling demanded a use of two potentiostats at the same time with the anode as working electrode. Thus the currents measured had to be multiplied by a factor of -1 to be in standard convention. Since the potentiostats measures the current on the working electrode.

The whole cell was submerged into a water bath which held a constant temperature at 25°C or 10°C during the experiments. The duration at both temperatures was 72,96 or 120 hours. A picture of the complete setup on the lab is shown in figure 3.6.

Figure 3.6: Picture of the setup on the lab. The cell is submerged in an water bath holding 25°C. The reference electrode is connected through a salt bridge. One of the potentiostats are pictured with a plot of the ongoing recordings

3.4 Sample cleaning and weighing

Before weight loss measurements were performed the coating had to be removed and the surfaces had to cleaned for corrosion products. Nail polish could be removed with acetone and the miccro lacquer was possible to peel off. The beewax were scraped of carefully with a plastic ruler before being boiled off for 50 seconds in distilled water. Removal of the corrosion products was performed with a cleaning procedure created out of ASTM G1 [27] and is shown in table 3.5 .

Table 3.5: Cleaning method for the different alloys after testing [27]

Alloy	Chemicals	Time	Temperature
X65	500mL HCl(SG.1.16) 3.5g Hexamethylenetetramine Distilled water to make 1000mL	30s x 6	25°C
6005 Al AlZnIn	50mL phosphoric acid(SG1.69) 20g Chromium (VI) oxide Distilled water to make 1000mL	10 min	90°C to boiling

The aluminium will not be attacked by the chromium phosphoric acid[24] and thus only one cleaning cycle is necessary. The steel will lose mass when immersed in the cleaning solution and thus 6 cleaning cycles were performed a with weight measurements between each cycle. All measurements were corrected for with a reference sample that had a know weight. For the steel the different cycles were plotted against the weight loss and found in point B in figure 6.1 which is found in the appendix.

3.5 Surface Characterization

The samples were visually inspected before and after testing. Photographs were taken with a Sony Xperia X phone. The samples were further studied with an SEM. Some parallels were run to study the formation of calcareous deposits of both the 6005 aluminium and the X65 carbon steel. The electron microscope used was an FESEM Seiss Ultra 55, Limited edition.

Chapter 4

Results

4.1 Electrochemical behaviour

4.1.1 Galvanic crevice corrosion for 72 hours with cathodic protection

Results at 25°C

In figure 4.1 parallel 1 and 2 for aluminium show an initial anodic peak before they start to decay. Parallel 1 starts decaying after 4 hours at 10 μA/cm^2 and decays steadily down to 1 μA/cm^2. Parallel 2 start decaying after 12 hours and has a anodic peak of 15 μA/cm^2, before decaying to 2 μA/cm^2. A logarithmic plot of parallel 1 and 2 found in the appendix presented in figure 6.2, which show that both are still decaying when the experiment is stopped. Parallel 3 deviates from the two other with a cathodic current during the entire experiment. The current moves in the anodic direction initially before steadily stabilizing at - 8 μA/cm^2.

The currents on X65 show similar behaviour with a cathodic current for the entire test period. The parallels start at different levels, but all steadily decay. Initially the decay is sharp and almost exponential before becoming linear after 30 hours. At the end of the experiments the currents are at - 23 $\pm$ 2 μA/cm^2

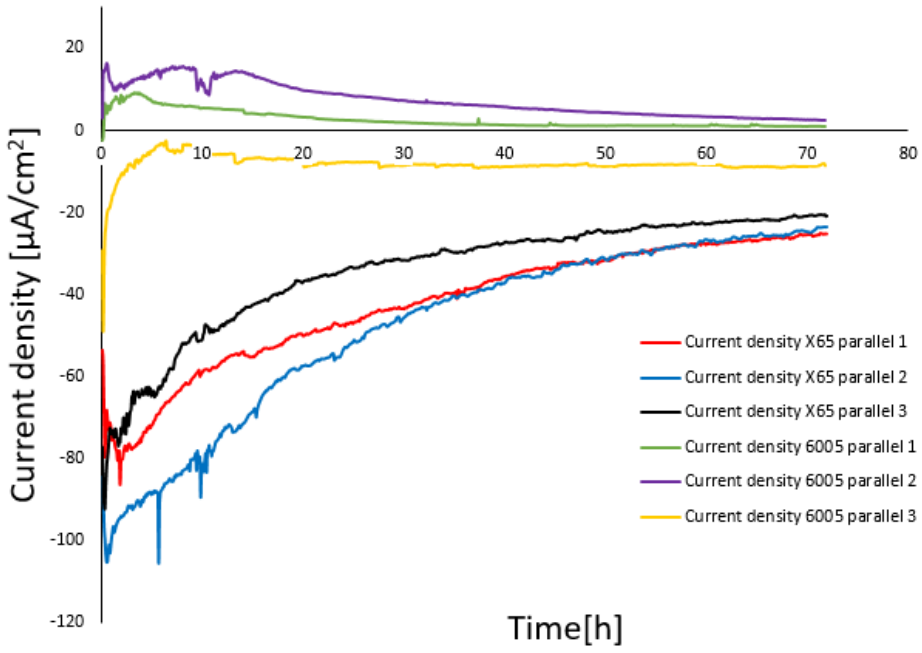

Figure 4.1: Plot of current as a function of time during galvanic crevice corrosion testing with X65, 6005 and AlZnIn as anode in synthetic seawater at 25°C. Parallel 1 and 2 is from previous work[25]

The potentials in figure 4.2 show similar behaviour with a stable potential during the entire experiment. The potential are held at - 1113 $\pm$ 5 mV vs SCE between the parallels.

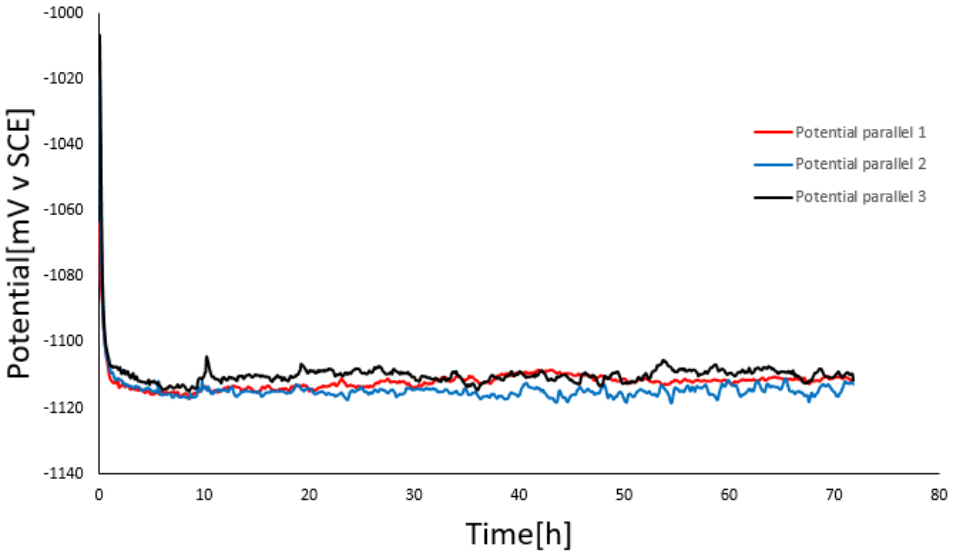

Figure 4.2: Potentials from galvanic crevice corrosion test with X65, 6005 and AlZnIn as anode in synthetic seawater at 25°C. Parallel 1 and 2 is from previous work[25]

Results at 10°C

In figure 4.3 the 6005 experience an anodic current during the entire test period. The current rises to 10 μA/cm^2 in the beginning before it starts to decay after 25 hours. A logarithmic plot of the current found in the appendix in figure 6.3 show a steady decay that starts at 40 hours and ends at 4 μA/cm^2 when the experiment is ended'

The X65 experience a cathodic current during the entire experiment. There is a cathodic peak of - 60 μA/cm^2 after 5 hours before the current decays in a linear fashion until the experiment is stopped. When the experiment is stopped the current is at - 32 μA/cm^2.

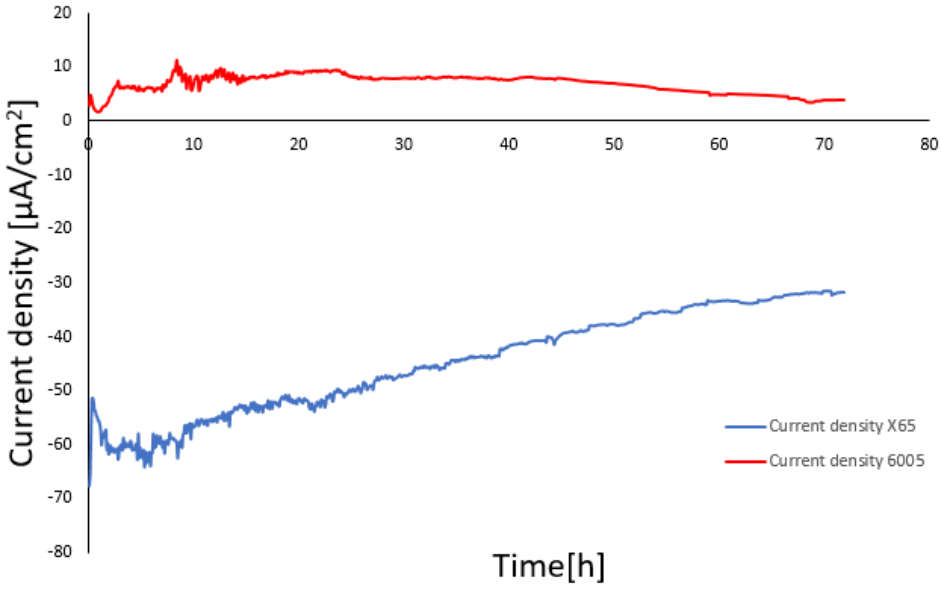

Figure 4.3: Plot of current as a function of time during galvanic crevice corrosion testing with X65, 6005 and AlZnIn as anode in synthetic seawater at 10°C

The potential in figure 4.4 drops in the initial hours before reaching a very stable potential of - 1122 mV vs SCE.

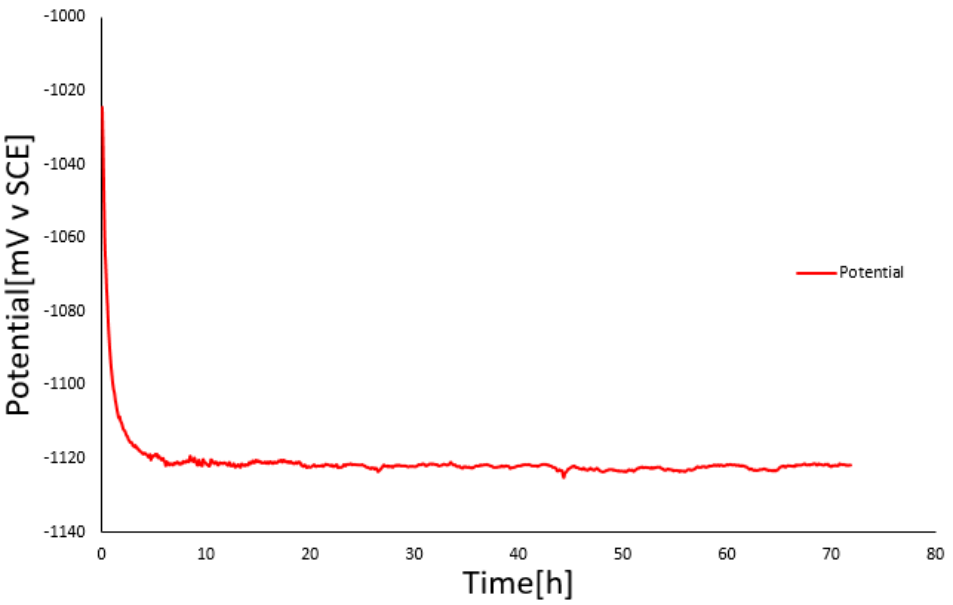

Figure 4.4: Potentials from galvanic crevice corrosion test with X65, 6005 and AlZnIn as anode in synthetic seawater at 10°C.

4.1.2 Galvanic crevice corrosion for 96 hours with cathodic protection

Results at 25°C

In figure 4.5 the 6005 experience an anodic peak in parallel 1 before decaying and stabilizing in the cathodic area. The current is stable at approximately - 4 μA/cm^2 after 40 hours until the end of the experiment. Parallel 2 show an initial anodic peak of 14 μA/cm^2 before decaying steadily to 1 μA/cm^2 at the end of the experiment. A logarithmic plot of the 2nd parallel in the appendix in figure 6.4 show that the current is still decaying when the experiment is stopped at 96 hours.

The steel parallels show same behaviour, but have different size on the cathodic currents. Parallel 1 starts at - 40 μA/cm^2 at ends at -8 μA/cm^2, while parallel 2 has a current of -80 μA/cm^2 initially, and ends at -25 μA/cm^2. Both have a sharp decay in the first 40 hours, which then becomes linear.

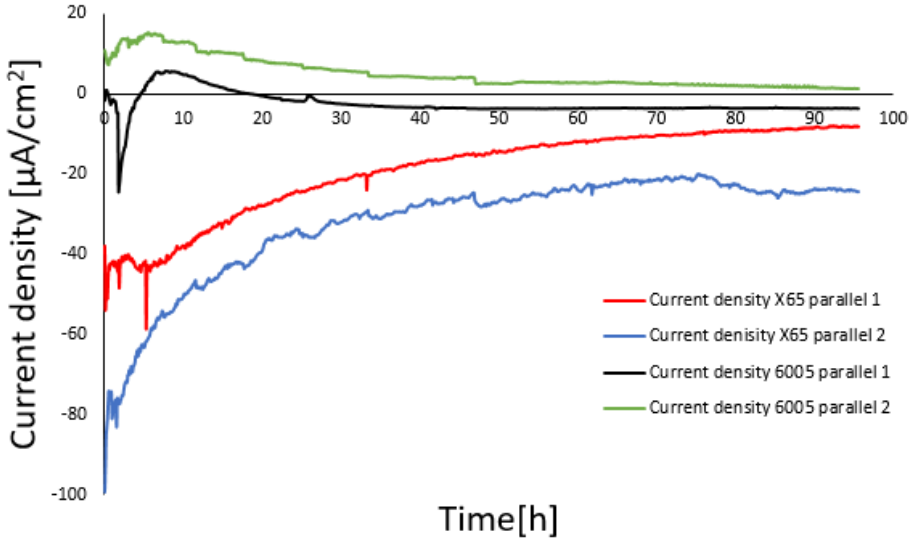

Figure 4.5: Plot of current as a function of time during galvanic crevice corrosion testing with X65, 6005 and AlZnIn as anode in synthetic seawater at 25°C. Parallel 1 is from previous work[25]

In figure 4.6 both parallels keep a stable potential between -1110 and 1120 mV vs SCE with parallel 2 being slightly more active.

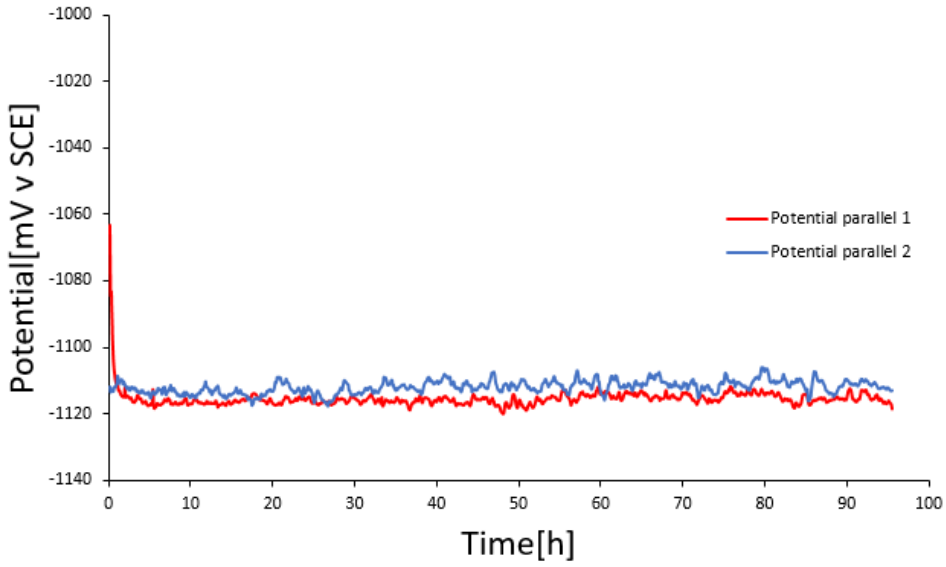

Figure 4.6: Potentials from galvanic crevice corrosion test with X65, 6005 and AlZnIn as anode in synthetic seawater at 25°C.Parallel 1 is from previous work[25]

Results at 10°C

The current on aluminium in figure 4.7 reaches an anodic peak of 20 μA/cm^2 after 15 hours before the current starts to decay down to 4 μA/cm^2 at 96hours . Logarithmic plot of the current after 20 hours can be found in the appendix in figure 6.5 and show that the current is still decaying when the experiment is ended.

The current on X65 is active in the cathodic region during the first 20 hours before it starts to decay. The decay almost linear after 20 hours and ends at -15 μA/cm^2.

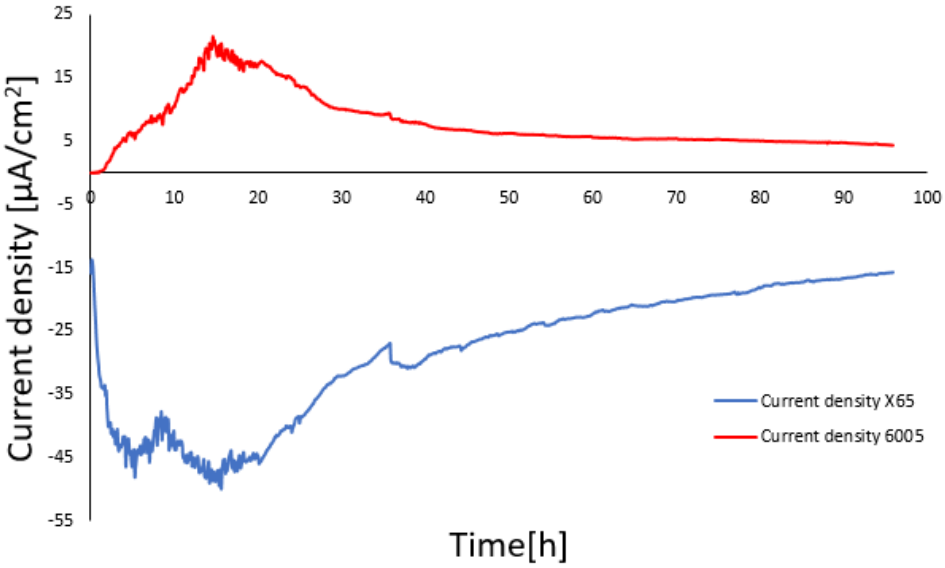

Figure 4.7: Plot of current as a function of time during galvanic crevice corrosion testing in synthetic seawater with X65, 6005 and AlZnIn as anode in synthetic seawater at 10°C.

The potential shown in figure 4.8 is stable at - 1122 mV vs SCE after an initial drop. The potential is very stable during the entire duration of the experiement.

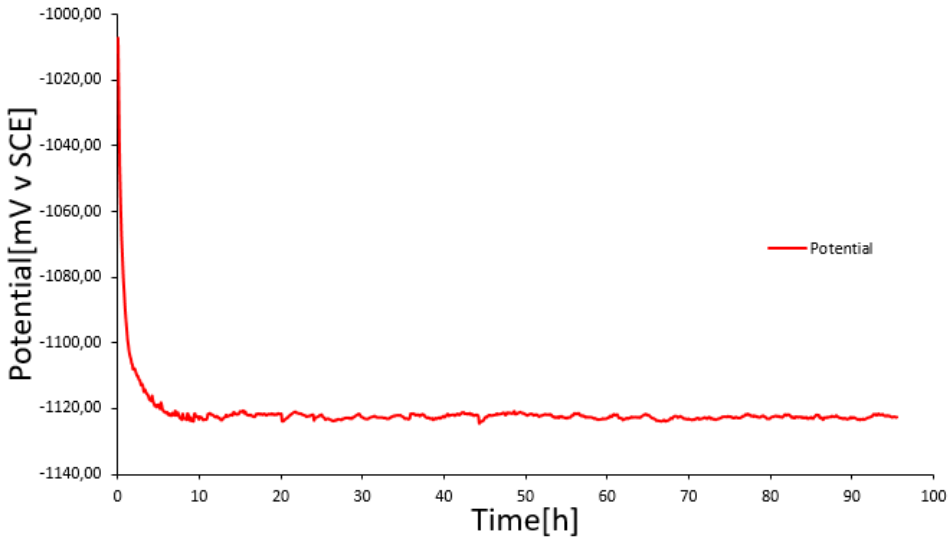

Figure 4.8: Potentials from galvanic crevice corrosion test with X65, 6005 and AlZnIn as anode in synthetic seawater at 10°C.

4.1.3 Galvanic crevice corrosion for 120 hours with cathodic protection

Results at 25°C

In figure 4.9 the current on aluminum show an initial anodic peak of 15 μA/cm^2 at 2 hours and starts to decay afterwards. The current reaches the cathodic region after 60 hours and stabilize at - 1 μA/cm^2.

The steel experience similar behaviour as before with a sharp decay until 40 hours and then a stable and linear decay. At the end of the experiment the current reaches - 11 μA/cm^2 and is still decaying.

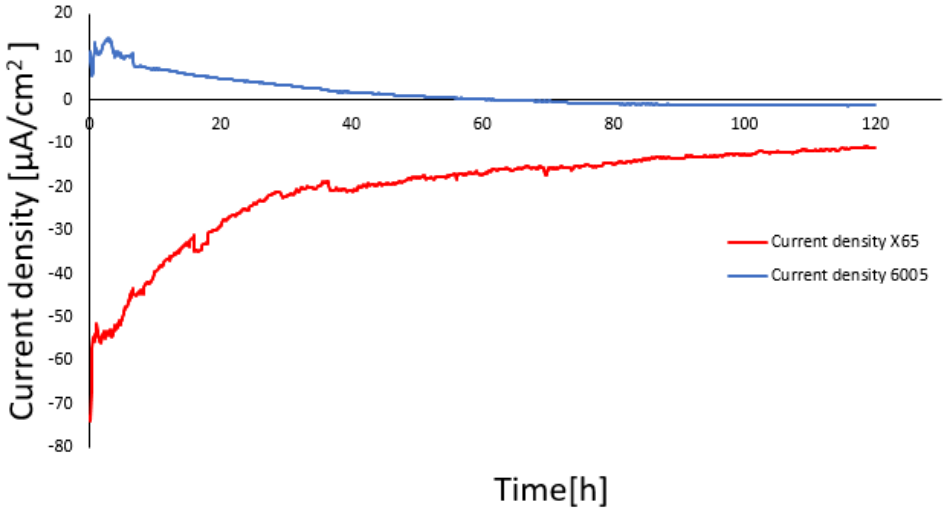

Figure 4.9: Plot of current as a function of time during galvanic crevice corrosion testing with X65, 6005 and AlZnIn as anode in synthetic seawater at 25°C.

The potential found in figure 4.10 is stable and varying between - 1111 and -1116 mV vs SCE.

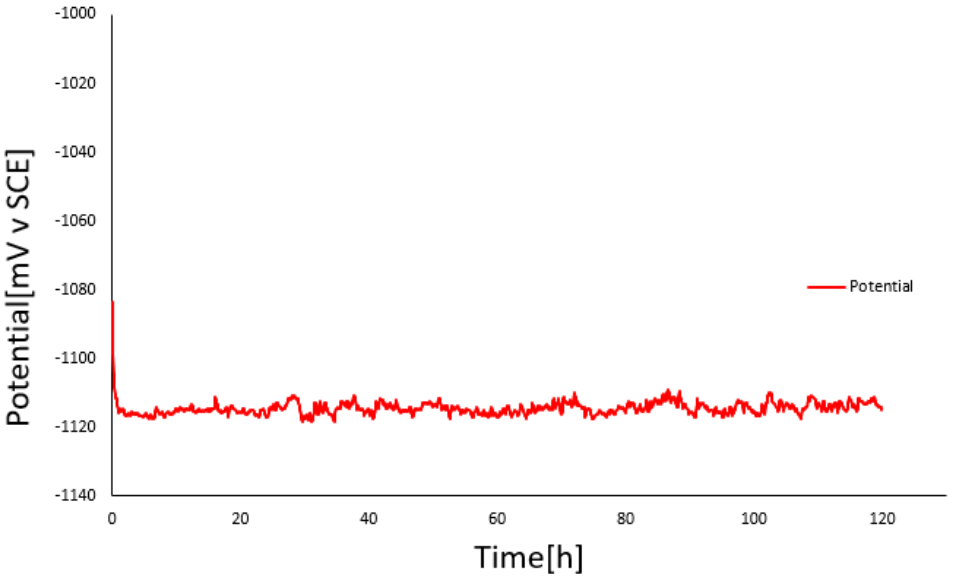

Figure 4.10: Potentials from galvanic crevice corrosion test with X65, 6005 and AlZnIn as anode in synthetic seawater at 25°C.

Results at 10°C

The current on aluminum in figure 4.11 is initially in the anodic region with a peak at 18 hours with a current of 14 μA/cm^2. The current the steadily decays and reaches the cathodic region after 100 hours before stabilizing at - 0.5 μA/cm^2.

The current found on steel is also active in the first 20 hours before it starts to decay. During the experiment it can be seen that the current ”jumps” in the cathodic direction from time to time. This behaviour stops after 90 hours. At the end of the experiment the cathodic current has reached - 30 μA/cm^2 and is still decaying.

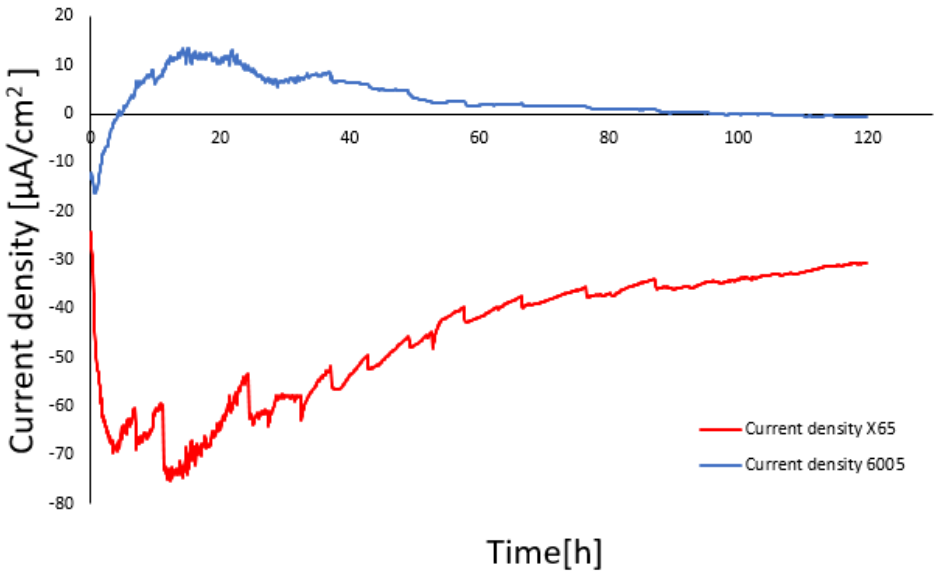

Figure 4.11: Plot of current as a function of time during galvanic crevice corrosion testing in synthetic seawater with X65, 6005 and AlZnIn as anode in synthetic seawater at 10°C.

The potential shown in figure 4.12 is very stable at - 1120 mV vs SCE. Some drops in potential can be seen which seem to be in conjunction with the current ”jumps” found on X65 from figure 4.11

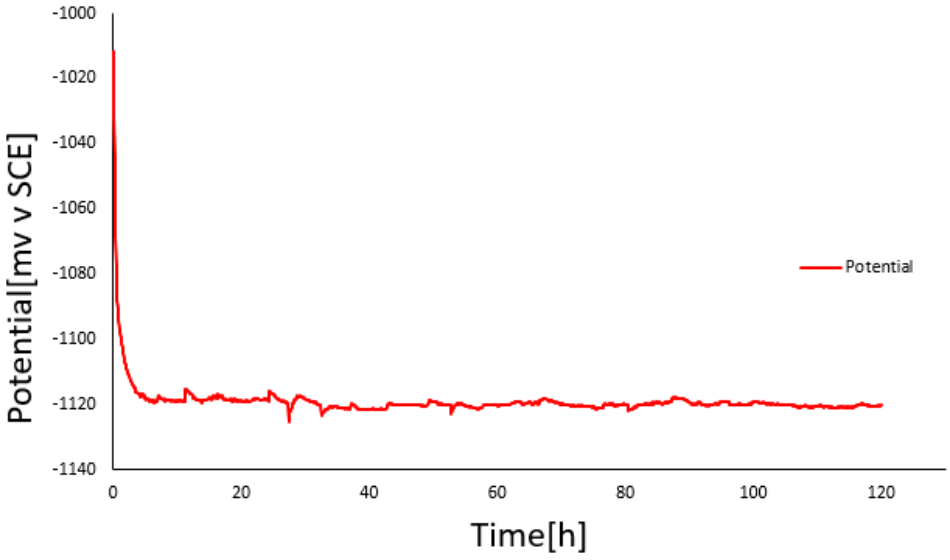

Figure 4.12: Potentials from galvanic crevice corrosion test with X65, 6005 and AlZnIn as anode in synthetic seawater at 10°C.

4.1.4 Galvanic crevice corrosion for 72 hours without cathodic protection

The current of carbon steel in figure 4.13 is in the cathodic region during the entire experiment. The current begins at - 1 μA/cm^2 before moving in the cathodic direction and ending at - 4.5 μA/cm^2.

The potential in figure 4.13 is at - 720 mV vs SCE initially. The potential then starts to decay gradually and ends up at - 830 mV vs SCE.

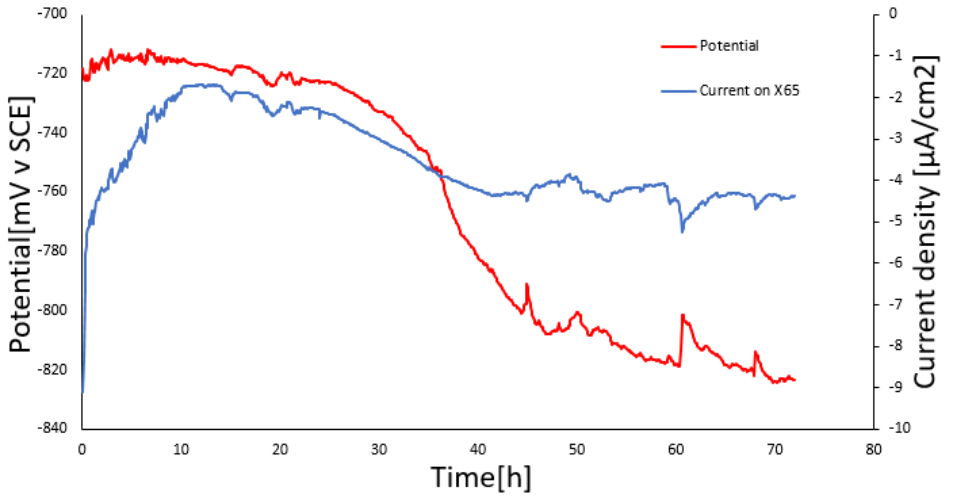

Figure 4.13: Potential and current density from galvanic crevice corrosion test with X65 and 6005 in synthetic seawater at 25°C.

4.2 Surface characterization

4.2.1 Macroscopic surface characterization

Here photographs of the surfaces from the experiments will be presented for the X65 and 6005. The morphology of the anode was the same for every experiment and thus not be presented. Pictures of the steel after chemical cleaning will neither be presented since there is no difference observable between the parallels and thus not of interest.

Surfaces from galvanic crevice corrosion at 25°C before chemical cleaning

In figure 4.14 a) and b) photographs of the metal surfaces from parallel 3 in figure 4.1 before chemical cleaning is presented. Both surfaces are covered with a calcareous layer. On the aluminium it can be seen that the layer is denser close to the edges. Deposits can also be observed on the outside of the teflon strips.

In c) and d) photographs of the metal surfaces from parallel 2 in figure 4.5 before chemical cleaning is presented. Both surfaces are covered with a calcareous layer. On the aluminium the calcareous layer is found to be thicker closer to the edge. Calcareous layer is also found on the outside of the teflon strip placement.

In e) and f) photographs of the metal surfaces from figure 4.9 before chemical cleaning is presented. Both surfaces are covered with calcareous deposits. The aluminium sample show a well developed layer close to the edges in the form of white strips. The picture indicate that the teflon strip did not stay in place during assembly of the crevice device.

(a) X65 72 hours at 25°C

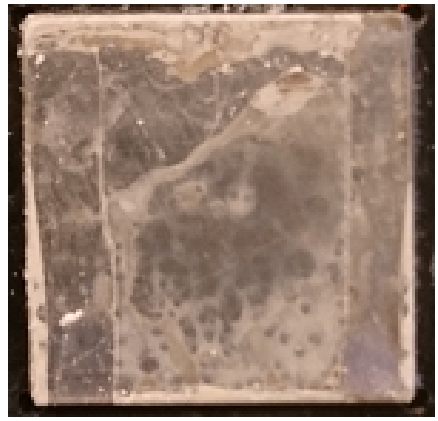

(b) 6005 72 hours at 25°C

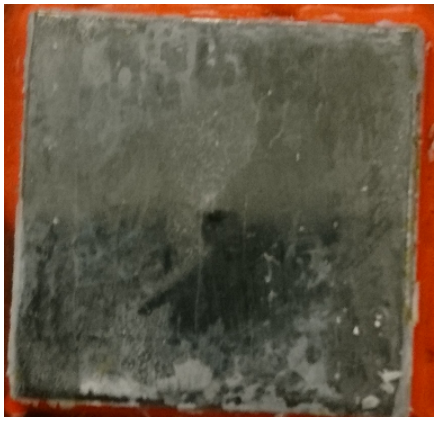

(c) X65 96 hours at 25°C

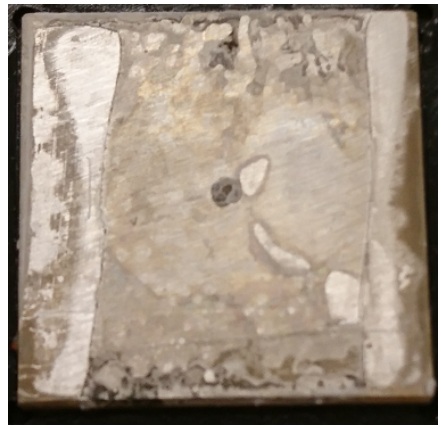

(d) 6005 96 hours at 25°C

(e) X65 120 hours at 25°C

(f) 6005 120 hours at 25°C

Figure 4.14: Images of surfaces from galvanic crevice corrosion tests with cathodic protection at 25°C .Images is taken before chemical cleaning

Aluminium from galvanic crevice corrosion at 25°C after chemical cleaning

Figure 4.15 a) show that the corrosive attack on aluminium is predominantly at the edge of the sample near the crevice mouth. It also seems that a region close to top of the sample was not covered with electrolyte.The sample photographed in b) show that the corrosive attack on aluminium is predominantly at the edge of the sample near the crevice mouth. Also a region placed in the center of the sample show pitting. The sample in c) show that the corrosive attack on aluminium is predominantly at the edge of the sample near the crevice mouth. Pitting in the middle of the sample and along the boundary of the teflon can be observed.

(a) Aluminium for 72 hours at 25°C

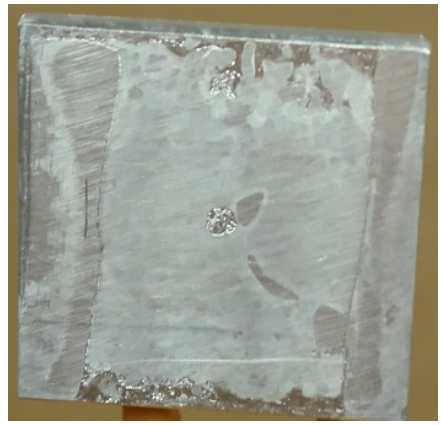

(b) Aluminium for 96 hours at 25°C

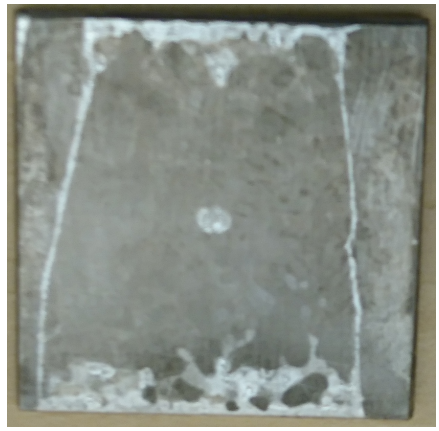

(c) Aluminium for 120 hours at 25°C

Figure 4.15: Photographs of 6005 surfaces after chemical cleaning

Surfaces from galvanic crevice corrosion at 10°C before chemical cleaning

In figure 4.16 photographs a) and b) are of the metal surfaces from figure 4.3 before chemical cleaning. Both surfaces are covered with calcareous deposits. On the aluminum sample the layer is thick on half of the sample as well as the edges near the crevice mouth.

In c) and d) photographs of the metal surfaces from figure 4.7 before chemical cleaning is shown. Both surfaces are covered with calcareous deposits. The layer covers both samples with a thick layer over the entire surface which also is found at the edges.

In e) and f) photographs of the metal surfaces from figure 4.11 before chemical cleaning is presented. Both surfaces are covered with calcareous deposits. The layer covers both samples with a thick layer over the entire surface which also is found at the edges.

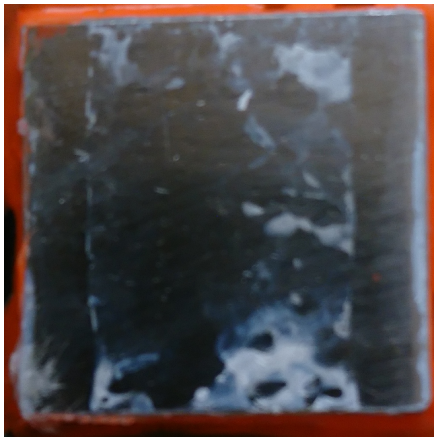

(a) X65 72 hours at 10°C

(b) 6005 72 hours at 10°C

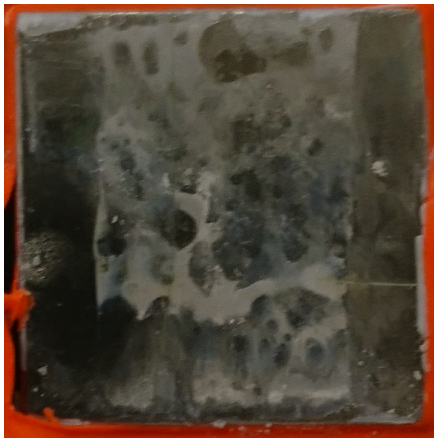

(c) X65 96 hours at 10°C

(d) 6005 96 hours at 10°C

(e) X65 120 hours at 10°C

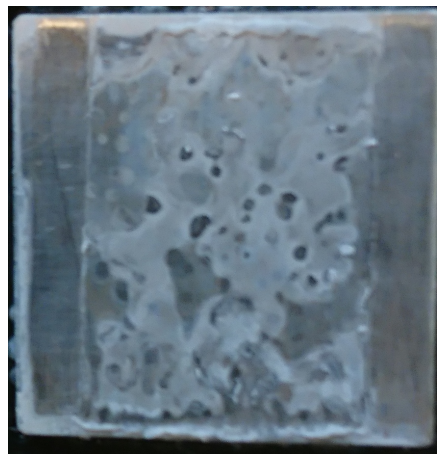

(f) 6005 120 hours at 10°C

Figure 4.16: Images of surfaces from galvanic crevice corrosion tests with cathodic protection at 10°C .Images is taken before chemical cleaning

Aluminium from galvanic crevice corrosion at 10°C before after chemical cleaning

In figure 4.17 all pictures reveal that the corrosive attack is spread out on the surface where the thick calcareous layer is found. A clear sign of pitting corrosion which is not only concentrated at the edge of the sample or in the center.

(a) Aluminium for 72 hours at 10°C

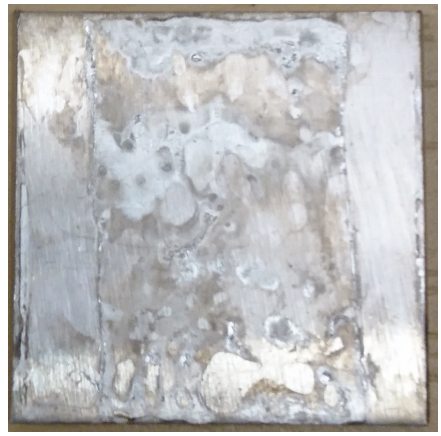

(b) Aluminium for 96 hours at 10°C

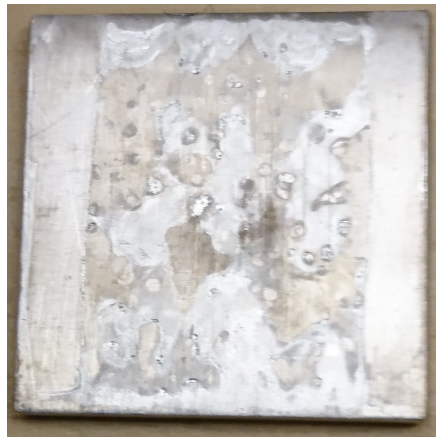

(c) Aluminium for 120 hours at 10°C

Figure 4.17: Photographs of 6005 surfaces after chemical cleaning

Galvanic Crevice corrosion for 72 hours without cathodic protection

From figure 4.18 surfaces from figure 4.13 is presented. It can be seen that both surfaces are covered by a layer which resembles calcareous deposits. The layer does not have the characteristic white colour. Orange products looking like rust can be seen near the edge of both samples and is especially clear on the aluminium.

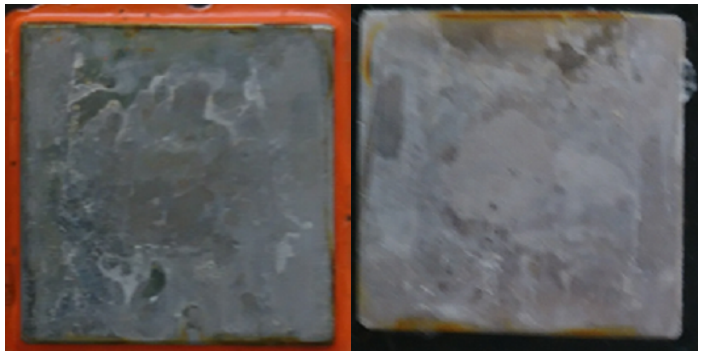

(a) X 65 steel from galvanic crevice corrosion testing without cathodic protection. Image is taken before chemical cleaning

(b) 6005 aluminium from galvanic crevice corrosion testing without cathodic protection.Image is taken before chemical cleaning

Figure 4.18

The figure 4.19 is showing the aluminium after chemical cleaning. The surface morphology is intact. No signs of pitting around the edges. And the black spot in the middle was further analyzed and concluded to be from mechanical damage.

Figure 4.19: Photograph of 6005 surface after chemical cleaning

Calcareous deposit analysis

As seen in figure 4.20 surfaces in a) and b) has as well developed white surface with calcareous deposits. The deposits are thickest at the edges of the samples. Picture in c) show a layer formed on the carbon steel. The layer does not have a characteristic white colour and orange colour can be seen near the edges. In picture d) no white layer can be seen, but a matte finish resembling the oxide layer is seen in the middle of the sample.

Around the edges orange products resembling rust can be observed

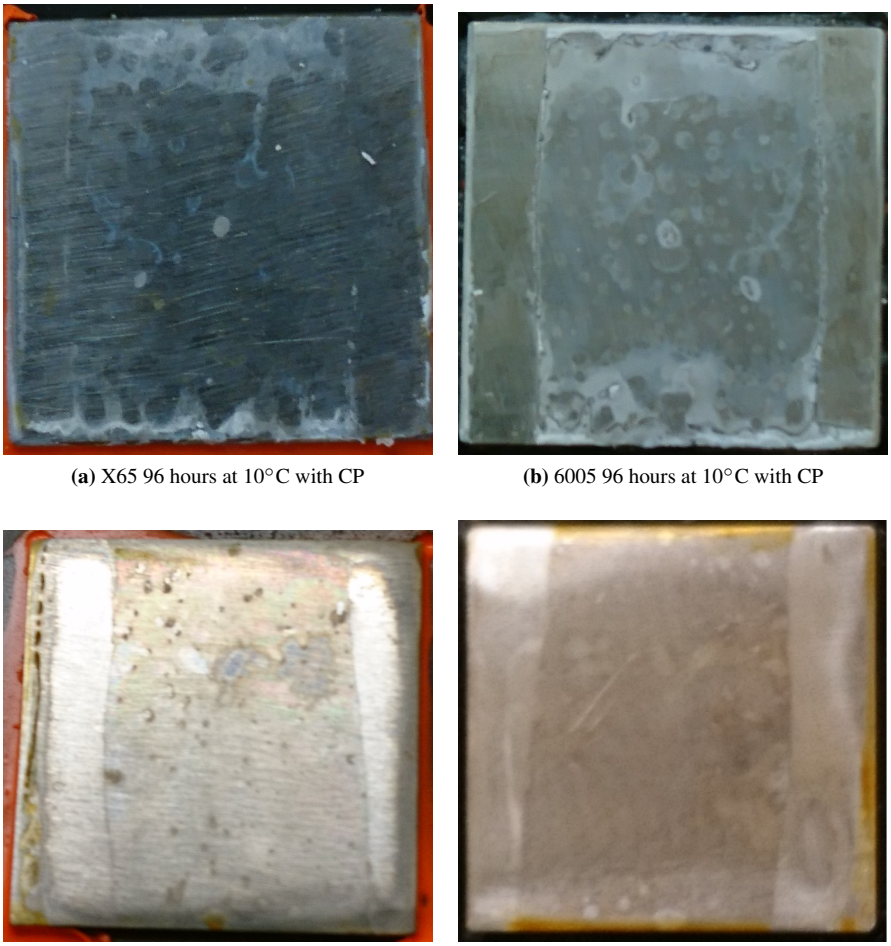

(a) X65 96 hours at 10°C with CP

(b) 6005 96 hours at 10°C with CP

(c) X65 96 hours at 10°C without CP

(d) 6005 96 hours at 10°C without CP

Figure 4.20: Pictures of parallels run for calcareous deposit analysis

4.2.2 Microscopic surface characterization

For reference, a picture of the surfaces prio to testing was taken. The stripes in the metal is due to the grinding and polishing. A complete folder with all SEM pictures taken is found in the attached ZIP file with the thesis.

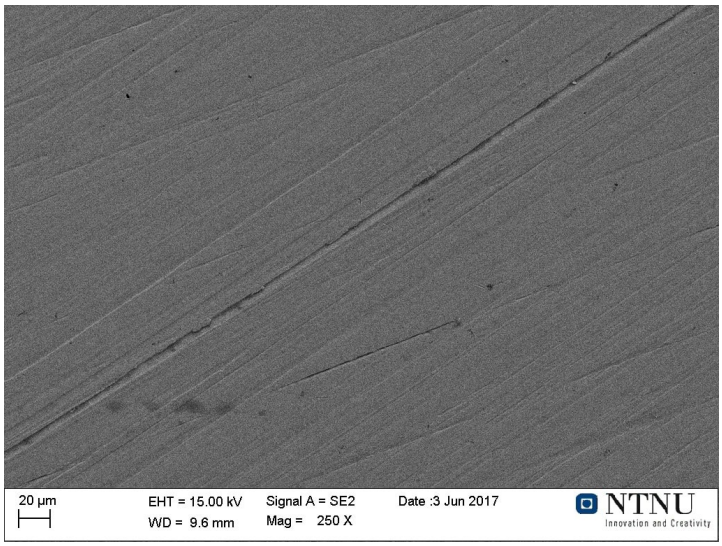

Figure 4.21: SEM Image of X65 carbon steel as received

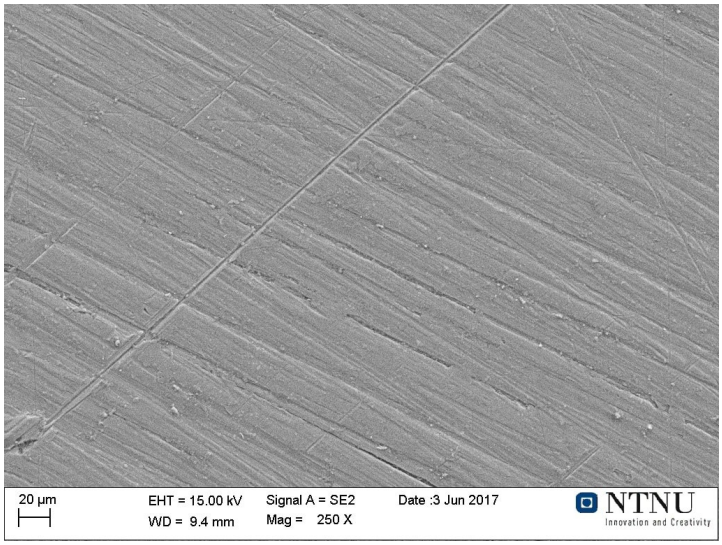

Figure 4.22: SEM Image of 6005 aluminium as received

Galvanic crevice corrosion for 72 hours at 25°C

The SEM micrograph presented in figure 4.23 is of parallel 3 in figure 4.1, which is photographed in a) in figure 4.17. Alkaline etching of the matrix can be observed to the left. A large pit with several intermetallic particles is to the left of the center. In the top left the corrosion attack is in the form of many hemispherical pits. Grain boundaries can also be observed. To the right the matrix is intact, but small pits with particles buried at the bottom can be observed. The same behaviour were found at the bottom of the sample and is shown in the appendix in figure 6.7. The matrix in the middle were found to be intact and without pits. This is shown in figure 6.6 in the appendix.

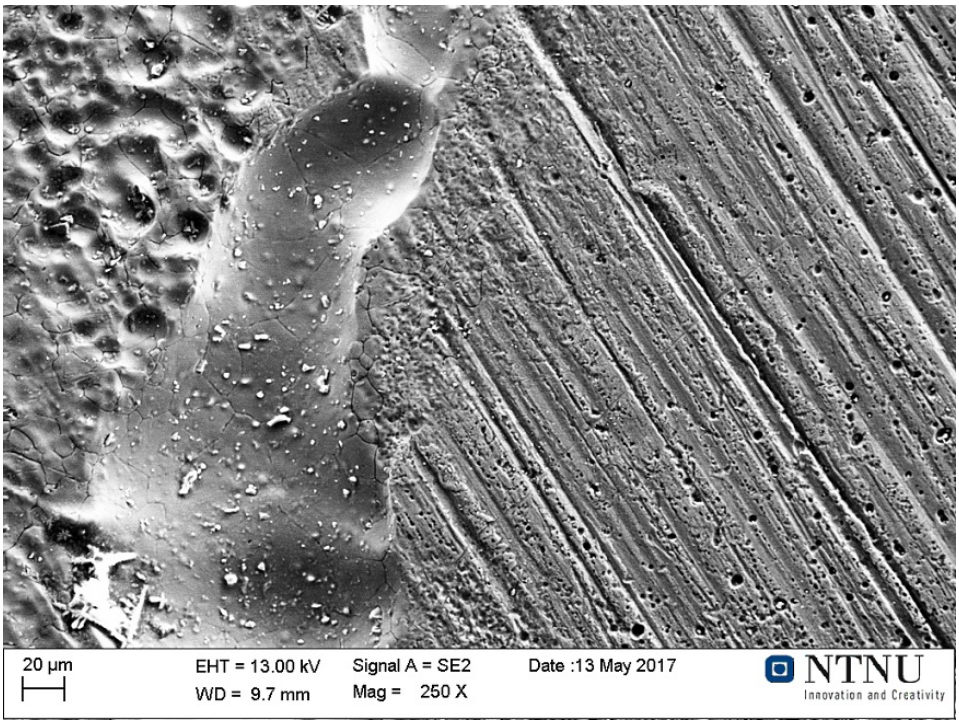

Figure 4.23: SEM Image of 6005 aluminum from galvanic crevice corrosion at 25°C run for 72 hours. Image is taken after chemical cleaning and is taken near the top of the sample

To confirm the intermetallic particles a point analysis with EDS was performed. The result can be found in figure 4.24 and the composition of the two points is given in table 4.1:

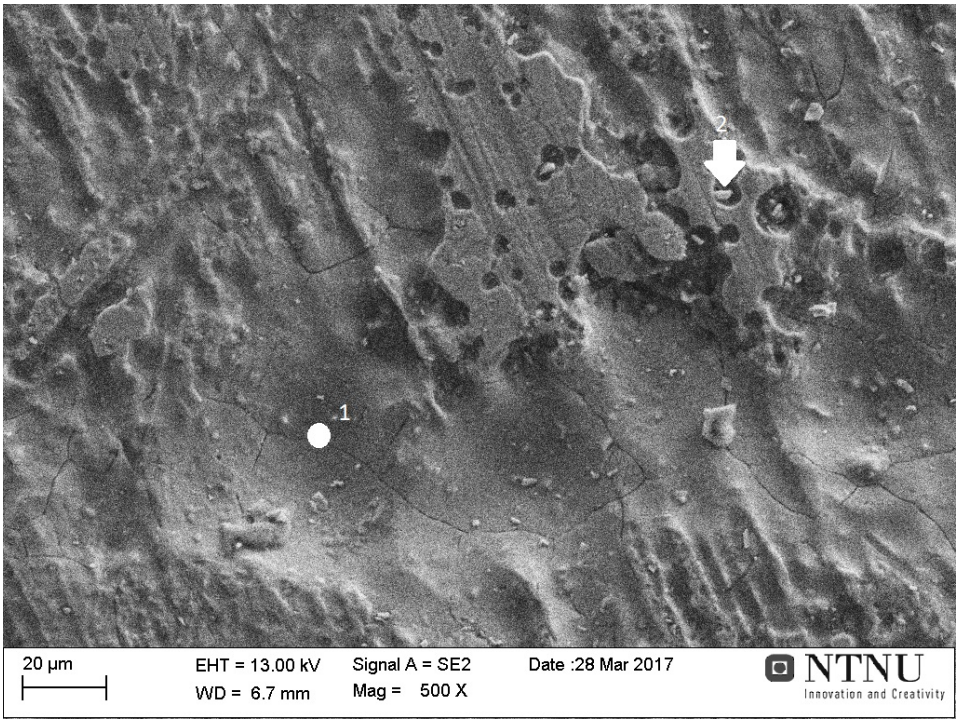

Figure 4.24: SEM Image of 6005 aluminum from galvanic crevice corrosion at 25°C run for 72 hours. Image is taken after chemical cleaning and near the top of the sample. The points were EDS analysis is performed is indicated in white

Table 4.1: EDS analysis of points in figure 4.24

Element	Point 1[wt%]	Point 2[wt%]
Al	52.9	34.7
O	47.1	41.8
Fe	-	18.5
Si	-	5.0
Tot	100	100

Galvanic crevice corrosion for 96 hours at 25°C

The SEM micrograph presented in figure 4.25 is of parallel 2 in figure 4.5, which is photographed in b) in figure 4.15. The figure show pit growth around the intermetallic particles in the middle of the sample. Image of the top of the sample is given in the appendix in figure 6.8 to give a reference on how far away from the edge the alkaline etching occurred. The figure show that the alkaline etching is visible 0.5 mm down into the crevice. Image of the bottom in figure 6.9 show the same behaviour as for previously

presented parallels.

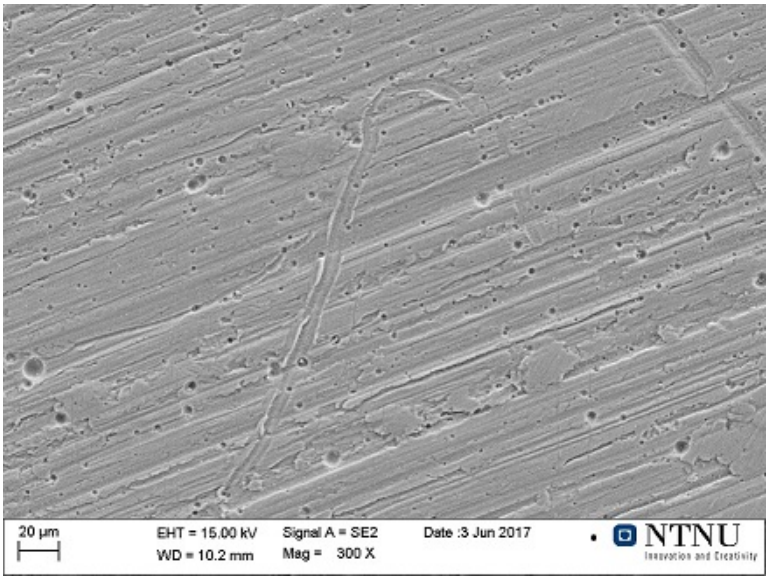

Figure 4.25: SEM Image of 6005 aluminum from galvanic crevice corrosion at 25° run for 96 hours. Image is taken after chemical cleaning and is taken in the middle of the sample

Galvanic crevice corrosion for 120 hours at 25°C

The SEM micrograph presented in figure 4.26 is from figure 4.9, which is photographed in c) in figure 4.15. The image show alkaline etching exposing grain boundaries in the top left of the picture. Hemispherical pits is found in the middle of the picture. Some of these pits has multiple intermetallic particles in them. The same behaviour as the previous parallels is found in the middle of the sample, presented in figure 6.11 in the appendix. The image of the top presented in figure 6.10 show that the alkaline etching occur approximately 0.3 mm into the crevice.

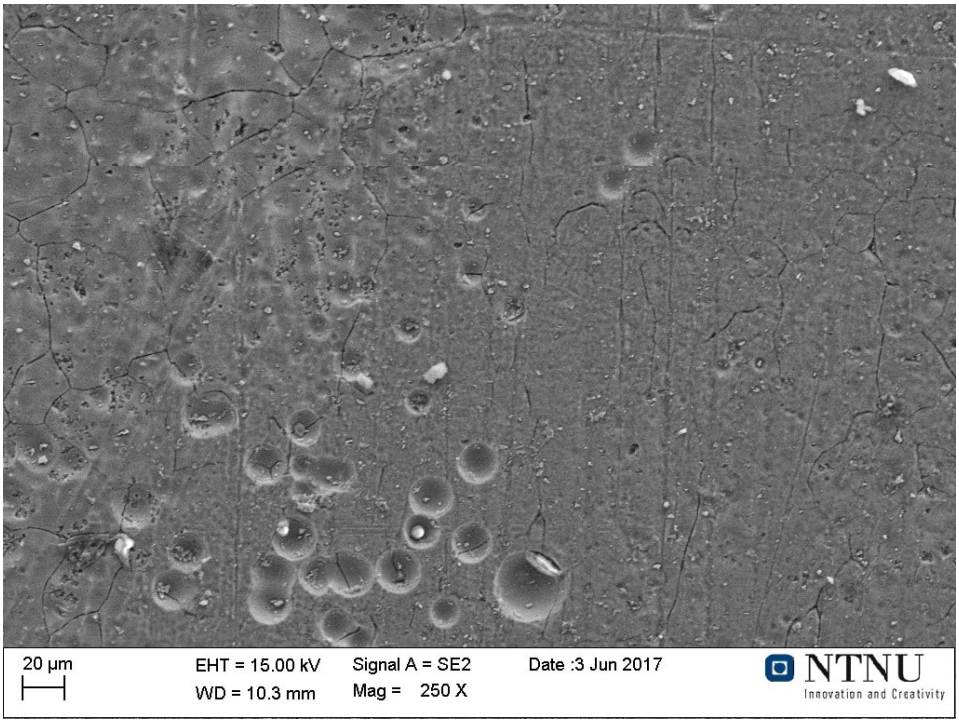

Figure 4.26: SEM Image of 6005 aluminum from galvanic crevice corrosion at 25°C run for 120 hours. Image is taken after chemical cleaning and is taken at the bottom of the sample

Galvanic crevice corrosion for 72 hours at 10°C

The SEM micrograph presented 4.27 is from figure 4.3, which is photographed in a) in figure 4.17. The image presents the middle of the sample were alkaline etching can be observed at the top of the image. In the bottom of the picture clusters of hemispherical pits, some with intermetallic particles can be seen. Image of the top of the sample in figure 6.12 show that the corrosive attack starts 0.5 mm into the crevice. Image of the bottom given in figure 6.13 show similar behaviour as for earlier parallels.

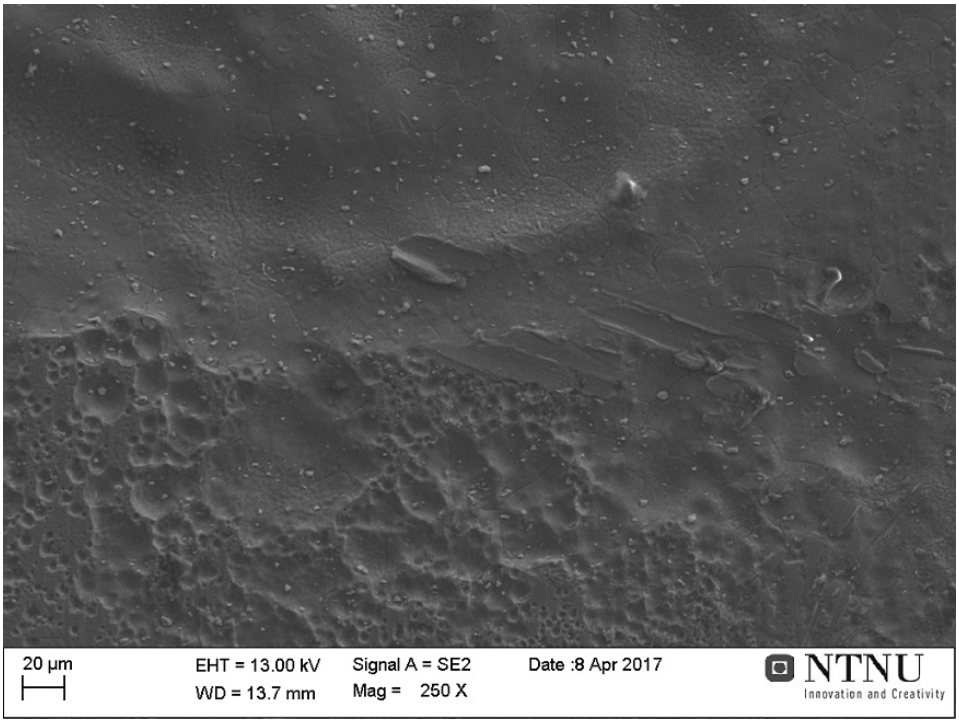

Figure 4.27: SEM Image of 6005 aluminum from galvanic crevice corrosion at 10°C run for 72 hours. Image is taken after chemical cleaning and is taken in the middle of the sample

Galvanic crevice corrosion for 96 hours at 10°C

The SEM micrograph presented 4.28 is from figure 4.7, which is photographed in b) in figure 4.17. The image show similar behaviour as found before with alkaline etching shown at the top of the picture. Hemispherical pits is also found in the middle and to the left. Alkaline etching of the matrix were found both at the top and the middle of the sample and is shown in figure 6.14 and 6.15 in the appendix.

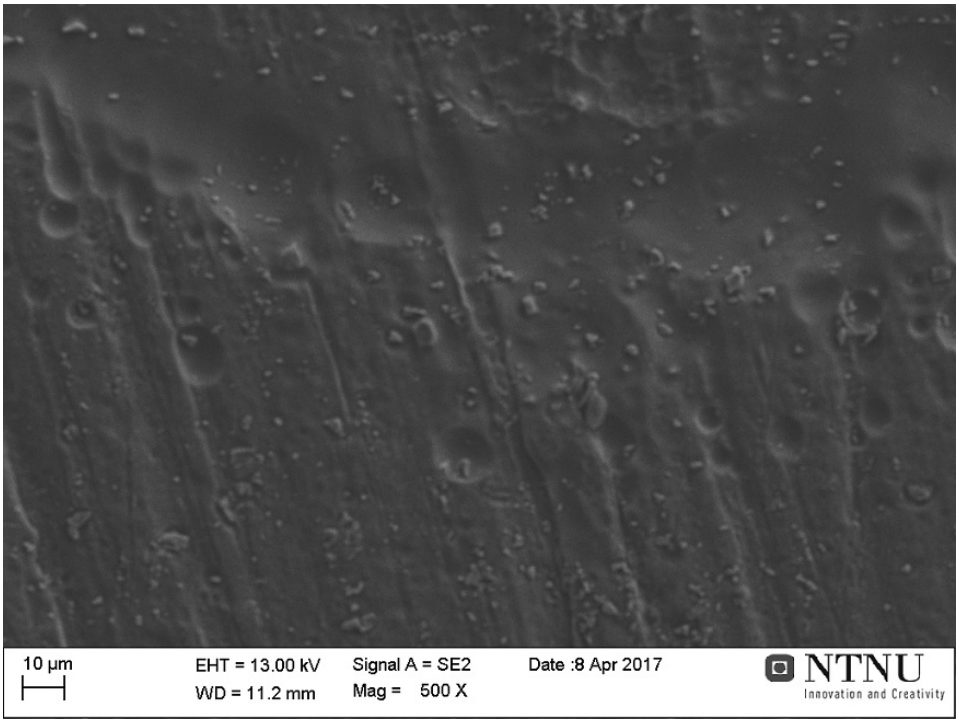

Figure 4.28: SEM Image of 6005 aluminum from galvanic crevice corrosion at 10°C run for 96 hours. Image is taken after chemical cleaning and is taken of the bottom of the sample

Galvanic crevice corrosion for 120 hours at 10°C

The SEM micrograph presented 4.29 is from figure 4.11, which is photographed in c) in figure 4.17. The image show alkaline etching pits which are separated by an intact matrix. Alkaline etching and buried intermetallic particles can be seen in a picture of the middle which is found in figure 6.16 in the appendix. In figure 6.17 the grain boundaries can be seen in an etched matrix at the bottom of the sample.

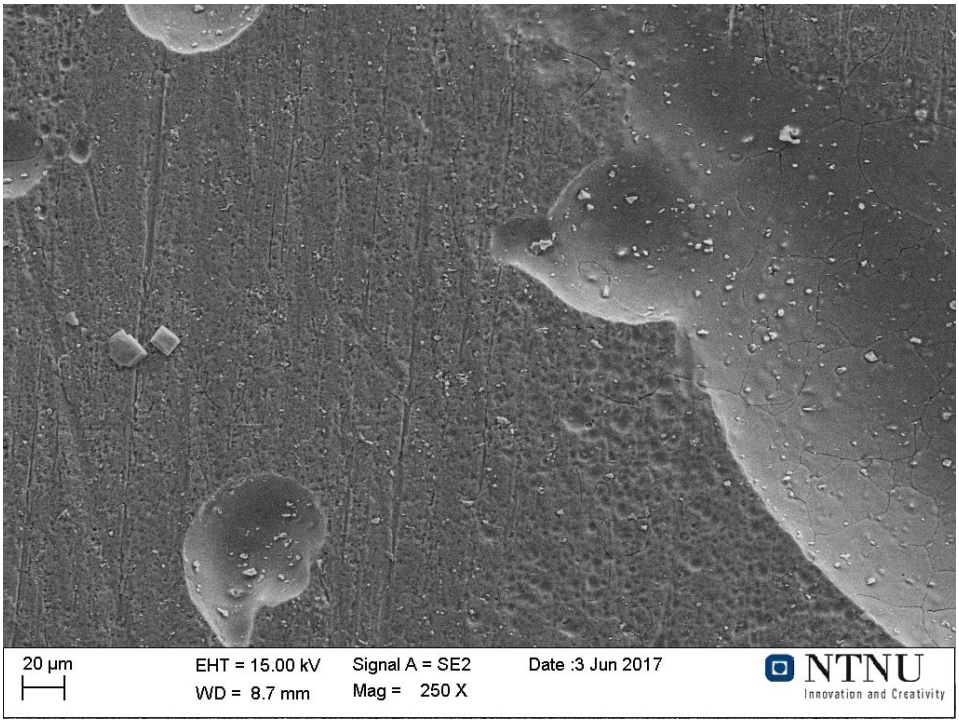

Figure 4.29: SEM Image of 6005 aluminum from galvanic crevice corrosion at 10°C run for 120 hours. Image is taken after chemical cleaning and is taken of the top of the sample

Galvanic crevice corrosion at 72 hours without cathodic protection

The SEM micrographs presented 4.30 is from figure 4.13 and is photographed in c) in figure 4.19. The image show an intact matrix with pitting from intermetallic particles. Some pits have particles buried at the bottom.

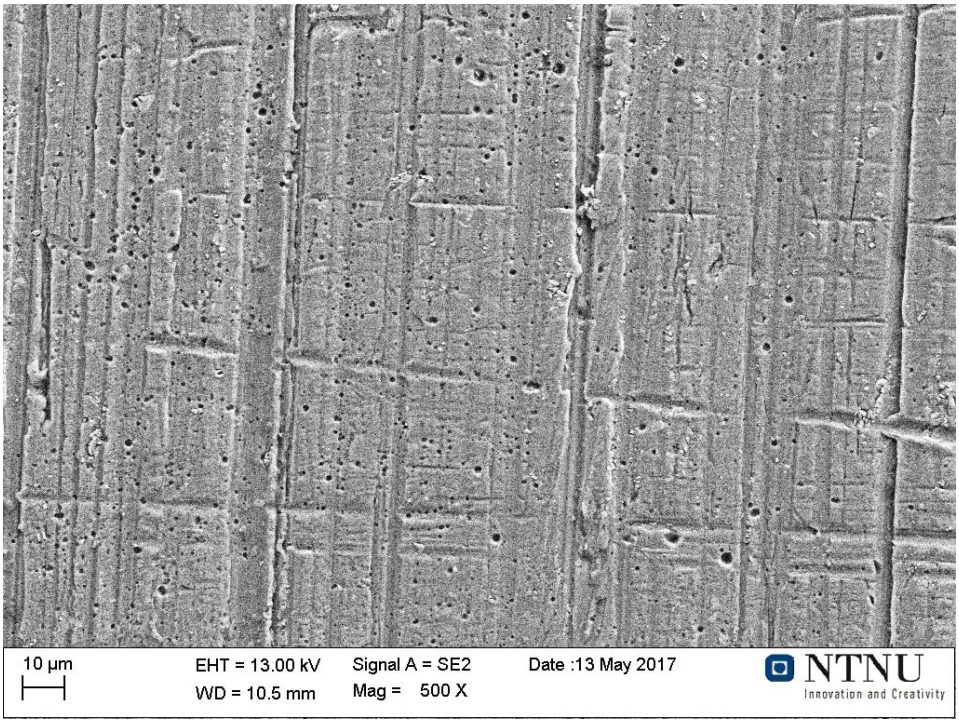

Figure 4.30: SEM Image of 6005 aluminum from galvanic crevice corrosion at 25°C run for 72 hours without AlZnIn anode. Image is taken after chemical cleaning and is taken of the top of the sample

In figure 4.31 a picture of the bottom show a corroded matrix in the middle of the picture.

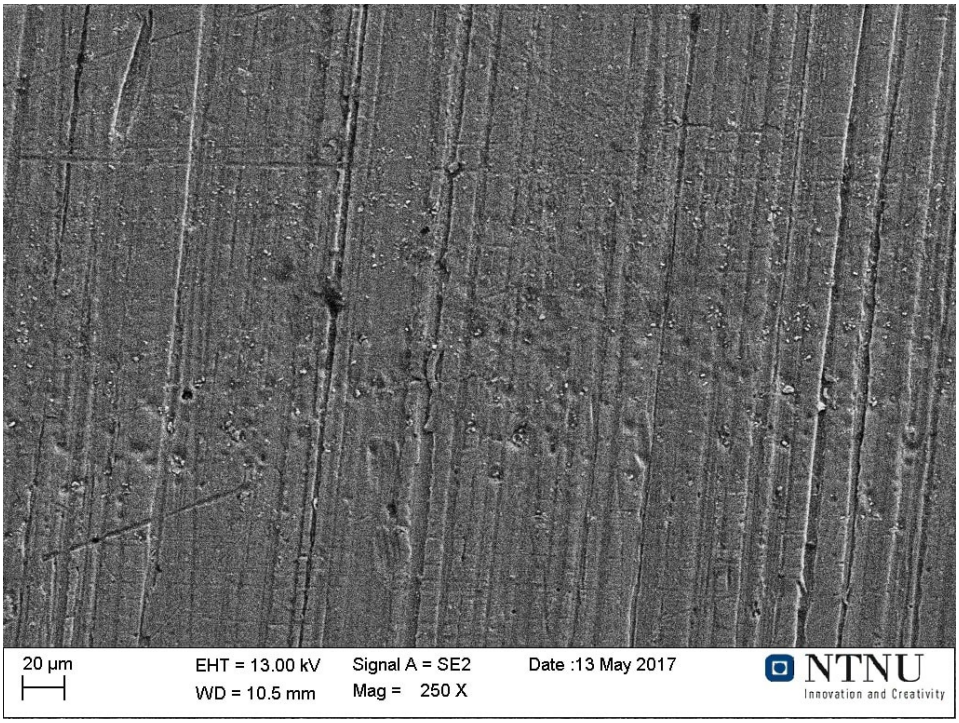

Figure 4.31: SEM Image of 6005 aluminum from galvanic crevice corrosion at 25°C run for 72 hours without AlZnIn anode. Image is taken after chemical cleaning and is taken at the bottom of the sample

Carbon steel in galvanic crevice corrosion for 120 hours

The image of the carbon steel presented in figure 4.32 was typical for all parallels performed at 25 °C. The image is from figure 4.9, which is pictured in e) in figure 4.14. The image show an entirely intact surface similar to the one received in figure 4.22.

In figure 4.33 an image of a steel surface after an experiment performed at 10 degrees is presented. The surface is now clearly deformed and seems to have experienced an uniform corrosion attack.

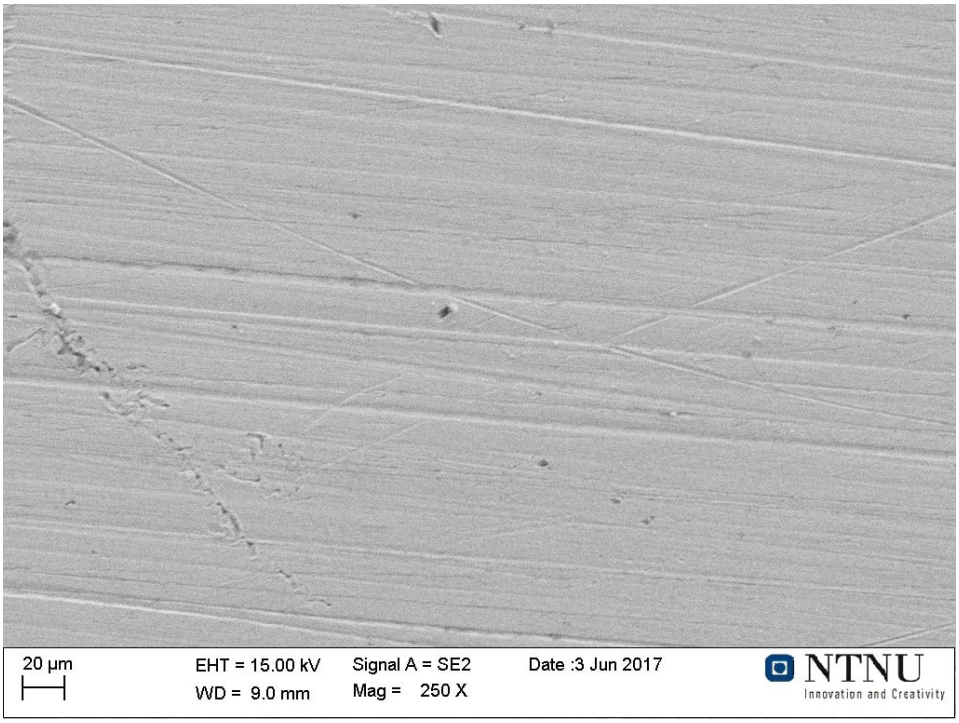

Figure 4.32: SEM Image of X65 carbon steel from galvanic crevice corrosion at 25°C run for 120 hours with cathodic protection. Image is taken after chemical cleaning and is taken of the top of the sample

Figure 4.33: SEM Image of X65 carbon steel from galvanic crevice corrosion at 10°C run for 120 hours with cathodic protection. Image is taken after chemical cleaning and is taken of the top of the sample

Calcareous deposit analysis

Without cathodic protection

The figure 4.34 show the steel surface photographed in c) in figure 4.20. The image shows a corroded surface with particles spread out over the entire surface. An EDS analysis is performed on the white area and given in table 4.2. The table show that the corrosion is primarily from iron with some traces of aluminium. The sodium is from the electrolyte.

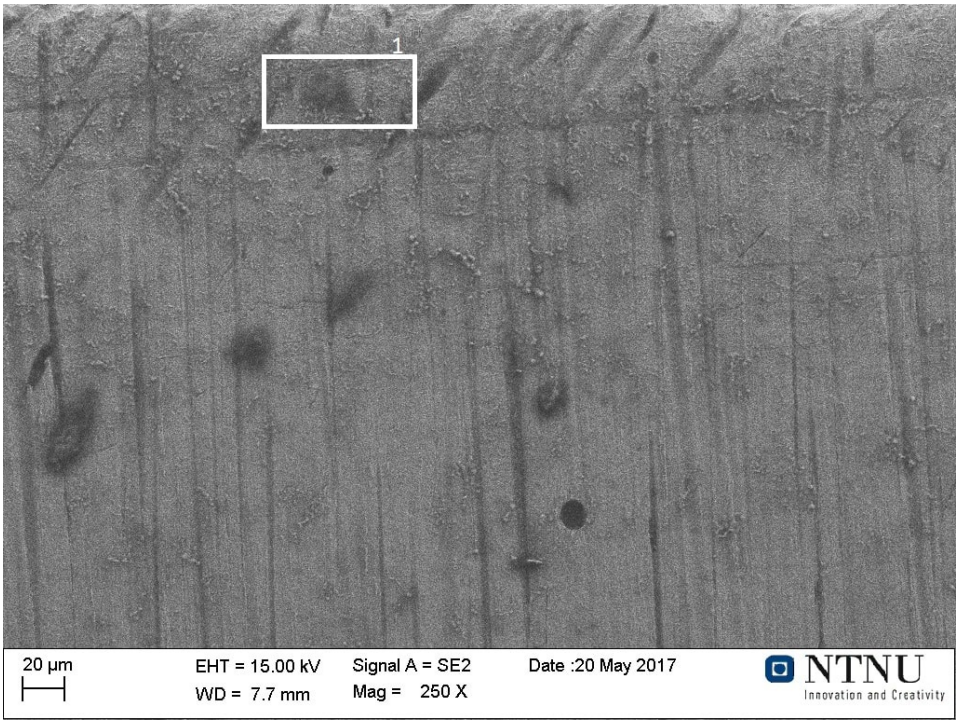

Figure 4.34: SEM Image of X65 carbon steel from galvanic crevice corrosion without cathodic protection at 10°C run for 96 hours. Image is taken before chemical cleaning and is taken of the top of the sample. EDS analysis is performed on the area marked in white

Table 4.2: EDS analysis of area marked in figure 4.34

Element	Area 1 [wt%]
Fe	73.4
O	23.2
Al	1.8
Na	1.6
Tot	100

The figure 4.35 show the aluminium surface photographed in d) in figure 4.20. It can be seen that the matrix is intact with small spherical particles located closer to the edge. An EDS analysis is performed on one of these particles with results given in table 4.3. The EDS analysis reveal that the particles are corrosion products from the carbon steel, containing mostly iron together with ions from the electrolyte.

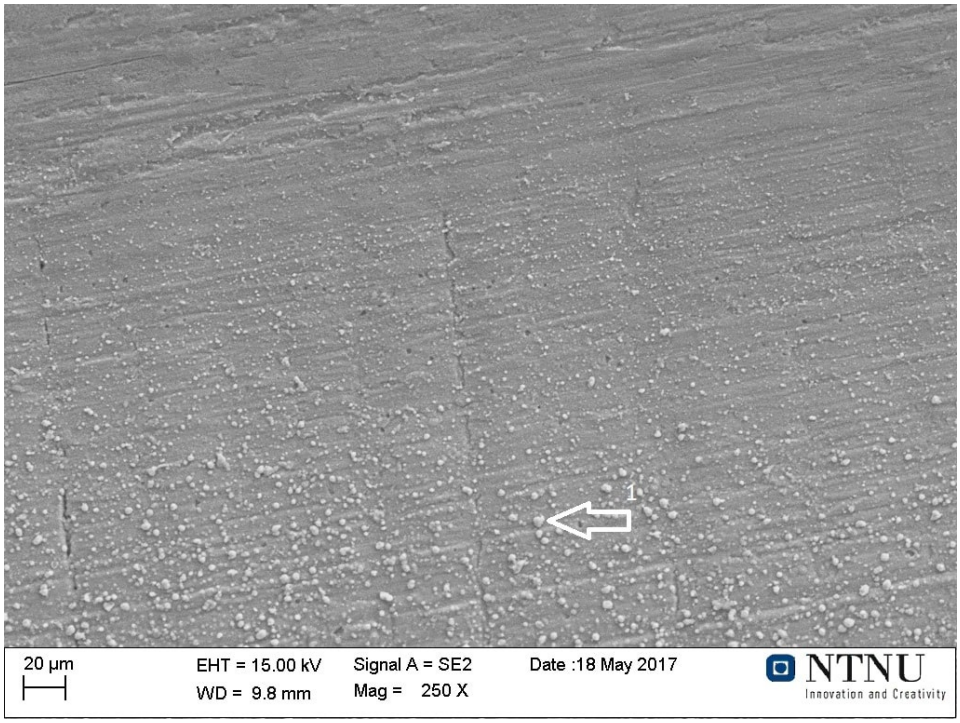

Figure 4.35: SEM Image of 6005 aluminum from galvanic crevice corrosion without cathodic protection at 10°C run for 96 hours. Image is taken before chemical cleaning and is taken at the bottom of the sample. EDS analysis is performed on the particle marked in white

Table 4.3: EDS analysis of particle marked in figure 4.35

Element	Point 1 [wt%]
Fe	63.2
O	24.2
Cl	3.9
Al	3.6
Na	2.0
Mg	1.3
Ca	0.7
S	0.7
K	0.6
Tot	100

With cathodic protection

The figure 4.36 show the steel surface photographed in a) in figure 4.20. A large layer of calcareous deposits can be seen distributed unevenly on the surface. In the areas marked in white an EDS analysis is performed. The black area is shown to indicate where on the sample the micrograph in figure 4.37 were taken. The EDS analysis presented in table 4.4 reveal that the calcareous layer on the steel is mostly made of magnesium. No trace of calcium is found in the analysis.

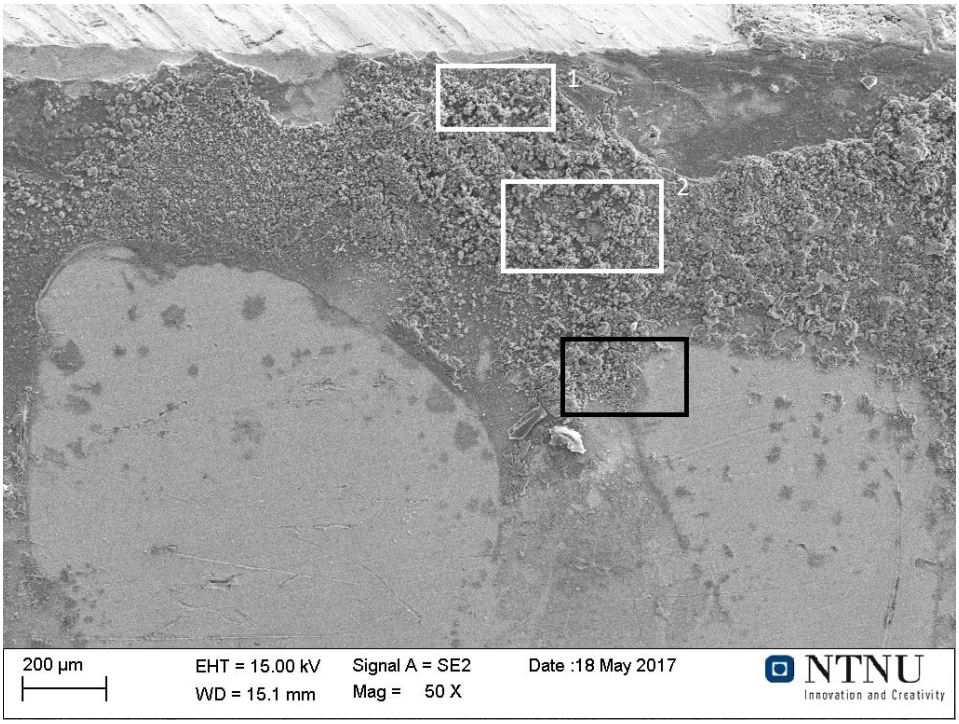

Figure 4.36: SEM Image of X65 carbon steel from galvanic crevice corrosion with cathodic protection at 10°C run for 96 hours. Image is taken before chemical cleaning and is taken of the top of the sample. EDS analysis is performed on the areas marked in white and the black area is indicating the area of figure 4.37

Table 4.4: EDS analysis of the areas in white figure 4.36

Element	Area 1[wt%]	Area 2[wt%]
Mg	43.3	39.4
O	36.3	33.5
Fe	8.9	-
Al	5.9	6.4
Cl	5.5	14.7
Na	-	4.4
K	-	1.6
Tot	100	100

The figure 4.37 is a closer look of the calcareous deposits formed on steel presented in figure 4.20 a). It is of the black area indicated on figure 4.36. Visible from the image, the characteristic needle structure of argonite can be seen. An EDS analysis of the needle structure was performed and the results are presented in 4.5. The EDS reveal the calcium phase on the needle shaped surface while magnesium is found on the adjacent area.

Figure 4.37: SEM Image of X65 carbon steel from galvanic crevice corrosion with cathodic protection at 10°C run for 96 hours.Image is taken before chemical cleaning and is taken of the area which was indicated in black on figure 4.36.EDS analysis is performed at the points indicated in black

Table 4.5: EDS analysis of the points in figure 4.37

Element	Point 1[wt%]	Point 2[wt%]
Ca	41.3	-
O	31.3	31.2
Al	14.2	10.0
Cl	9.7	16.8
Mg	3.2	26.4
Na	-	12.2
K	-	3.4
Tot	100	100

An EDS analysis of the layer at the bottom is found in the appendix in figure 6.18. The EDS analysis in table 6.1 show large amounts of magnesium and aluminium corrosion products. There is also found calcium iniside the layer.

The figure 4.38 show the aluminium surface photographed in b) in figure 4.20. A large layer of calcareous deposits can be seen distributed unevenly on the surface. In the areas marked in white an EDS analysis is performed. The image show that close to the edge, the calcareous layer are formed in clusters of spheres. The EDS analysis presented in table 4.6 reveal that these spherical deposits are rich on calcium. The layer further down into the crevice contains more magnesium and calcium could not be traced. Further down in the crevice the aluminium matrix is visible. Thus an image of this area were performed inside the black rectangle as is indicated in the figure.

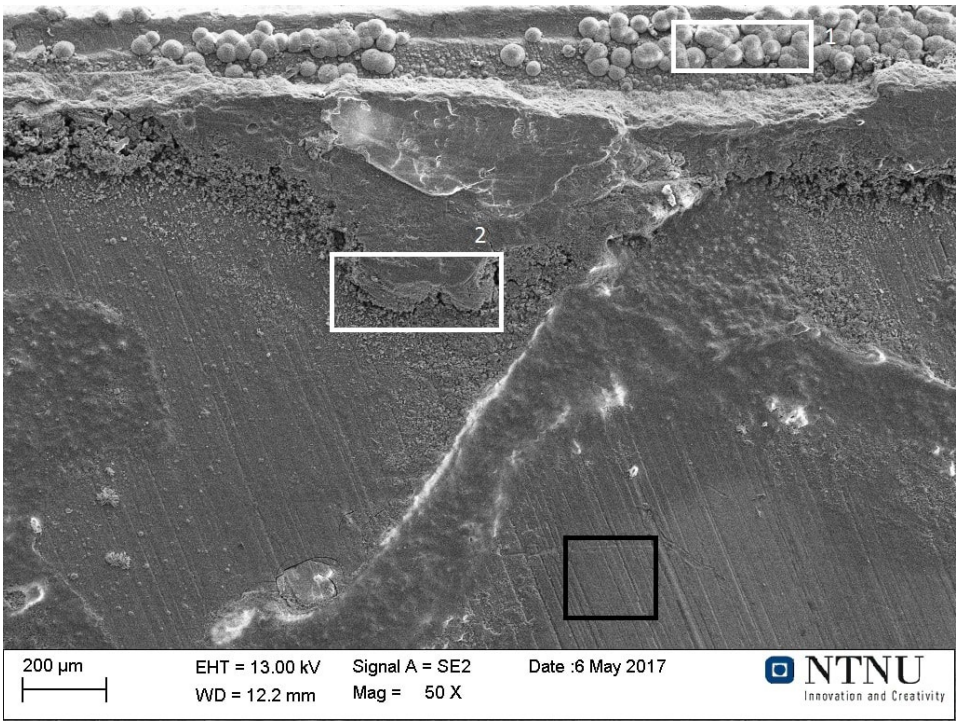

Figure 4.38: SEM Image of 6005 aluminium from galvanic crevice corrosion with cathodic protection at 10°C run for 96 hours. Image is taken before chemical cleaning and is taken of the top of the sample. EDS analysis is performed on the areas marked in white and the black area is indicating the area of figure 4.39

Table 4.6: EDS analysis of the areas in white in figure 4.38

Element	Area 1[wt%]	Area 2[wt%]
O	49.1	47.7
Ca	22.0	-
C	14.8	4.5
Mg	11.3	34.1
Na	1.2	1.4
Al	0.8	6.0
Cl	0.8	4.1
S	-	0.6
Tot	100	100

Figure 4.39 show the area below the thick calcareous layer in figure 4.38. The surface of the aluminum can be seen, but seems to be covered by a thin layer. This is investigated by an EDS analysis on the marked area which is presented in the table 4.7. These results reveal high amounts of oxygen and some magnesium which indicate calcareous formation on top on the oxide layer.

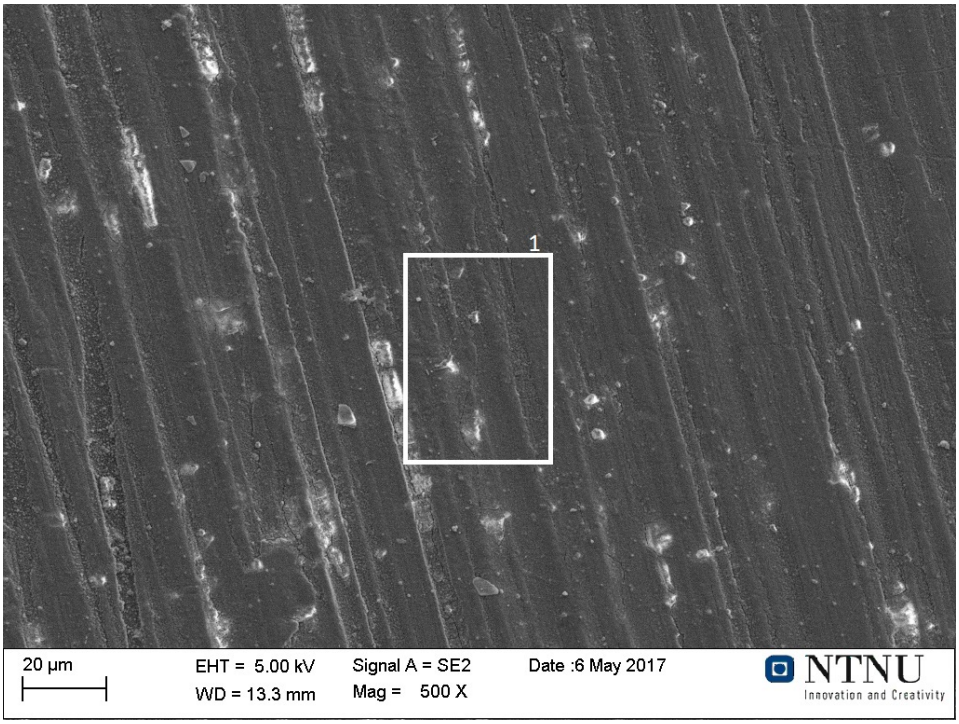

Figure 4.39: SEM Image of 6005 aluminium from galvanic crevice corrosion with cathodic protection at 10°C run for 96 hours. Image is taken before chemical cleaning and is taken of the area which was indicated in black on figure 4.38. EDS analysis is performed on the area marked in white

Table 4.7: EDS analysis of the area in figure 4.39

Element	Area 1[wt%]
O	50.1
Al	36.5
Mg	7.3
C	4.3
S	1.8
Tot	100

4.3 Weight loss and pH measurements

4.3.1 Galvanic crevice corrosion at 25°C

Table 4.8: Weight loss measurements for X65 carbon steel, 6005 aluminium and AlZnIn in galvanic corrosion with three metal and two metal coupling with a simulated crevice. The experiments are performed at 25°C and the unit for the weight loss is $\frac{mg}{cm^2}$

Parallel	X65	6005	AlZnIn
1(72h)	0	0.36	3.68
2(72h)	0	0.32	1.64
3(72h)	0	0.21	2.07
Without CP(72h)	0.32	0.29	-
1(96h)	0	0.32	1.47
2(96h)	0.04	0.29	1.57
1(120h)	0	0.39	1.50

4.3.2 Galvanic crevice corrosion at 10°C

Table 4.9: Weight loss measurements for X65 carbon steel, 6005 aluminium and AlZnIn in galvanic corrosion with three metal coupling with a simulated crevice. The experiments are performed at 10°C and the unit for the weight loss is $\frac{mg}{cm^2}$

Parallel	X65	6005	AlZnIn
72h	0.21	0.36	1.46
96h	0.11	0.46	1.50
120h	0.11	0.43	1.50

4.3.3 pH measurements

The pH measurements were performed by placing a pH strip on the crevice after ended experiment. They are presented in table 4.10 below. All parallels performed with a AlZnIn

anode show an alkaline pH of either 9 or 10. The parallel of galvanic crevice corrosion without cathodic protection show an slightly acidic environment with a pH of 5.

Table 4.10: pH measurements performed after conducted experiment of electrolyte inside crevice

Parallel	pH
1(72h,25c)	10
2(72h,25c)	9
3(72h,25c)	9
Without CP(72h,25c)	5
(72h,10c)	10
1(96h,25c)	9
2(96h,25c)	10
(96h,10c)	10
(120h,25c)	9
(120h,10c)	10

Chapter 5

Discussion

5.1 Potentials

The potentials for all parallels are as expected very stable due to the mechanism described in figure 2.13. The potential vary a bit more at 25 °C and is also shifted a few mV in the anodic region in comparison to the potentials at 10°C. With a more cathodic potential hydrogen evolution will be favoured. This also seems to be the case when the current behaviour between 10°C and 25°C are taken into consideration. The currents decay in a more linear fashion at 10°C, which is an indication of hydrogen evolution being dominant. The potential without AlZnIn is in the range of the aluminium in figure 2.12. This is expected as aluminium will then act as an anode.

5.2 Carbon steel

The measurements on steel show that there is a steady decrease in current required of the anode. This is expected since the potential is sufficiently low. This keeps the reductions on the the surface at a high rate, and thus facilitate formation of calcareous deposits. In the parallel performed without cathodic protection in figure 4.13, the same characteristic decay is not found. Here an increase in current is experienced when the potential becomes more active. Thus the calcareous scale will not form as readily in a two metal coupling compared to a three metal coupling. The picture in figure 4.18 show a layer resembling calcareous deposits, but the pH measurement in table 4.10 show a value inside the crevice which is below the theoretical values for initiation[12],[13]. A parallel without CP at 10 °C show a very thin layer in figure 4.20 c), compared to what is seen in a) where the anode has been connected . There is a clear difference in the parallels without cathodic protection between the two different temperatures. This is probably due to the fact that calcareous deposits form faster at higher temperatures due to faster kinetics. A SEM micrograph with EDS analysis in figure 4.34 and table 4.2 reveal that the surface is covered with corrosion products. This result is not totally reliable due to the fact that if a calcareous layer formed

on the surface it would probably be too thin for an EDS analysis to detect. The electron beam could probably penetrate through the thin layer and thus not detect any calcareous compounds. It's however clear from all photos and the SEM micrograph of the uncleaned steel surface that calcareous formation is faster with the anode connected. The weight loss measurement also confirm this in table 4.8, where the parallel without the AlZnIn anode is the only one with a significant weight loss found on the steel.

Experiments at 25 °C see a sharp decrease in current at the beginning, when the anode is connected. This indicates the oxygen reduction reaction decreasing due to migration restrictions inside the crevice as well as the $CaCO_3$ formation. The "linear" behaviour after the initial sharp decrease is seen in every experiment. This in turn is due to hydrogen evolution becoming the dominant reduction reaction. The weight loss measurements at 25 °C show a complete protection of the steel. One parallel showed weight loss, but this is below the error margin of the analytical weight and thus not significant. The SEM micrograph of a steel surface from 25 °C shown in figure 4.32 give no signs of corrosion. Thus the steel is well protected from crevice corrosion at 25 °C which has been concluded in earlier works [24],[25].

With experiments conducted at 10 °C the steel current show a more active behaviour at the beginning of the experiment. The sharp initial decrease in current is not found. In figure 4.7 and 4.11 an increase can be seen at the start of the experiments. With a decrease in temperature the solubility of oxygen will increase even if the diffusion is lower. Calcium is more soluble at lower temperatures and thus the calcareous layer will be less protective at lower temperatures due to less $CaCO_3$ forming. Studies by Barchiche et al [11] found that temperature would not effect the layers ability to reduce current at the potentials found in this report. This is not the case when a crevice is present as is clear from the electrochemical data. Thus a possible explanation for the different behaviour in the beginning is that the larger amount of oxygen cause a larger demand for current before being depleted. With more calcium solved the calcareous layer is less effective at reducing the current. The reduction rate will be high and the surface is kept alkaline and favouring $Mg(OH)_2$ formation . The currents on aluminum show active peaks which are "mirroring" the behaviour of the carbon steel at 10 °C. The peaks are most likely from cathodic corrosion which in turn is a result of the oxygen reduction in equation (2.2) that cause the alkaline environment to develop. So the activity in the beginning is most likely a combination of the large amount of oxygen inside the crevice and the slower kinetics of the calcareous layer at lower temperatures. After the initial activity a linear decay is observed for all parallels which indicate that hydrogen evolution is the dominant reaction. The "jumps" experienced in figure 4.11 might also be explained by H_2 evolution as the gas could be trapped inside the crevice, but eventually detaches, causing a new area to be exposed. Even if it was hypothesized that the slower kinetics of the calcareous layer caused an active current in the beginning, the pictures in figure 4.16 show a more developed layer at 25 °C. This might be due to the fact that the steel experience corrosion at this temperature. The porous corrosive products will then act as barriers for the electrolyte and thus create an environment which favour calcareous formation, and hence catalyze the process[31]. The weight found in table 4.9 show that the steel is not completely protected at 10 °C the SEM image in 4.33 also show a corroded surface. The weight loss is however

small and not significant. When looking at the electrochemical behaviour, steel seems to be well protected even at lower temperatures.

5.3 Aluminium

Without cathodic protection the aluminum experience an anodic current during the entire experiment. This is expected since it's less noble in comparison to steel. The mass loss show that the 6005 is not able to protect the steel. The picture in 4.20 d) show no signs of calcareous deposits, but rather an intact oxide layer. The clear pitting morphology from the three metal coupling is not seen picture 4.19 either. The closer analysis from figure 4.30 show that the matrix is intact, but corrosion around intermetallic particles can be seen. Considering the potential during the experiment it's likely that these pits are the acid pits which was described in the theory. These pits initiate at the top of the experimental pourbaix diagram in figure 2.6 which is in the potential range of what was seen in figure 4.13. From the pourbaix diagram it can also be seen that in this potential region the aluminium will be susceptible to a general or uniform corrosive attack. This is probably what is observed in figure 4.31 where the aluminium show corrosion at the bottom of the sample. The weight loss is not larger than for the comparable parallels with cathodic protection. The aluminum does not suffer from cathodic corrosion in this instance and thus not show a large mass loss. However considering the potential and current behaviour it's expected that the aluminium will continue to corrode. Measurements performed by Røstbø in figure 2.15 show the largest corrosion rate in a crevice without cathodic protection.

All the currents on aluminum at 25 °C show an initial anodic peak before starting to decay towards the cathodic region. The parallels that did not reach the cathodic region during the experiment was still decaying as is evident from the plots presented in the appendix. The exception being parallel 3 in figure 4.1 where the current is in the cathodic region during the entire experiment. The pictures in figure 4.14 b) and 4.15 does show that possibly a smaller amount of the surface was exposed to the electrolyte. The current on steel for the same parallel is also less cathodic compared to the other parallels. Thus indicating that the reduction inside rates on steel inside the crevice probably were lower. This in turn would cause the alkalinity inside the crevice to increase at a slower rate and thus less of the aluminium matrix being harmed by alkaline etching. This can be backed up by the weight loss measurements which are the lowest for parallel 3 at 72 hours. Less weight loss is of course to be expected with a cathodic current found on aluminium during the entire experiment. Parallel 1 at 96 hours in figure 4.5 also go into the cathodic region early in the experiment. This parallel also has the smallest cathodic current on steel which thus repeats the argument of a slower alkalization inside the crevice. The parallel were performed in the authors specialization project and from pictures in the report a large area inside the crevice was not covered with electrolyte[25]. So both behaviours can be explained due to experimental error, but this will be discussed further later. Some of the samples show corrosion right at the center of the sample. This looks like it comes from the hole in the back where the sample is connected. With a surface polished down to close to the screw hole a small sharp peak can possibly be found in the center of the sample. This is a weakness in the experimental as it seems to only have happened at a select few of the

parallels. The pitting attack is in general located at the edges, which is expected due to the mechanism described in the theory and presented in figure 2.10.

SEM pictures reveal both cathodic corrosion and particle detachment for all parallels at 25 °C. This is in conjunction with the electrochemical behaviour were both anodic peaks and a decay in current can be found. If the with the discussed experimental errors are excluded, the weight loss show a decrease in corrosion rate as a function of time. This is expected as the anodic currents decrease or move into the cathodic region. Thus the results indicate that protection of aluminium is and that the system will be able to stabilize at 25 °C. Further testing with longer experiments will give a clear picture if the aluminium is kept in the passive region and thus be protected. The initial results are promising, but lack statistical evidence.

The current behaviour on aluminium at lower temperature is the same as for steel with a longer period of activity before a steady decay starts. This indicate an increase in alkaline etching which is evident from the pictures in figure 4.17, where the pitting attack cover a larger surface. As discussed earlier is this probably due to the slower formation of calcareous deposits in conjunction with a larger amount of dissolved oxygen. The SEM micrographs also show that alkaline etching occurs on the entire surface during experiments run at 10 °C. The only parallel which enters the cathodic region is the 120 hour parallel. Looking at the logarithmic plots in the appendix it can be seen that the current decays at a slower rate at 10 °C. This is expected and is well in conjunction with the weight loss in table 4.9 where a higher corrosion rate is found on aluminium compared to parallels performed at 25 °C. One thing to note is that a higher mass loss is found at 96 hours then at 120 hours. The electrochemical data in figure 4.7 predict this since the anodic current is larger than what is seen in figure 4.11.The larger weight loss at 10 °C seems to make for a more uniformly distributed and thicker calcareous layer, which in turn can make the deposits block the surface faster. Thus it would be interesting to run experiments for even longer(maybe weeks?) to look on the effect it has on mass loss. The electrochemical behaviour show promising results with a clear indication that the currents become cathodic and the oxidation reactions happen predominantly on the anode. The large forming of calcareous deposits will also be positive due to blocking of the crevice. Weight loss show that the corrosion might slow down with time, but again lacks statistical results. The SEM micrographs confirms the alkaline etching in the middle of the samples, but also show buried and detached intermetallic particles. All things considered anodic protection of aluminum seems possible at 10°C, but will need further testing before a decisive conclusion can be made.

5.4 Calcareous formation in three metal galvanic crevice corrosion.

The calcareous layer form more readily with the AlZnIn anode system. This is evident from figures 4.34 and 4.35, where only corrosion products is found at the surface. This is expected considering the pH inside the crevice being shifted in the acidic region.

The calcareous layer found on steel during cathodic protection is well developed at the edge as seen in figure 4.36. Further down into the crevice the layer is less developed. This is likely due to a higher amount of oxygen present this close to the bulk solution which gives a subsequent higher amount of reduction reactions at the crevice mouth. The EDS analysis presented in table 4.4 found that the layer consisted mainly of magnesium compounds close to the edge. This is expected due to the high reduction rate causing alkalinity at the surface. Earlier works had found the calcium phase to be close to the surface[24] at 25°C, then located in a magnesium matrix. EDS analysis of the bottom in figure 6.18 found this. The calcium was embedded in magnesium and corrosion products from aluminum. Thus the magnesium phase can be found over the entire exposed surface, while the calcium phase is distributed non uniformly inside the magnesium matrix. Further down in the crevice argonite needles could be found on the steel sample as seen in figure 4.37. Here the crevice the oxygen supply is lower and thus the reduction reactions occur at a slower rate. This will facilitate better for $CaCO_3$ since the reduction reactions on the surface is most likely slower.

The layer found on aluminium presented in figure 4.38 show the same behaviour with a thick layer at the edge. The EDS data presented in table 4.6 show a calcium rich spherical formed phase right at the edge. The spherical shape indicate that the deposits are formed around intermetallic particles. This explanation goes well in conjunction with the acid environment which can develop inside these pits in chloride containing electrolytes. This might also be due to the fact that at the edge is close to the bulk which has a pH of 8.2. This will might be able to keep the environment at a more favourable pH for $CaCO_3$ formation. Further investigation of the edge with a cross section could provide with interesting results. Deeper down the crevice a larger amount of magnesium phase is found and no calcium phase is detected. This is shown in figure 4.39 and table 4.7. Thus the calcium phase does not precipitate uniformly on aluminum either. It's however not proof that the calcium phase does not form at these places since the EDS analysis could have penetrated through calcium containing compounds. For further investigation with a more surface sensitive analysis like GD-OES could answers these questions.

5.5 Experimental procedure and sources for error

The crevice device and placement of the teflon strips cause some practical problems. Especially when the strips "slip" and cause a different area to be exposed. It was also not possible to coat the edges if the sample was to thick because then the crevice could be blocked. Thus the areas exposed are not controlled precisely with the current setup. The best way to solve this in future projects would be to change to a more sophisticated setup. Most known problems with the experimentation were linked to this. The coating on the coupling in the crevice device would some time also fail, causing the copper wire to be exposed to the solution. One way to avoid this would be to apply a heat shrink tube after the cable shoe has been connected. Otherwise did the miccro lacquer isolate well when it was held intact. The beewax that were used on the anodes has been recommended to be replaced earlier [24],[25]. This is not due to poor coating properties, but rather the difficulty in removing it effectively. The wax also has a tendency to stick too all equipment

which is in contact with it. In earlier works a different coating called “Micro-shield” stop of lacquer has been used on the same anodes[29]. This coating experienced only problems when high amounts of gas development occurred on the anode surface, which is not the case for these experiments and thus might be a suitable alternative.

The pH measurements are very uncertain. They do however show the difference between galvanic crevice corrosion with or without AlZnIn anode, but the measurements are not reflecting the real pH inside the crevice. The weight loss measurements will have a degree of uncertainty due to the fact that the solution remove both corrosion products and the metal for steel samples. Such small weight losses are however an indication of good corrosion protection which is the point of the project. Since experiments are conducted at different time intervals the the corrosion rate will not be constant through the experiment. Which such small areas as has been used the weight loss measurements carry uncertainty and some of the weight loss was at the edge of the error margin for the analytical weight. With an introduction of a larger area, small deviations would be easier to avoid and the weight loss measurements would be more precise.

As mentioned will the EDS analysis performed not give a precise representation on what is at the very top of the film covering the surfaces. Problems with detecting the intermetallic particles also occurred and is likely due to a large accelerating voltage, which in turn penetrates through the particles. One idea could be to analyze the l-shell energy of the calcium which is at lower eV.

Synthetic seawater will cause different result than what is found at real conditions. This is due to the fact that it doesn’t have the same buffer capacity and the factor of marine growth is not possible to simulate. This can change the formation of the calcareous layer and the difference in chemistry can change the corrosion rates. Short experiments will also not replicate real conditions were structures are submerged for several years.

5.6 Suggestions for further work

Here follows a short summary of suggestions for further work.

- Perform further testing with the crevice corrosion to get statistical results
- Perform test in natural seawater
- Perform tests with a photo cell which can monitor the formation of calcareous deposits
- Utilize GD-OES or XRD in conjunction with the EDS analysis to further investigate the calcareous deposits
- Introduce nitrogen bubbling the further investigate the effect of hydrogen evolution inside the crevice
- Try out different alloying the aluminium to see if they are more or less susceptible to crevice corrosion and alkaline etching

- Increase the area of the samples to eliminate some of the uncertainty due to the low weight loss measurements
- Develop a more sophisticated way to conduct crevice test which can monitor the pH levels and the potential as a function of distance inside the crevice. Like the tests performed by Li et al [22]
- Analyze the corroded specimens in a light microscope and measuring the pit depth
- Perform cross section SEM analysis of specimen at the edge of the crevice with calcareous deposits.

Chapter 6

Conclusions

Studies of cathodic protection of X65 carbon steel and 6005 aluminium in a crevice with and without a AlZnIn anode was performed. And here is what that was found

- Crevice corrosion show complete protection of steel at 25°C and low corrosion rates at 10°C. This show that protection of steel in galvanic crevice corrosion with three metal coupling is possible.
- Calcareous deposits form on both steel and aluminum during crevice corrosion with three metal coupling. This will decrease the current requirement for both surfaces
- In cathodic protection with a crevice present, aluminium will experience a anodic current and corrosion initially. This current will decay slowly and turn into an cathodic current indicating that the aluminium is protected. This is true for experiments at both 25°C and 10°C.
- In galvanic crevice corrosion the pH inside the crevice was found to be alkaline after ended experiment with a pH of 10 and 9 with cathodic protection. Without cathodic protection the environment is acidic with a pH of 5.
- Aluminium experience more alkaline etching at a lower temperature inside a crevice. This could be detrimental to the structure and needs to be further investigated.

References

[1] Christian Knutsen, Ivar Kvale, Jan Halvor Nordlien, et al. Aluminium applied for subsea structures" possibilities and challenges. In *The Eleventh International Offshore and Polar Engineering Conference*. International Society of Offshore and Polar Engineers, 2001.

[2] DET NORSKE VERITAS, DNV-RP-B401. Cathodic protection design. 2010.

[3] Kemal Nisancioglu. Corrosion basics and engineering, kompendium, 1994.

[4] R.E. Andresen, P.O, and Bardal E, Gartland. C8th international congress on met. corrosion, mainz, proceedings, 2,. pages 1333–1339, 1981.

[5] Norsok Standard. m-503 cathodic protection. 1997.

[6] Z. Ahmad. *Principles of Corrosion Engineering and Corrosion Control*. Elsevier, 2006.

[7] Ph Refait, M Jeannin, R Sabot, H Antony, and S Pineau. Corrosion and cathodic protection of carbon steel in the tidal zone: Products, mechanisms and kinetics. *Corrosion Science*, 90:375–382, 2015.

[8] S Elbeik, ACC Tseung, and AL Mackay. The formation of calcareous deposits during the corrosion of mild steel in sea water. *Corrosion science*, 26(9):669–680, 1986.

[9] Trine Okstad, Øyvind Rannestad, Roy Johnsen, and Kemal Nisancioglu. Significance of hydrogen evolution in cathodic protection of steel in seawater. *Corrosion*, 63(9):857– –865, 2007.

[10] SH Salleh, S Thomas, JA Yuwono, K Venkatesan, and N Birbilis. Enhanced hydrogen evolution on mg (oh) 2 covered mg surfaces. *Electrochimica Acta*, 161:144–152, 2015.

[11] Chems Barchiche, Claude Deslouis, Otavio Gil, Philippe Refait, and Bernard Tribollet. Characterisation of calcareous deposits by electrochemical methods: role of sulphates, calcium concentration and temperature. *Electrochimica Acta*, 49(17):2833–2839, 2004.

[12] Trine Okstad. Hydrogenutvikling ved katodisk beskyttelse av karbonstal i naturlig sjøvann,master's thesis. Master's thesis, NTNU, 2005.

[13] Yuanfeng Yang, James David Scantlebury, and Elena Victorovna Koroleva. A study of calcareous deposits on cathodically protected mild steel in artificial seawater. *Metals*, 5(1):439–456, 2015.

[14] NL Sukiman, AE Hughes, GE Thompson, JMC Mol, N Birbilis, SJ Garcia, and X Zhou. *Durability and corrosion of aluminium and its alloys: overview, property space, techniques and developments*. INTECH Open Access Publisher, chapter 2 ,2012.

[15] GG Perrault. The role of hydrides in the equilibrium of aluminum in aqueous solutions. *Journal of The Electrochemical Society*, 126(2):199–204, 1979.

[16] Ph Gimenez, JJ Rameau, and MC Reboul. Experimental ph potential diagram of aluminum for sea water. *Corrosion*, 37(12):673–682, 1981.

[17] Kemal Nisancioglu. in corrosion behaviour and protection of copper and aluminium alloys in seawater. pages 145–155. CRC Press, 2007.

[18] Kemal Nisanciglu and Torgeir Wenn. Corrosion and cathodic protection of aluminium in flowing seawater,12th scandinavian corrosion congress . Eurocorr 92, 1992.

[19] R Gundersen and K Nisancioglu. Cathodic protection of aluminum in seawater. *Corrosion*, 46(4):279–285, 1990.

[20] M.G Fontana. *Corrosion engineering*. McGraw-Hill Book Company, chapter 3 ,1967.

[21] A.J Betts and Boulton L.H. Crevice corrosion: review of mechanisms, modelling, and mitigation. *British Corrosion Journal*, 28(4):279–296, 1993.

[22] Z Li, F Gan, and X Mao. A study on cathodic protection against crevice corrosion in dilute nacl solutions. *Corrosion Science*, 44(4):689–701, 2002.

[23] Galvanic series of metals in seawater. `http://www.nordhavn.com/resources/tech/images/Galvanic_Series.pdf`. Accessed: 02.09.2016.

[24] Sondre Røstbø. Cathodic protection of steel-aluminium galvanic couples for a new generation of lightweight subsea structures. Master's thesis, NTNU, 2016.

[25] Harald Solli. Cathodic protection of steel-aluminium galvanic couples for a new generation of light-weight subsea structures, specialization project,. Master's thesis, NTNU, 2016.

[26] Are Berging. Alternating current corrosion of steel in seawater. Master's thesis, NTNU, 2015.

[27] ASTM International. ASTM G1-03(2011). Standard practice for preparing, cleaning, and evaluating corrosion test specimens. west conshohocken. 2011.

[28] ASTM International. ASTM D1141-98(2013). Standard practice for the preparation of substitute ocean water, west conshohocken. 2013.

[29] Kari Forthun. Alternating current corrosion of aluminium sacrificial anodes. Master's thesis, NTNU, 2013.

[30] Kemal Nisancioglu. Personal communication, NTNU, 2016.

[31] Kemal Nisancioglu. Personal communication, NTNU, 2017.

List of Symbols

Here follows a short list of the symbols used in the report

Symbol	Explanation	Unit
E_{corr}	Corrosion potential	V
E_P	Protection potential	V
E_{rev}	reversible potential	V
E_C	Coupling potential	V
I_{Net}	Net current	A
$I_{ox,N}$	Oxidation current of metal N	A
$I_{red,N}$	Reduction current of metal N	A
$I_{ox,M}$	Oxidation current of metal M	A
$I_{red,M}$	Reduction current of metal M	A
$I_{corr(M-\underline{N})}$	Corrosion current of metal N due to galvanic coupling of metal M	A
$I_{corr(\underline{M}-N)}$	Corrosion current of metal M due to galvanic coupling of metal N	A
i_{corr}	Corrosion current density	A/cm^2
i_P	Protection current density	A/cm^2

Appendix

Appendix A: Cleaning method for carbon steel

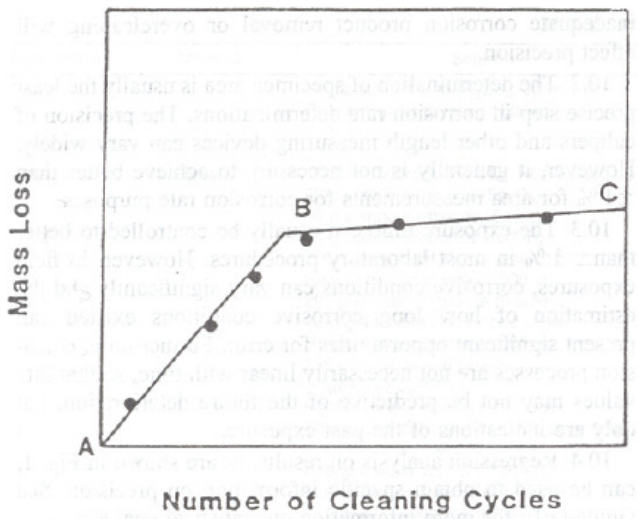

Figure 6.1: Schematic illustration how to find weight loss with multiple cleaning cycles [27]

Appendix B: Additional electrochemical measurements and supplemental plots

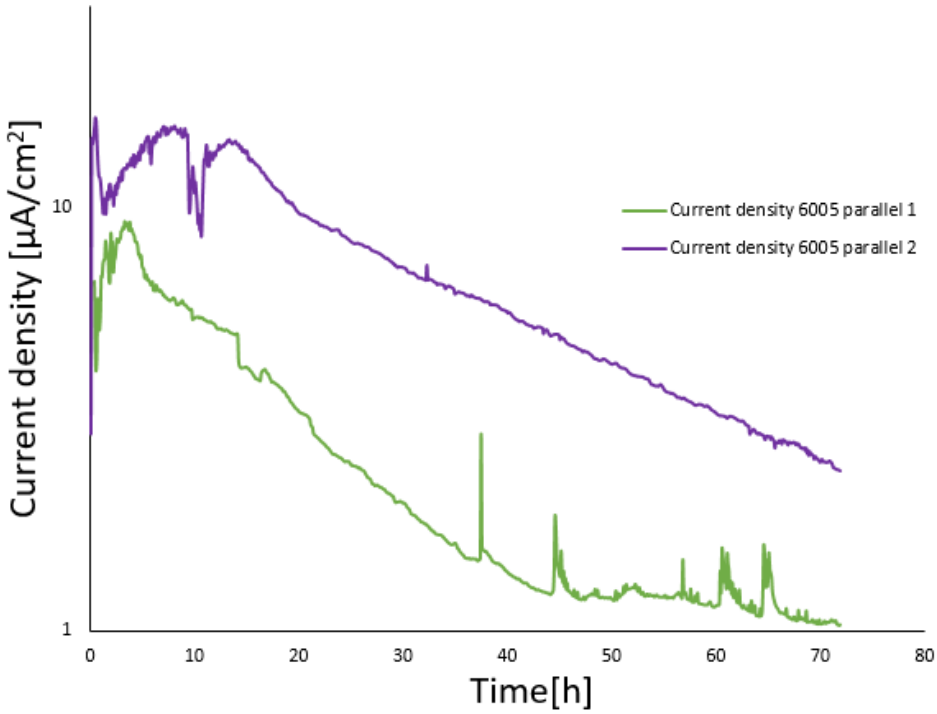

Figure 6.2: Logarithmic representation of currents on 6005 aluminium for parallel 1 and 2 from figure 4.1.

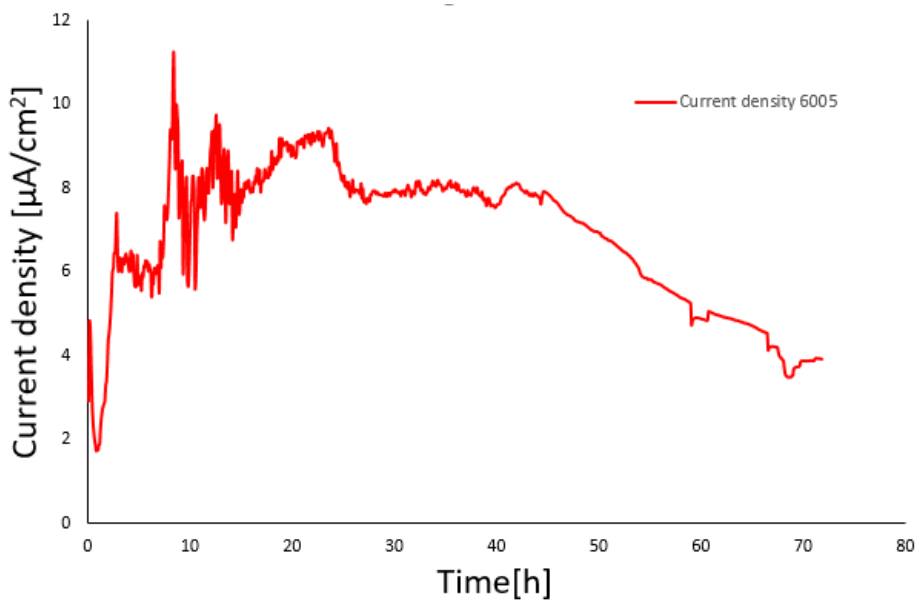

Figure 6.3: Logarithmic representation of current on 6005 aluminium from figure 4.3.

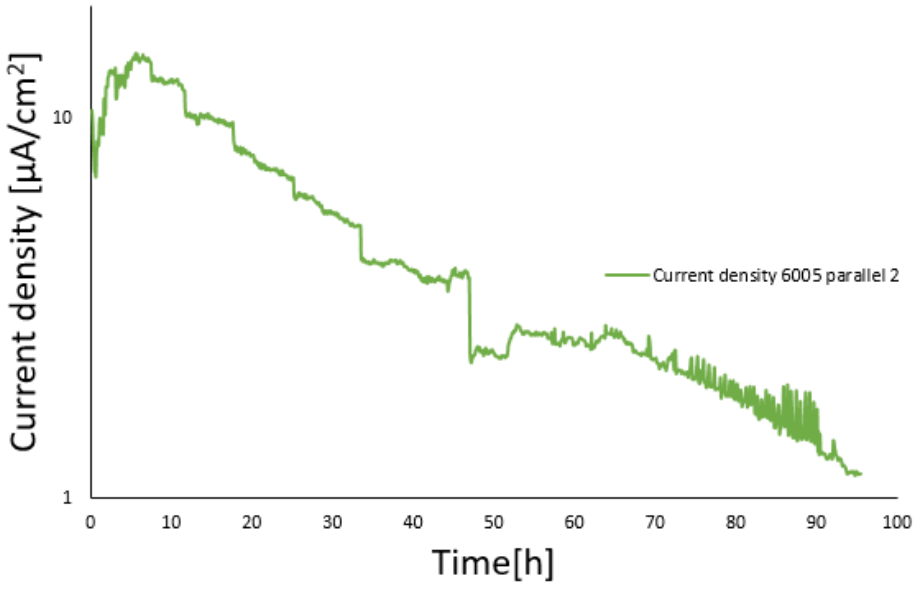

Figure 6.4: Logarithmic representation of currents on 6005 aluminium for parallel 2 from figure 4.5.

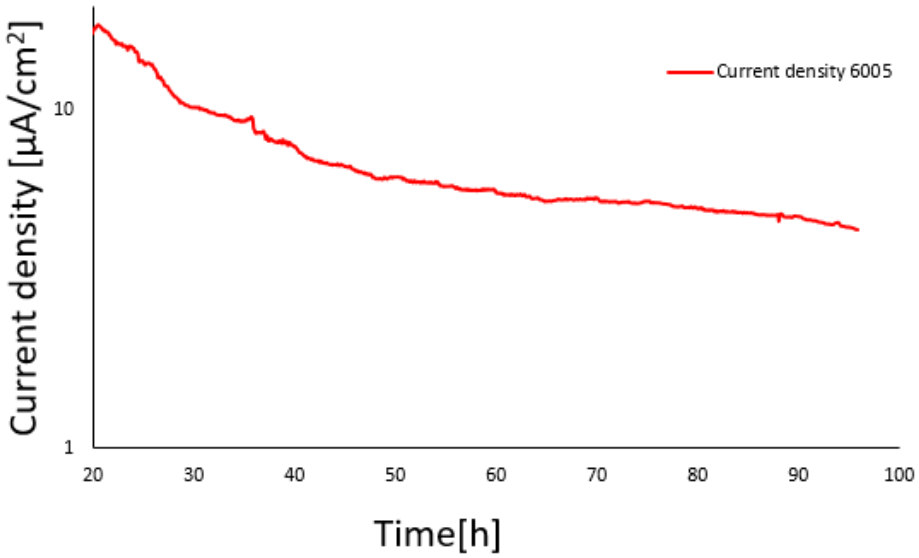

Figure 6.5: Logarithmic representation of current on 6005 aluminium after 20 hours from figure 4.7.

Appendix C: Additional SEM Images

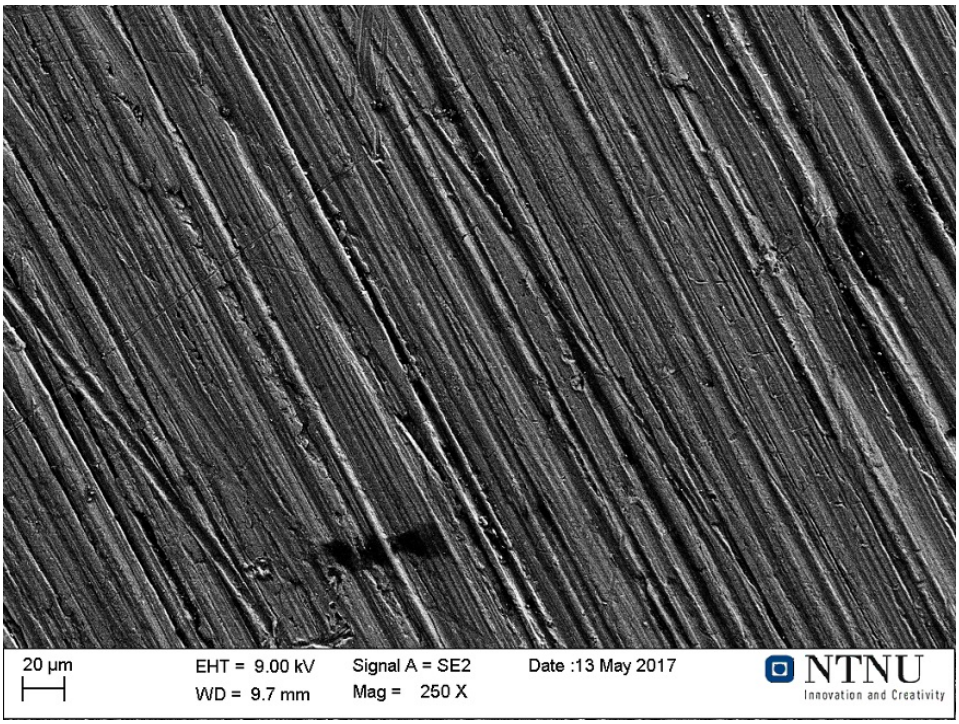

Figure 6.6: SEM Image of 6005 aluminum from galvanic crevice corrosion at 25° run for 72 hours. Image is taken after chemical cleaning. Image is taken in the middle of the sample

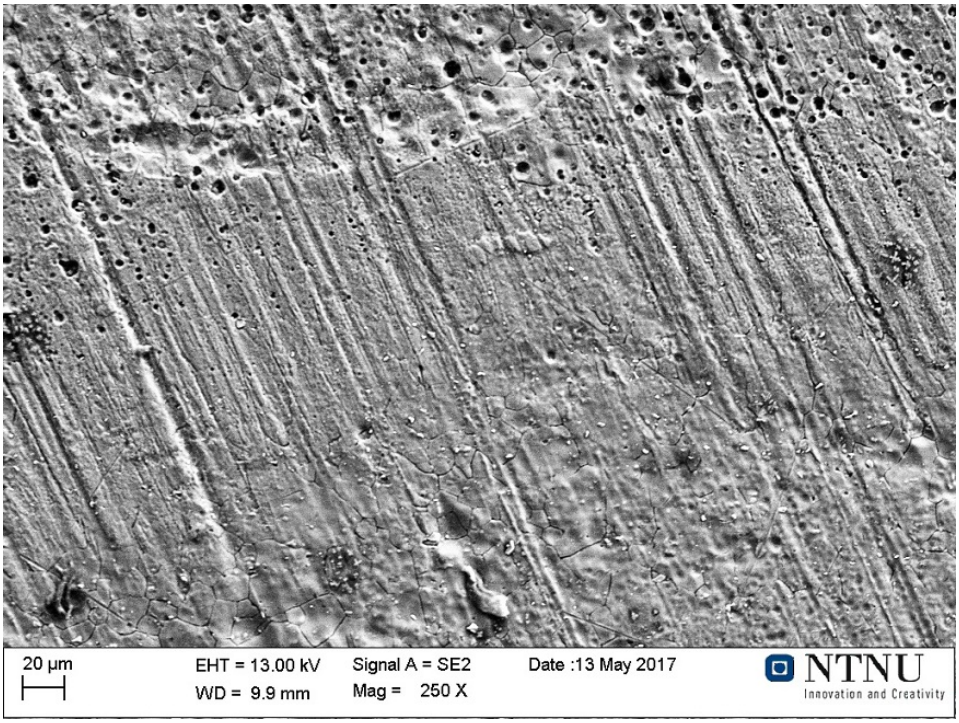

Figure 6.7: SEM Image of 6005 aluminum from galvanic crevice corrosion at 25° run for 72 hours. Image is taken after chemical cleaning. Image is taken near the bottom of the sample

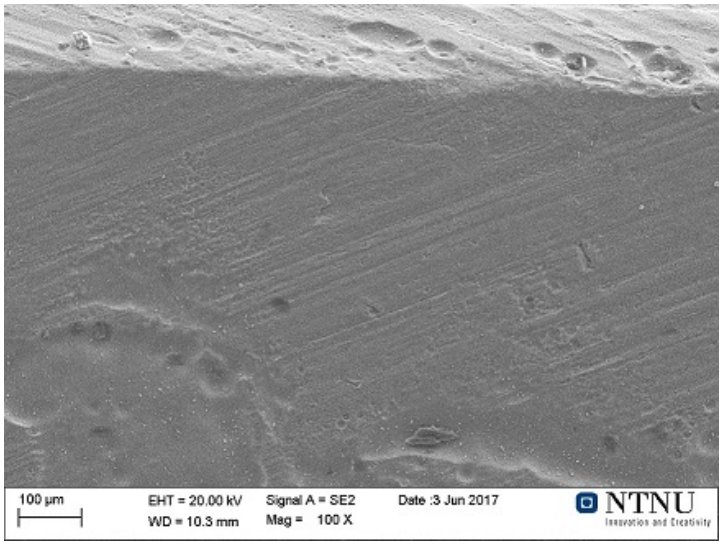

Figure 6.8: SEM Image of 6005 aluminum from galvanic crevice corrosion at 25° run for 96 hours. Image is taken after chemical cleaning and is taken of the top of the sample

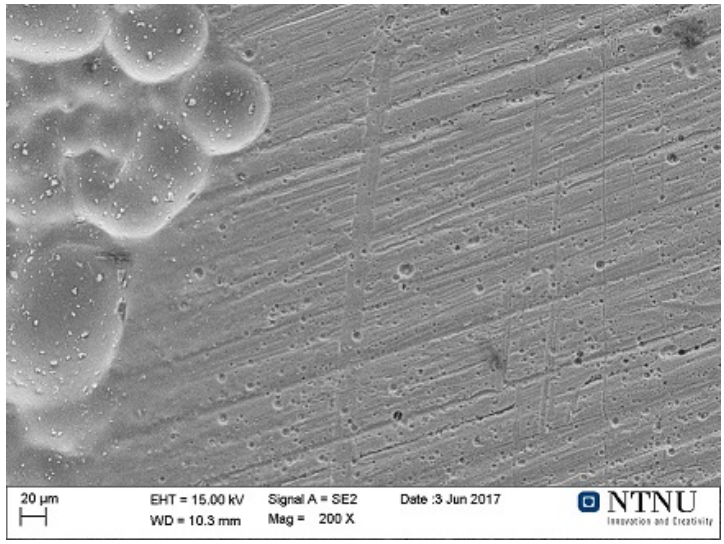

Figure 6.9: SEM Image of 6005 aluminum from galvanic crevice corrosion at 25° run for 96 hours. Image is taken after chemical cleaning and is taken near the bottom of the sample

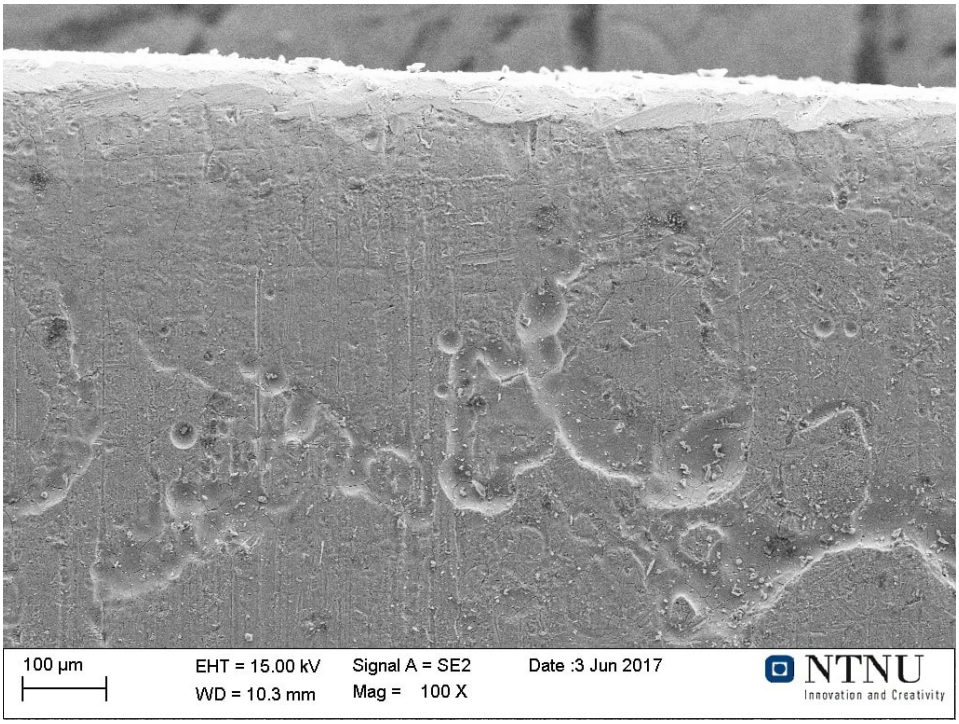

Figure 6.10: SEM Image of 6005 aluminum from galvanic crevice corrosion at 25° run for 120 hours. Image is taken after chemical cleaning and is taken near the top of the sample

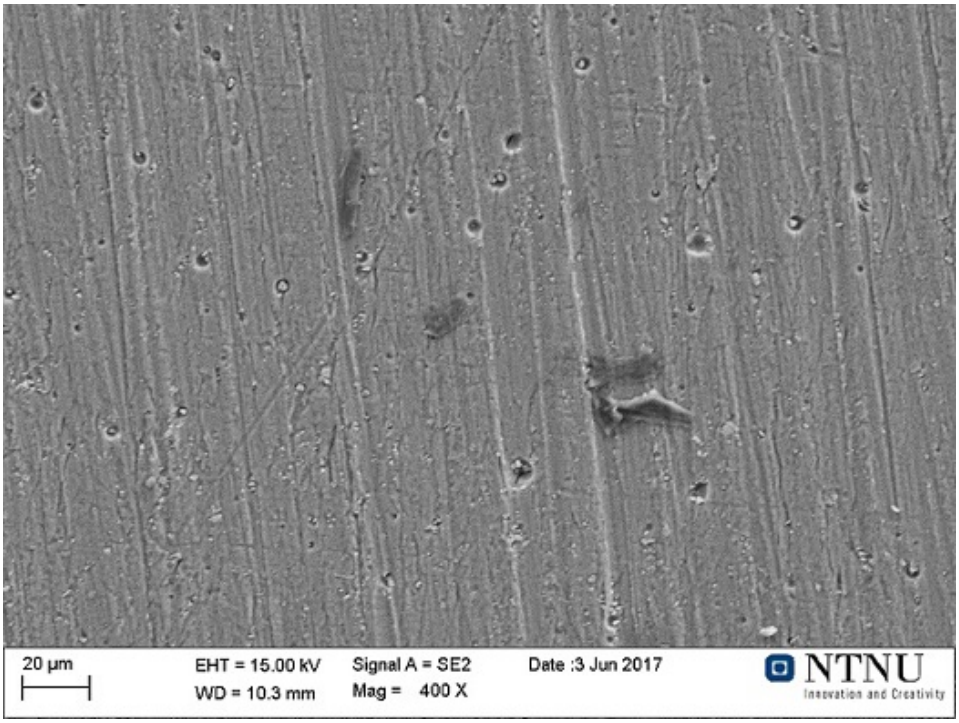

Figure 6.11: SEM Image of 6005 aluminum from galvanic crevice corrosion at 25° run for 120 hours. Image is taken after chemical cleaning and is taken in the middle of the sample

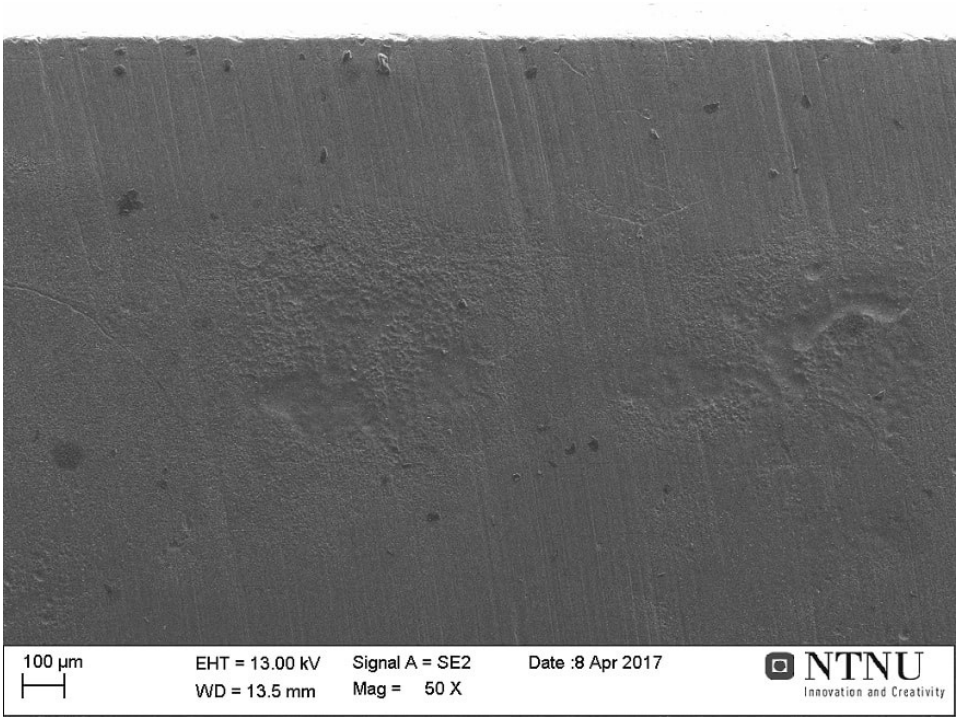

Figure 6.12: SEM Image of 6005 aluminum from galvanic crevice corrosion at 10° run for 72 hours. Image is taken after chemical cleaning and is taken near the top of the sample

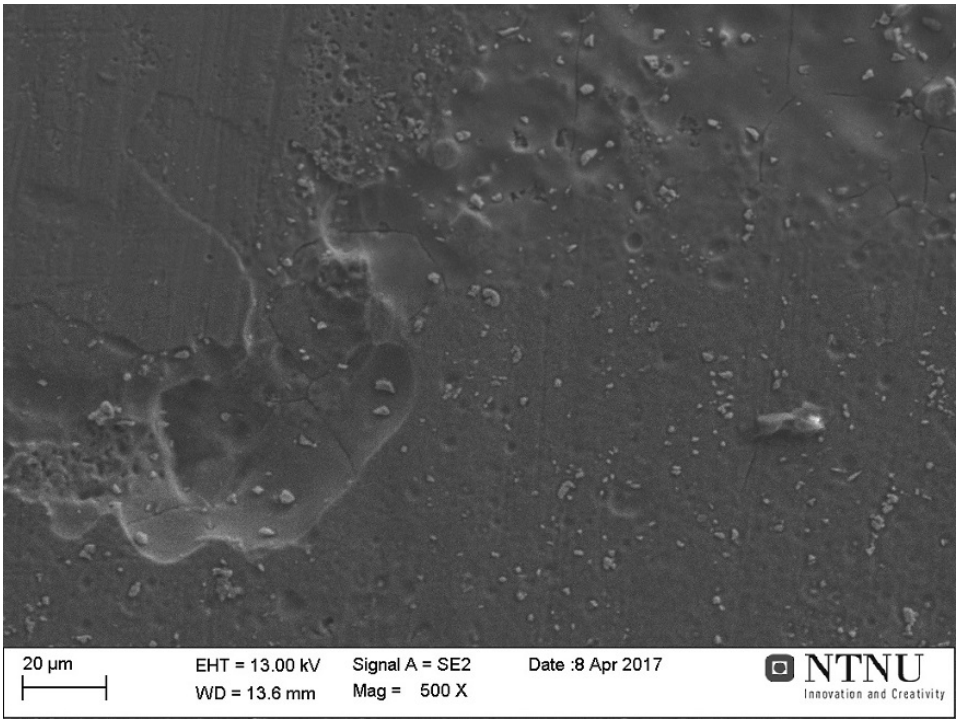

Figure 6.13: SEM Image of 6005 aluminum from galvanic crevice corrosion at 10° run for 72 hours. Image is taken after chemical cleaning and is taken near the bottom of the sample

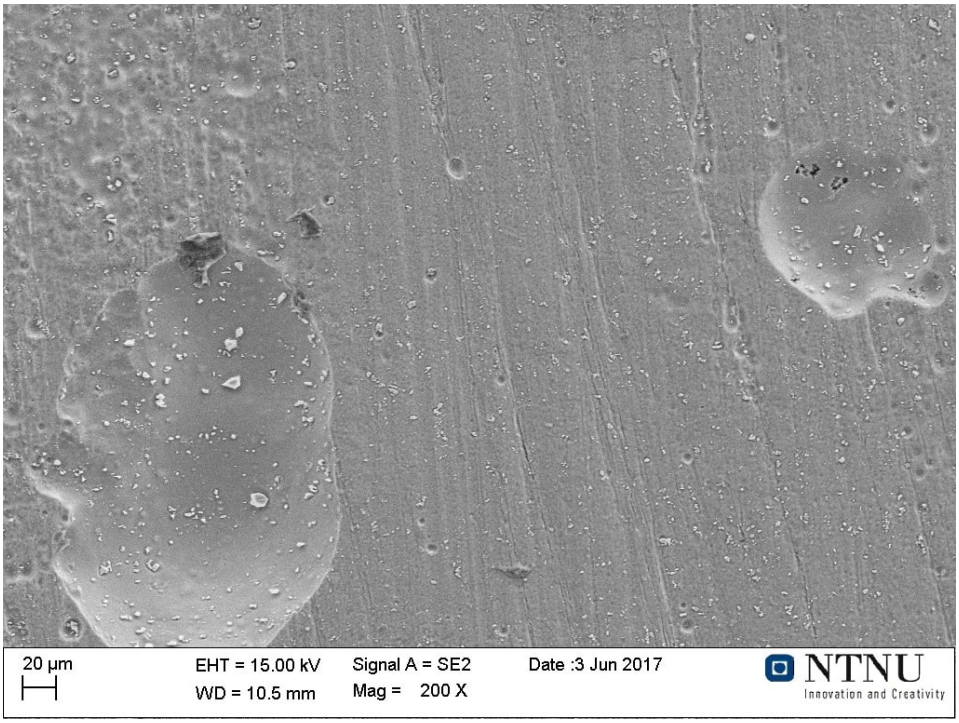

Figure 6.14: SEM Image of 6005 aluminum from galvanic crevice corrosion at 10° run for 96 hours. Image is taken after chemical cleaning and is taken of the top of the sample

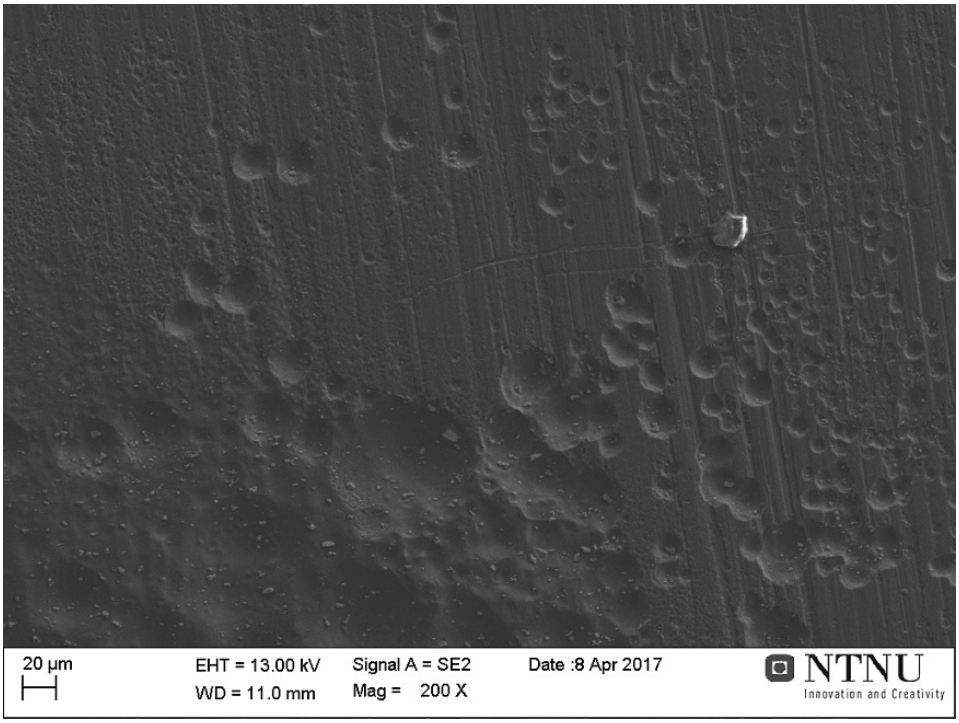

Figure 6.15: SEM Image of 6005 aluminum from galvanic crevice corrosion at 10° run for 96 hours. Image is taken after chemical cleaning and is taken in the middle of the sample

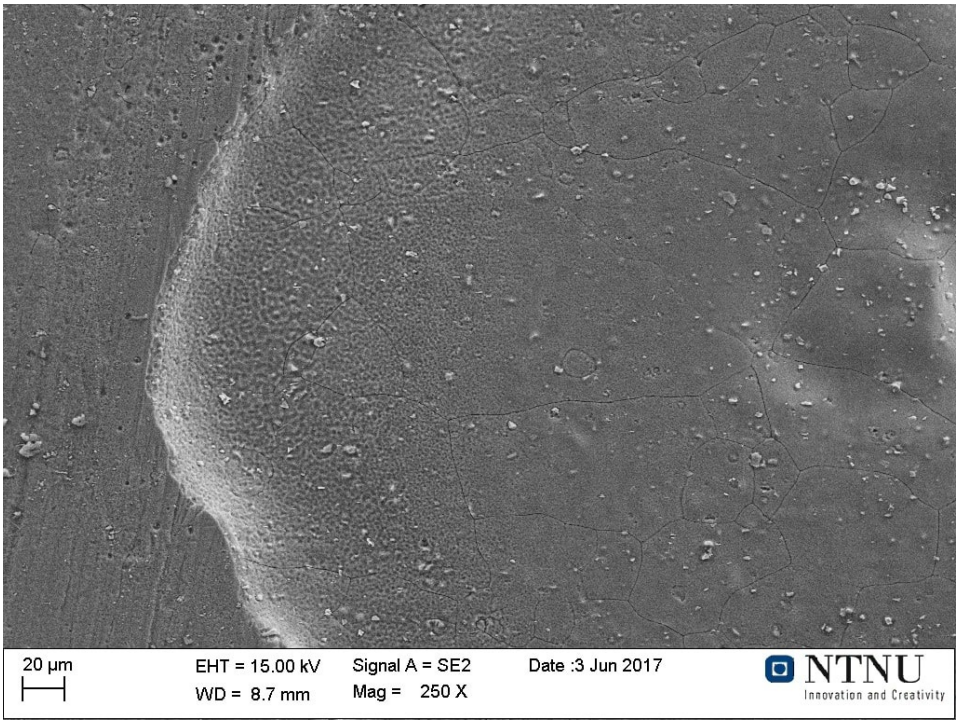

Figure 6.16: SEM Image of 6005 aluminum from galvanic crevice corrosion at 10° run for 120 hours. Image is taken after chemical cleaning and is taken in the middle

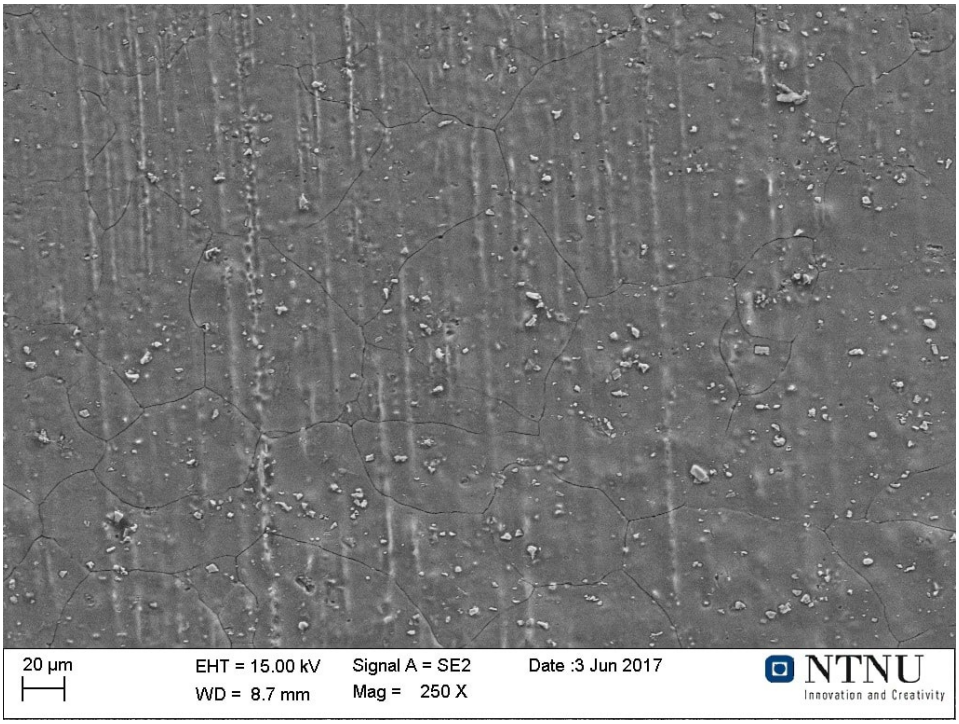

Figure 6.17: SEM Image of 6005 aluminum from galvanic crevice corrosion at 10° run for 120 hours. Image is taken after chemical cleaning and is taken of the bottom of the sample

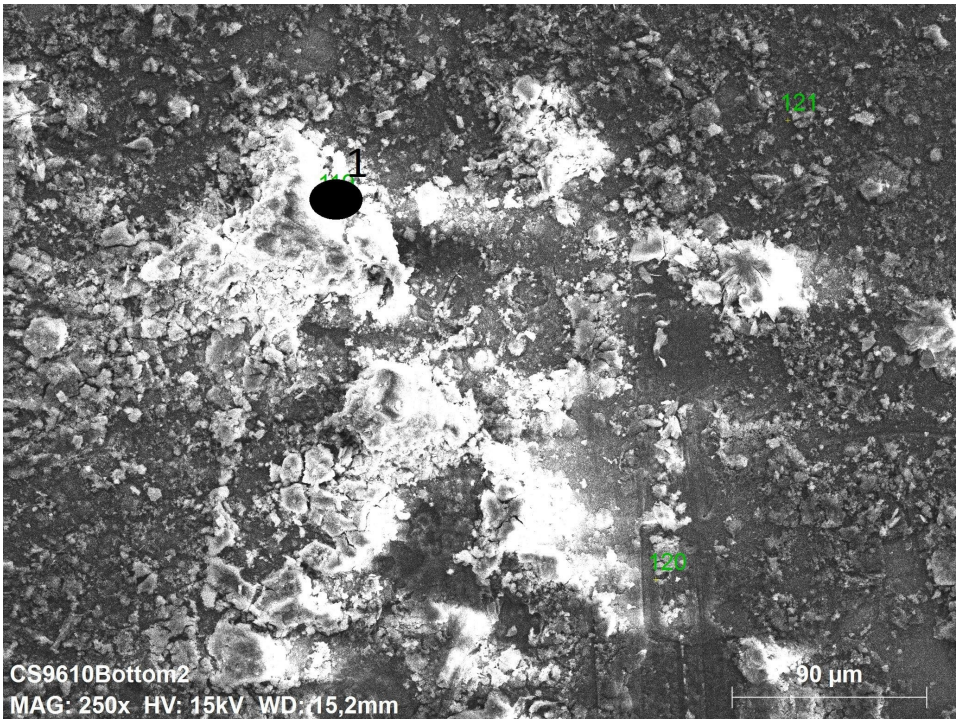

Figure 6.18: SEM Image of X65 carbon steel from galvanic crevice corrosion with cathodic protection at 10°C run for 96 hours. Image is taken before chemical cleaning and is taken at the bottom of the sample

Table 6.1: EDS analysis of the black area figure 6.18

Element	Area 1[wt%]
O	36.4
Mg	28.6
Al	11.4
Cl	10.1
Ca	5.0
Na	3.6
K	2.6
S	2.5
Tot	100